Sede Amministrativa: Università degli Studi di Padova

Dipartimento di *Scienze Biomediche*

SCUOLA DI DOTTORATO DI RICERCA IN : Bioscienze Biotecnologie
INDIRIZZO: Neurobiologia
CICLO XXV

RECIPROCAL NEURON-ASTROCYTE SIGNALING IN EPILEPTIC SEIZURE GENERATION AND PROPAGATION

Direttore della Scuola: Ch.mo Prof. Giuseppe Zanotti
Coordinatore d'indirizzo: Ch.mo Prof. ssa Daniela Pietrobon
Supervisore: Ch.mo Prof. Giorgio Carmignoto

Dottorando : Mario Cammarota

INDEX

INTRODUCTION

The idea that astrocytes – the main population of glial cells in the brain – are active partners of neurons in many aspects of brain functions represented a *Copernican Revolution* in neurobiology. Astrocytes, which were for many years considered just like the cement (from Greek *glia* i.e. glue) that keeps neuronal cells together, have now been moved from the periphery to the centre of the universe of information processing in the brain providing a radically different point of observation in the study of brain physiology. This new view of brain activity turns around the discovery of a bidirectional communication between neurons and astrocytes, a process called *gliotransmission*. Astrocytes respond to neurotransmitters and through a Ca^{2+} dependent mechanism release neuroactive substances that induce functional changes in neurons. In spite of the resistances opposed against the desertion of the neuronal dogma, a large amount of evidence collected during the last three decades contributed to reshape the concept of synaptic communication, considering astrocytes - together with the pre- and post- synaptic membranes - a fundamental element of the *tripartite synapse.* In other words, astrocytes participate transversally to information processing in the brain by modulating both synaptic transmission and different forms of plasticity.

This new consciousness of astrocytes as active elements in brain physiology, naturally suggests that these glial cell can potentially be involved in the development of brain disorders. Indeed many studies revealed that dysfunctions in astrocyte-neuron signaling can be directly involved in many pathologies including Alzheimer's disease, Parkinson disease, amyotropic lateral sclerosis and epilepsy.

The main goal in my thesis was to understand how the release of gliotrasnmitters by astrocytes, in particular glutamate, may influence two distinct phases of epileptic activity: the generation and the propagation of a focal seizure.
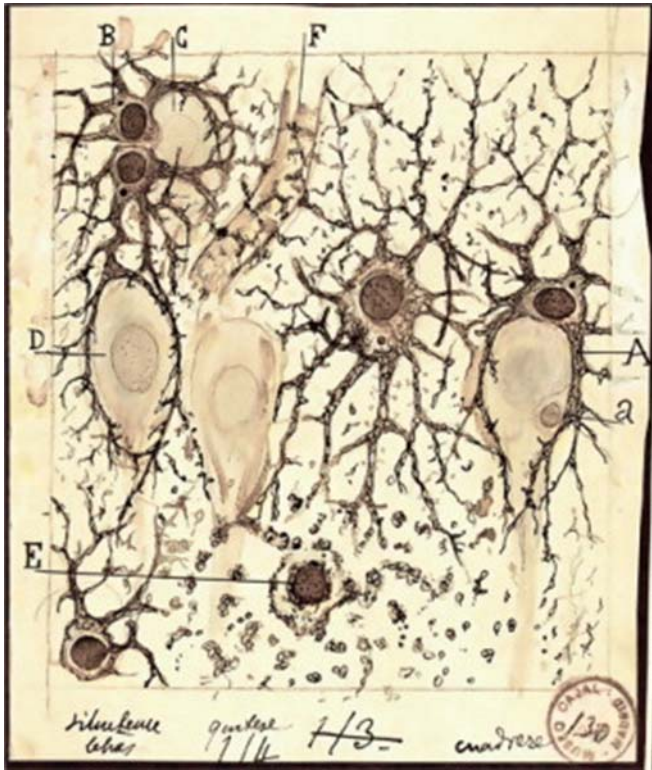
NEURONS TALK TO ASTROCYTES

Figure 1: Original drawing of Santiago Ramon y Cajal showing the intimate morphological connection between neurons and astrocytes.

The information flow in the brain is conveyed by electrical signals. Astrocytes do not have a density of Na^+ channels sufficient to generate an action potential and they respond to depolarizing steps with a linear current-tension characteristic. In other words, they are unable to elaborate the information using a language based on electrical signals. For this reason astrocytes have been segregated for many years at the periphery of the brain. Nevertheless, clues for a possible neuron-to-astrocyte signalling came from morphological studies, which revealed an intimate connection between the astrocytes processes and the synapse (see Figure 1; (Peters et al., 1991);(Dani et al., 1992);(Ventura and Harris, 1999).

In the early 90s, taking advantage of the novel Ca^{2+} imaging techniques, different groups provided the first evidence that astrocytes display a form of excitability mediated by Ca^{2+} signal changes in response to neuronal activity (see Figure 2; (Dani et al., 1992); (Porter and McCarthy, 1996); (Pasti et al., 1997). In both cell cultures and acutely isolated hippocampal slices, the stimulation of glutamatergic afferents evoked Ca^{2+} oscillations in astrocytic cytoplasm. In the following years, the pioneering observation of an astrocytic Ca^{2+} signaling was extended to different brain regions (Perea et al., 2009); for a review see (Volterra and Meldolesi, 2005), associated to many neurotransmitters and factors (for a review see (Haydon and Carmignoto, 2006), and, more recently, reported also in living animals in response to sensorial stimuli (Navarrete et al., 2012) and during locomotor activity (Nimmerjahn et al., 2009). Despite astrocytes speak a different language with respect to that of neurons - which is based on intracellular Ca^{2+} change and not on electrical signals - it seems,

3

however, that they can understand neurons. In the two following paragraphs I address two important issues related to neuron-to-astrocyte signalling: i) what is the mechanism that induces Ca^{2+} oscillations in astrocytes? ii) how Ca^{2+} oscillations are codified in the astrocyte to convey signals to neurons.?
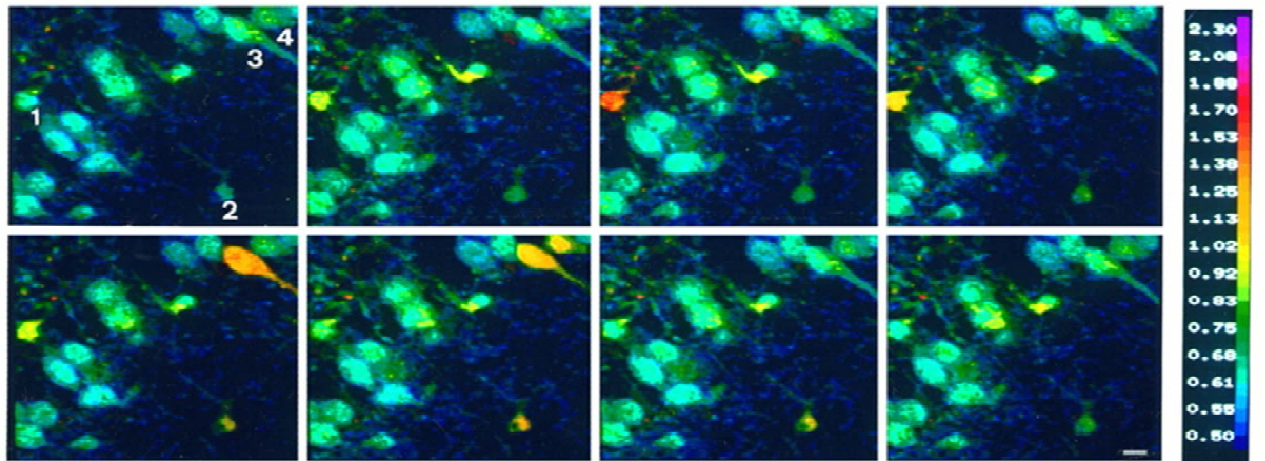

Figure 2: Stiimulation of mGluRs induces Ca^{2+} oscillations in hippocampal cells. Time series of the changes occurring in two astrocytes (labeled 1-2) and two pyramdal neurons (labeled 3-4). From Pasti et al., J Neuroscie 1997;17:7817-7830

Ca^{2+} SIGNALLING IN ASTROCYTES

A signaling based on Ca^{2+} dynamics is present in all eukaryotic cells and it generally plays a crucial role in many cellular processes such as muscle contraction, gene expression, metabolic reactions, etc… Generally speaking, Ca^{2+} is the fundamental ion in cellular communication, providing the link between input signals coming to the cells and output signals. In particular, Ca^{2+} is the key molecule for chemical transmission in the nervous system: it couples the electrical excitability (input) with the exocytosis of neurotransmitters from the pre-synaptic terminal (output). During the action potential discharge at the pre-synaptic terminal, exocytosis requires that very high concentrations of Ca^{2+} (10-50 μM) were reached in proximity of the compartment specialized for releasing transmitters, the *active zones*, in order to induce the fusion of the vesicles with pre-synaptic membrane. This process occurs at the time scale of a few milliseconds and it thus implies a very fast mechanism and requires a huge Ca^{2+} source. This source is constituted by voltage-gated Ca^{2+} channels (VGCCs) which are abundntly expressed at the pre-synaptic membrane.

As we anticipated above, Ca^{2+} is the substrate for astrocytes excitability. Ca^{2+} elevations in astrocytic cell body occur with slow kinetics (1-10 seconds time scale), and are indeed very much slower compared with the kinetics which characterize Ca^{2+}

increase at the neuronal terminals.. Not surprisingly astrocytes lack a fast source of Ca^{2+}: VGCCs expressed by astrocytes have minor implications in cellular signalling (Carmignoto et al., 1998), and no evidence have been reported for the presence in astrocytes of other possible fast sources of Ca^{2+}, like the Ca^{2+}-permeable glutamate NMDA receptor (Teichberg, 1991). The most important mechanism for Ca^{2+} elevations in astrocytes is the activation of G-protein-coupled receptors. When a neurotransmitter binds to a GPCR, Phospholipase C (PLC) hydrolyzes Phosphatidylinositol 4,5-bisphosphate (PIP2) generating Diacil Glycerole (DAG) and Inositol 1,4,5-triphosfate (IP3) which binds to IP3 receptor inducing Ca^{2+} release from endoplasmatic reticulum. Astrocytes express many receptors that can be activated by different neurotransmitters, such as glutamate, D-serine, ATP, GABA, which are usually released by the pre-synaptic terminal. Also the post-synaptic neuron may activate astrocytes Ca^{2+} signal through the release of retrograde messenger such as endocannabinoid (Navarrete and Araque, 2008); (Navarrete and Araque, 2010).

A totally different mechanism of Ca^{2+} signaling in astrocytes was recently described by Shigetomi and colleagues (Shigetomi et al., 2011). Taking advantage of a membrane-tethered, genetically encoded Ca^{2+} indicator (Lck-GCaMP3), they observed Ca^{2+} signals which appeared as flashes at localized spots of the membrane. They were able to demonstrate hat this type of Ca^{2+} signalling is mediated by Ca^{2+} influx through transient receptor potential A1 (TRPA1) channels.

ASTROCYTES CODING OF NEURONAL INPUT

The most compelling problem in the study of neuron-astrocyte interactions is our defective understanding of how the Ca^{2+} signals are codified by astrocytes. Differently from neurons, where the action potential represents a sort of basic unit of the electrical excitability in these cells, the language spoken by astrocytes lacks a similar hall mark. Ca^{2+} oscillations in astrocytes may have different patterns, in terms of frequencies and amplitude, and these differences may be translated into different functional outputs. A possible reason of our unsatisfactory understanding of the code used by astrocytes could be the fact that, at least until few years ago, scientists have monitored Ca^{2+} signals exclusively at the level of the astrocytic cell body. Astrocytes displays long lasting (one to ten seconds) Ca^{2+} elevations in their soma, mainly in response to a very intense neuronal activity. In other words, a somatic Ca^{2+} elevation

5

could occur only when neuronal activity reaches a certain threshold and the frequency of these oscillations increased according to an increasing intensity of the neuronal activity (Pasti et al., 1997); (Matyash et al., 2001).

A fundamental step forward in our understanding of Ca^{2+} signalling in astrocytes was given by two recent studies that by revealing that the spatio-temporal scale of the Ca^{2+} activity at the astrocyte processes unveil a totally new world previously hidden with features rather different from those of the Ca^{2+} signal at the level of the cellular body (Di Castro et al., 2011); (Panatier et al., 2011). Authors showed that low levels of neuronal activity, such as spontaneous synaptic events, may induce Ca^{2+} increases in tiny compartments (1-4 um) of the astrocytic processes. These signals occur randomly with a frequency significantly higher than that of similar events at the cell body), and are relatively short-lasting (less than a second rise time; *focal Ca^{2+} transients*). On the other hand, a single action potential generates a robust and long response (few seconds; *Expanded Ca^{2+} transients*) occurring synchronously in several of these compartments. The authors demonstrated that these Ca^{2+} signaling control a process of glutamate release which influences synaptic transmission at this spatial-temporal scale. Astrocytes are able to detect action potential-dependent synchronization of local synaptic activity, and to coordinate their response accordingly, thereby providing a very fine substrate for the detection and the modulation of local synaptic activity.

All in all, somatic Ca^{2+} signaling appears to be the tip of the iceberg of a very more complex and intricate network of signals. They represent a class of responses that can occur only above a fixed threshold and reflect a more intense and coordinated neuronal network activity.
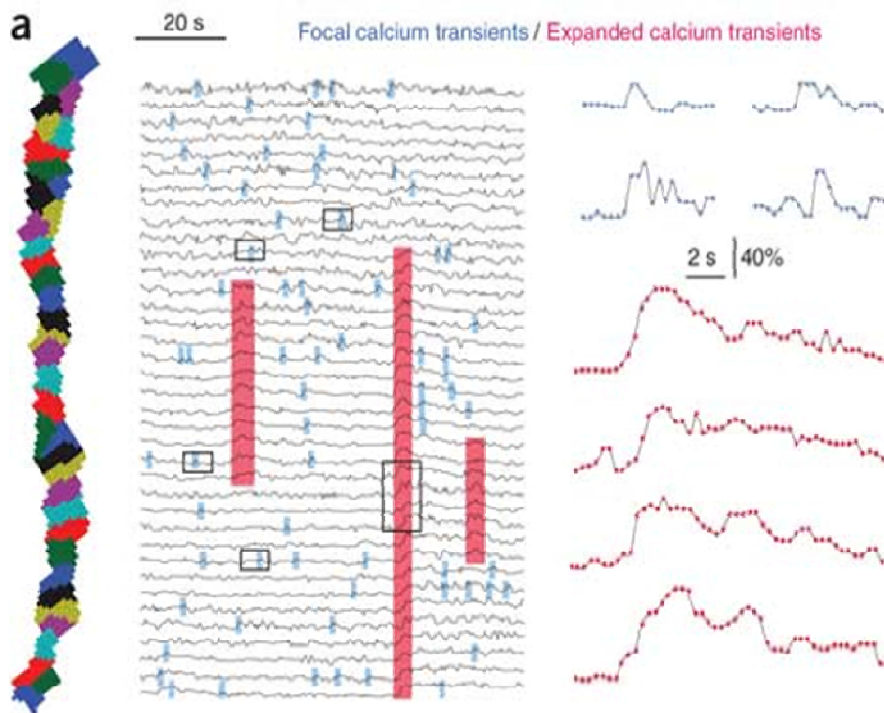
Figure 3: Ca²⁺ activity in an astrocytic process. Left: process reconstruction and subdivision in subregions of ~ 1μm. Middle: traces showing occurrence of Ca²⁺ peaks in contigous process subregions.- Red highlights identify expanded Ca²⁺ events, relative high-amplitude transients with recurrent pattern in several subregions. Blue highlights identify focal Ca²⁺ events, small transients often limited to one subregion. Righ: magnified traces of boxed examples of focal and expanded Ca²⁺ events. From Di Castro et al., Nature Neurosci 14, 1276-1284 (2011).

ASTROCYTES RESPOND TO NEURONS

Although astrocytes can release gliotransmitters by different mechanisms including transporters and hemichannels, the great importance of Ca²⁺ signalling in the intercellular communication and the neuronal activity dependence of Ca²⁺ oscillations in astrocytes, strongly suggest that the output of astrocytes, i.e. the gliotransmission, might be fundamentally a Ca²⁺-dependent process. First of all, researchers focused their attention on the possible similarities between the release of transmitters from astrocytes and the Ca²⁺-dependent exocytosis of neurotransmitter from neurons. A major role in the regulated secretion of vesicles in neurons is played by the proteins of the SNARE complex, which are involved in the processes of docking and fusion of the vesicles. Astrocytes have been showed to express several proteins of SNARE complex, i.e., synaptobrevin II, the Ca²⁺ sensor synaptotagmin IV, syntaxin and the homolog of SNAP-25, SNAP-23, suggesting that a regulated Ca²⁺- dependent exocytosis may occur in astrocytes too. Other kinds of evidence support the notion of Ca²⁺-dependent exocytosis in astrocytes. The exocytosis process was directly monitored in cultured astrocytes using TIRF microscopy (Bezzi et al., 2004); (Bowser and Khakh, 2004); (Malarkey and Parpura, 2011) and the fusion of the vesicles with

7

the astrocytic membrane was measured as changes in the membrane capacitance (Kreft et al., 2004); (Zhang et al., 2004).

MODULATION OF SYNAPTIC ACTIVITY AND PLASTICITY

Do the transmitters released by astrocytes influence neuronal activity? Do they modulate synaptic transmission? Do they affect synaptic plasticity? Although until today we have not definitive answers to these questions, a huge amount of experimental data obtained transversally in all brain regions studied allow us to state that astrocytes *has the potential* to do release gliotrasnmitters that deeply influence synaptic transmission..

Astrocytic modulation of synaptic transmission is; however, a multifaceted world as it can result in both potentiation and depression of synaptic transmission. The overall nature of the gliotransmitter effects on neuronal activity depends on many different factors: the type of gliotransmitter released, the neuronal receptor activated, the type of neuron targeted, the brain region in which gliotranmsission takes place. The release of glutamate acting on pre-synaptic mGluRs, for example, was demonstrated to potentiate synaptic transmission in hippocampal CA3-CA1 synapses (Perea and Araque, 2007), but the same effect can be provided by the activation of NMDARs in a different region of the hippocampus, the dentate gyrus (Jourdain et al., 2007). Analogously, the release of ATP by astrocytes, which is readily metabolized in adenosine by specific enzymes in the extracellular space, has been showed to be linked to both inhibitory and excitatory effects activating A1 and A2A receptors respectively (Serrano et al., 2006); (Pascual et al., 2005); (Panatier et al., 2011). An additional factor of complexity is the spatial extensions of astrocytic processes. For example, a Ca^{2+} signal induced locally at an active synapse can travel intracellularly and triggers the release of gliotransmitters in different and distant sites. Astrocytes activated by endocannabinoids in the hippocampus have been shown to enhance synaptic transmission in relatively distant synapses, while neurotransmission was depressed by the direct effect of the endocannabinoid at the presynaptic membrane expressing CB1 cannabinoid receptors (Navarrete and Araque, 2008); (Navarrete and Araque, 2010). Similarly, the ATP released by astrocytes upon the stimulation of a high active synapse was observed to depress other synapses aftre its conversion to adenosine (heterosynaptic depression; (Serrano et al., 2006)).

8

Long lasting effects on synaptic efficacy were associated to astrocytes. Also in this context many variables determine the effect of astrocytes modulation of neuronal network. The gliotransmitter glutamate mediates a form of spike-timing dependent depression of excitatory transmission in neocortex (Min and Nevian, 2012), but, at the same time, was associated to an mGluR dependent and NMDA independent form of long term potentiation (LTP) in the CA1 region of the hippocampus. Here, this form of plasticity requires the coincidence between postsynaptic activity and astrocyte Ca^{2+} signalling (Perea and Araque, 2007). A different form of LTP in the same hippocampal CA1 region was associated to the release of another gliotransmitters, D-serine, which acts as NMDAR co-agonist, and is necessary for the induction of this kind of NMDA dependent LTP (Henneberger et al., 2010). Also cholinergic activity evoked by sensory stimulation was shown to evoke an astrocytes dependent LTP. Authors showed that the activation of a Ca^{2+} signaling in astrocytes, and the consequent gliotransmission is required to this form of plasticity (Takata et al., 2011); (Navarrete et al., 2012).
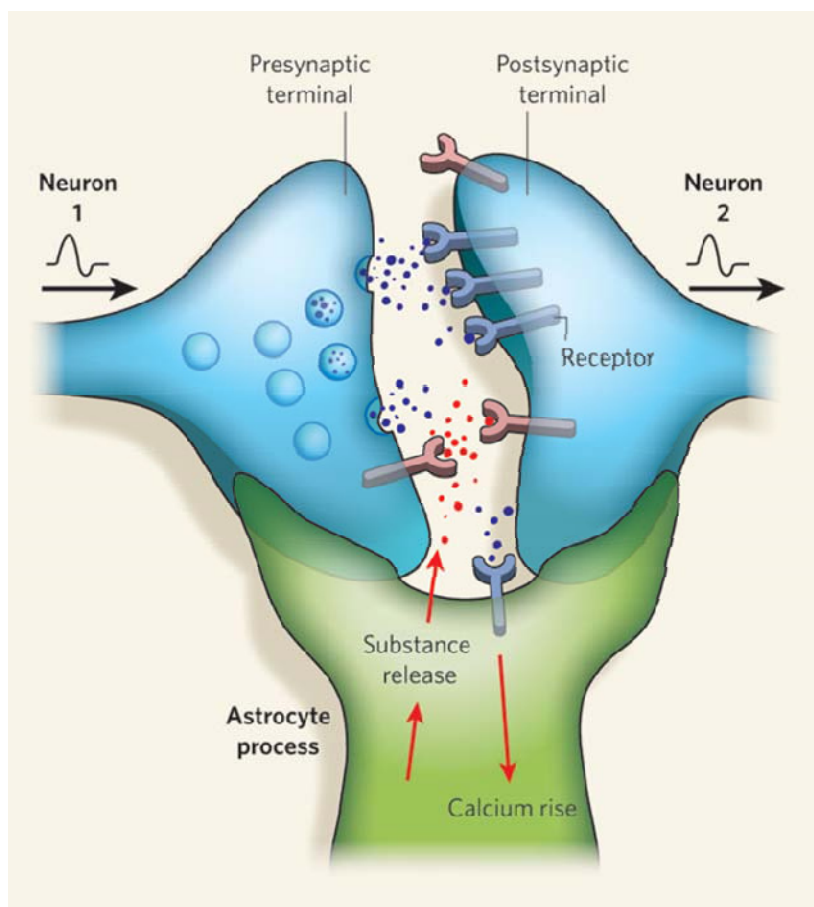

Figure 4: Picture illustrating a model of the tripartite synapse. Transmitters released by presynaptic neurons can activate Ca^{2+} rises in astrocytes which in turn release substances which act back to neurons to either inhibit or enhance neuronal activity. From Allen and Barres, Nature 457, 675-677 (2009)

THE ROLE OF ASTROCYTES IN EPILEPSY

The term epilepsy is referred to a chronic neuro-pathological condition characterized by recurrent seizures provoked by anomalous and hyper-synchronous neuronal discharges which originate from the hyperactivity of the neurons from a restricted cerebral region – the *epileptogenic focus* – and then propagate to other regions possibly involving the whole brain. Seizures can arise in a plenty of different ways, and a clinical classification has been made in 1981 by the *Commission on classification and terminology of the international league against epilepsy*. The 3% of the total world population is affected by this condition, that in a 30% percentage of cases is pharmacological untreatable, the only possible solution being the surgical ablation of the portion of tissue which generates the seizures. Epileptic activity is conventional characterized by three different phases (Pinto et al., 2005):

i)   *generation* which consists in the transition from a local and asynchronous neuronal hyperactivity restricted to the epileptogenic focus, to a synchronous activity involving large neuronal populations

ii)   *propagation* which consists in the recruitment to the epileptiform activity of neuronal population distant from the epileptogenic focus

iii)   *termination* which consists in the sudden and synchronous cessation of the crisis

The increase in astrocytes number, morphological changes of their soma and processes, together with functional changes – a complex condition generally termed *reactive astrogliosis* – have been for a long time associated to brain disorders, and in particular to epilepsy. Although a causative role for astrogliosis in epileptogenesis has been never demonstrated, gliosis, which can be reveald from an increase in the expression of glial fibrillary acidic protein (GFAP), was observed in different epileptic tissues: both in patients (tissues obtained by surgical ablation or postmortem) and in animal models (such as pilocarpine or kainite induced epilepsy; (Seifert et al., 2006). More interestingly, was also shown that seizure often generate in proximity to gliotic brain tissue (McKhann et al., 2000). Thus, the hypothesis that astrocytes dysfunctions can contribute to epileptogenesis can be reasonably advanced.

How astrocytes can be connected to epileptic activity? In the next paragraphs I give a rapid sketch of two view of the astrocyte role in epilepsy. The first is related to K^+ buffering and glutamate uptake, while the second is emerging from recent results and it is directly related to the action of gliotransmission in epileptiform activities (for a review see (Losi et al., 2012)).

K^+ BUFFERING

Since even small elevations in extracellular K+ concentration ($[K^+]_o$) might lead to a significant depolarization in neurons and to an increase in the activity of the neuronal network, the homeostasis of K^+ is considered to be both a fundamental aspect in the control of the general excitability in the neuronal network and a possible causal factor in epilepsy. The high and rapid permeability of astrocytes to K^+ makes them very important in the control of $[K^+]_o$ homeostasis. Astrocytes are able to spatially redistribute K^+ from areas characterized by an high $[K^+]_o$ to neighboring regions which have a lower $[K^+]_o$. Due to their ability of spatial buffering of K^+, astrocytes have been hypothesized to play a crucial role in epileptic activity in the clearance of the large $[K^+]_o$ increase due to intense action potential firing during epileptic activity (Kuffler et al., 1966). The K^+ channels responsible for the high astrocytic K^+ permeability are rectifying K+ channels (Kir channels). These channels are characterized by high open probability at resting potential and by a channel conductance proportional to $[K^+]_o$ (Olsen and Sontheimer, 2008). For these reasons Kir channels can be effectively activated by large $[K^+]_o$ increases, and they mediate small $[K^+]_o$ efflux from depolarized cells and large influx at hyperpolarized potentials. Among the sixteen distinct Kir channel subunits, the most estensively studied is type 4.1, which is interestingly largely expressed in astrocytes in many brain regions (Takumi et al., 1995); (Li et al., 2001).

Altered Kir4.1 expression and activity has been observed in epileptic tissues from human patients and experimental animal models (Lenzen et al., 2005); (Inyushin et al., 2010). These observations do not dissect out if Kir4.1 dysfunctions were actively involved in epileptogenesis or if they were just a mere consequence of epileptic activity.

11

GLUTAMATE UPTAKE

Another important factor which can influence neuronal network excitability is the dynamics of glutamate concentrations in the extracellular space. A crucial role in taking up the glutamate released by excitatory neurons is played by five different excitatory amino acid transporters EAAT1-5. Among this group, EAAT1 and EAAT2 (GLAST and GLT-1 in rodents, respectively) are selectively expressed in astrocytes, they have the function of regulating the extracellular glutamate concentration (Tanaka et al., 1997). While elevated levels of glutamate have been reported in human epileptic tissues, there are no definitive results about the contribution of EAAT levels in epileptogenesis: some studies revealed a down regulation of astrocytic glutamate transporters level (Mathern et al., 1999); (Proper et al., 2002); (Sarac et al., 2009), others did not observed alterations (Tessler et al., 1999); (Eid et al., 2004).

THE ROLE OF GLIOTRANSMISSION (GLUTAMATE)

The hypersyncrhonization which characterized epileptic activity has been considered for long time a pure neuronal phenomenon until glutamate released by astrocytes was revealed to be an extrasynaptic source that could synchronize groups of neurons from different brain regions. Two different studies demonstrated that glutamate released upon the stimulation of the metabotropic receptors in astrocytes is able to induced synchronous N-methyl-D-aspartic acid (NMDA) mediated slow inward currents (SICs) in pyramidal neurons (Fellin and Carmignoto, 2004); (Angulo et al., 2004). Using paired patch-clamp recordings from pyramidal neurons, authors showed that SICs occurred with a high level of synchrony whenpair of neurons were located within a reciprocal distance of 100 μm. Furthermore, Ca^{2+} imaging experiments revealed that astrocyte Ca^{2+} elevations could be followed by the synchronous activation of spatially dinstinct domains of neurons. The power of astrocytes in synchronizing groups of neurons raises the hypothesis that astrocytes – and in particular glutamatergic gliotransmission – can be involved in the process of ictogenesis. In other words, the observation that Ca^{2+} oscillation in astrocytes could evoke synchronous response in groups of neurons, seems to sugges that this group of neurons could represent – *in embryo* - an epileptogenic focus. This thesis was strongly supported by a controversial study by Nedergaard's group, which showed that in five different

12

experimental models of pharmacological induced epilepsy, 70-90% of paroxysmal depolarizing shift (PDSs), i.e. interictal spikes, were insensitive to tetrodotoxin (TTX) application (Tian et al., 2005). The interpretation given by the authors was that PDSs coincide with SICs and that seizure activity may have a pure astrocytic basis. However, the observation reported by Tian et al. was in contrast with previous and subsequent studies showing that TTX efficiently blocks PDS. Moreover, as was reviewed by Weteringhton et al., (Wetherington et al., 2008) a huge amount of data supports the notion that SICs and PDSs are rather different cellular events. SICs have been demonstrated to be mediated exclusively by NMDA receptors, while PDSs were reported to be in large part D-AP5 insensitive. In spite of these possible contradictions against a hypothesis of an astrocytic basis of epilepsy, the possibility that glutamate released by astrocyte could be an important factor in epileptic discharge generation was never ruled out. In the Results we are going to report a recent work from our laboratory (Gomez-Gonzalo et al., 2010) showing how the contribute of astrocytic glutamate, although not sufficient, is very important to set the threshold for ictal discharge.
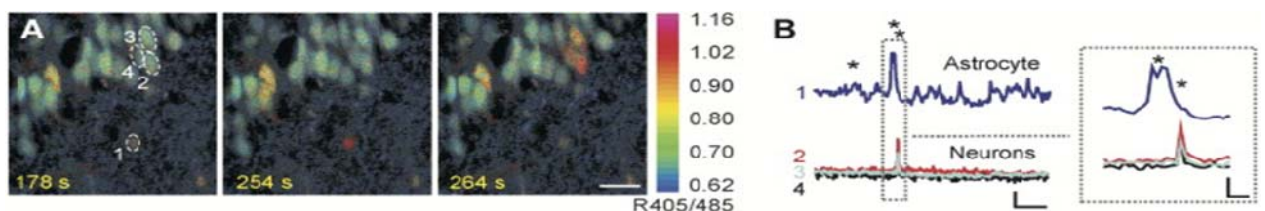
Figure 5: Ca2+ changes occurring in one astrocyte (1) and three neurons (2,3,4) upon low Ca2+ stimulation. Sampling rate, 2s. Scale bar, 20 μm. B Time course of the response from the same cells indicated in A. From Fellin et al., Neuron 43, 729-743 (2004).

THE ROLE OF GLIOTRANSMISSION (ATP)

Glutamate is not the only gliotransmitter released by astrocytes which plays a relevant role in the control of epileptic discharges. ATP is released by astrocytes through different mechanisms, both Ca^{2+} dependent and Ca^{2+} independent (Coco et al., 2003); (Pascual et al., 2005). Although ATP can act directly on neurons and astrocytes respectively through the activation of P2 and P2Y receptors (for a review see (Kumaria et al., 2008)), the main effect of ATP on epileptic discharges is exerted by its metabolite adenosine (Ado). Ado is a strong suppressor of neurotransmitters release, activating A1 receptors on neuronal pre-synaptic terminals. Haydon's group, taking advantage of a transgenic mouse characterized by impaired gliotransmission,

13

demonstrated that astrocytic ATP mediates an important form of synaptic transmission: etherosynaptic depression (Pascual et al., 2005); (Serrano et al., 2006). This result put astrocytes at the center of the stage of the purinergic signaling in synaptic transmission, opening the way to possible implications of this signaling in the control of epileptic discharges. Is today well established that Ado is a potent anticonvulsant, and astrocytes are very important regulators in Ado metabolism, since they are a major source of an enzyme that efficiently degrades Ado, adenosine kinase (ADK; (Gouder et al., 2004); (Boison, 2005)). The genetic reduction of ADK was shown to prevent seizure and reduce epileptogenesis in animal models of epilepsy (Hubert et al., 2001); (Li et al., 2007); (Li et al., 2008).

SUMMARY OF THE RESULTS

This brief introduction about gliotranmsission and its role in epilepsy represents the background on which the experimental results obtained during my PhD program are built on. In the following section I am going to present these results. In the fist chapter (2.1) I am going to describe the experimental model developed in our lab and used for all the experiments described in this thesis. In cortical slices of young rodents perfused with 4-AP and low Mg^{2+}, activation of layer V-VI by local NMDA applications evolved into an ictal discharge that propagated to the entire cortex. In this way we have the unique opportunity to repetitively evoke an ictal discharge from the same restricted site, and thus to study the cellular events at the basis of ictal discharge initiation. Using this model we next investigated the role of gliotranmsission in ictal discharge generation. Chapters 2.2 and 2.3 present results about the contribution of astrocytic glutamate in setting the threshold for ictal discharge generation obtained using respectively an experimental and a computational approach. The next chapters are dedicated to ictal discharge propagation. Chapter 2.4 is a study in which we

demonstrated that Parvalbumin-expressing fast-spiking interneuron, the most abundant GABAergic interneurons population, are crucial in controlling the spatio-temporal features of the recruitment of pyramidal neurons during the propagation of ictal discharge. Starting from these results, in chapter 2.5, we show how the manipulation of this GABAergic signaling by the stimulation of an individual Parvalbumin-expressing fast-spiking interneuron can prevent ictal discharge propagation. Finally, chapter 2.6 present preliminary data about the interaction between this GABAergic signals and astrocytes.

RESULTS

FULL-LENGTH ORIGINAL RESEARCH

A new experimental model of focal seizures in the entorhinal cortex

Gabriele Losi, Mario Cammarota, Angela Chiavegato, Marta Gomez-Gonzalo, and Giorgio Carmignoto

Department of Experimental Biomedical Sciences and CNR Institute of Neuroscience, University of Padova, Padova, Italy

SUMMARY

Purpose: Despite intensive studies, our understanding of the cellular and molecular mechanisms underlying epileptogenesis remains largely unsatisfactory. Our defective knowledge derives in part from the lack of adequate experimental models of the distinct phases that characterize the epileptic event, that is, initiation, propagation, and cessation. The aim of our study is the development of a new brain slice model in which a focal seizure can be repetitively evoked at a precise and predictable site.

Methods: Epileptiform activities were studied by fast Ca^{2+} imaging coupled with simultaneous single and double patch-clamp or extracellular recordings from neurons of entorhinal cortex (EC) slices from Wistar rats and C57BL6J mice at postnatal days 13–17.

Results: In the presence of 4-aminopyridine (4-AP) and low Mg^{2+}, activation of layer V–VI neurons by local

N-methyl-D-aspartate (NMDA) applications evolved into an ictal discharge (ID) that propagated to the entire EC. NMDA-evoked IDs were similar to spontaneous events. IDs with similar pattern and duration could be repetitively triggered from the same site by successive NMDA stimulations. The high ID reproducibility is an important feature of the model that allowed testing of the effects of currently used antiepileptic drugs (AEDs) on initiation, propagation, and cessation of focal ictal events.

Conclusions: By offering the unique opportunity to repetitively evoke an ID from the same restricted site, this model represents a powerful approach to study the cellular and molecular events at the basis of initiation, propagation, and cessation of focal seizures.

KEY WORDS: Epileptogenesis, Seizures, Entorhinal cortex, Calcium, NMDA.

Temporal lobe epilepsy (TLE) is the most frequent form of partial seizures in adults and is frequently resistant (30%) to the currently used antiepileptic therapies. In TLE, seizure discharges initiate at restricted epileptogenic foci in hippocampus, entorhinal cortex (EC), and amygdala before spreading to large portions of the brain. A crucial step in the pathophysiology of this type of epilepsy is thus to understand how the ictal discharge (ID) is generated at these restricted loci (Jefferys, 1990; McNamara et al., 2006; Baulac & Pitkanen, 2008). By using pharmacological tools to generate an imbalance between excitatory and inhibitory activities, previous studies in acute brain slices (Traub & Wong, 1982; Tsau et al., 1998; Avoli et al., 2002; Pinto et al., 2005; Trevelyan et al., 2006) and the whole guinea pig brain preparation (de Curtis et al., 1998; Uva et al., 2005; Gnatkovsky et al., 2008) provided important insights into the molecular mechanisms and signaling pathways that contribute to epileptiform activities, including focal seizures. In particular, the use of the proconvulsant 4-aminopyridine (4-AP) and reduced Mg^{2+} to induce IDs in brain slices of EC and hippocampus has been largely used in the last two decades (Voskuyl & Albus, 1985; Rutecki et al., 1987; Perreault & Avoli, 1989; Avoli et al., 2002). However, the early cellular events that develop at a restricted brain site before ID generation and predispose neurons to seizures remain poorly defined. Indeed, in the currently used models, the epileptic discharge arises randomly from multiple foci (Demir et al., 1998; Tsau et al., 1998; Pitkänen et al., 2006). The inability of these models to predict both the site and the timing of ID generation hampers the study of the early cellular events that precede the initiation of a focal seizure.

We describe herein a model in EC slices from young rodents that allowed us to trigger at a precise timing repetitive IDs from the same restricted site. This model uses pressure pulses applied to an *N*-methyl-D-aspartate (NMDA)–containing glass pipette to stimulate the NMDA receptor of a limited number of layer V–VI neurons from young rat EC slices, in the presence of the proconvulsant

16

4-AP and reduced Mg^{2+}. Laser scanner microscope, fast imaging of Ca^{2+} signals from neurons and simultaneous patch-clamp recordings from pairs of neurons or field potentials, revealed that the NMDA-induced episode of local neuronal hyperactivity was regularly followed, with a few-second delay, by an ID that propagated to adjacent and distant neuronal populations. By generating a predictable ictogenic site, this model offers the opportunity to investigate the early events that at this site predispose neurons to seizures. The high reproducibility of the ID represents an additional important feature of this model that in an initial series of experiments allowed us to gain insights into the mechanisms of currently used antiepileptic drugs (AEDs).

MATERIALS AND METHODS

Brain slices and dye loading

All experimental procedures were authorized by the Italian Ministry of Health; all efforts were made to minimize the number of animal used and their suffering. Coronal cortical-hippocampal slices were obtained from Wistar rats and C57BL6J mice at postnatal days 13–17 as described previously (Fellin et al., 2004). Briefly, brain was removed and transferred to ice-cold cutting solution containing (in mM): 120 NaCl, 3.2 KCl, 1 KH_2PO_4, 26 $NaHCO_3$, 2 $MgCl_2$, 1 $CaCl_2$, 10 glucose, 2 Na-pyruvate, and 0.6 ascorbic acid at pH 7.4 (with 5% CO_2/95% O_2). Slices were obtained with a Leica Vibratome VT1000S (Mannheim, Germany) in the presence of the NMDA receptor inhibitor kynurenic acid (2 mM). Slices were recovered for 15 min at 37°C and then loaded with the Ca^{2+} sensitive dye Oregon Green 488 BAP-TA-1 acetoxymethyl ester (OGB-1 AM, 20 μm; Invitrogen, Carlsbad, CA, U.S.A.) for 60 min at 37°C. Dye loading was performed in the cutting solution containing sulfinpyrazone (200 μM), pluronic (0.12%), and kynurenic acid (1 mM). After loading, slices were recovered and kept at room temperature in the presence of 200 μM sulfinpyrazone.

Electrophysiology and Ca^{2+} imaging

Brain slices were continuously perfused in a submerged chamber (Warner Instruments, Hamden, CT, U.S.A.) with (in mM): 120 NaCl, 3.2 KCl, 1 KH_2PO_4, 26 $NaHCO_3$, 1 $MgCl_2$, 2 $CaCl_2$, 10 glucose, and 0.2 sulfinpyrazone at pH 7.4 (with O_2 95%, CO_2 5%). Whole-cell patch-clamp recordings in rat brain slices were performed using standard procedures with one or two Axopatch-200B amplifiers (Molecular Devices, Union City, CA, U.S.A.), as reported previously (Fellin et al., 2004). Typical pipette resistance was 3–4 MΩ. Data were filtered at 1 kHz and sampled at 5 kHz with a Digidata 1320 interface and pCLAMP8 software (Molecular Devices). Whole-cell intracellular pipette solution was (in mM): 140 K-gluconate, 2 $MgCl_2$, 0.3 ethylene glycol bis(2-aminoethyl ether)-N,N,N′N′-tetraacetic acid (EGTA), 4 Na_2ATP, 0.4 Na_2GTP, 10 4-(2-hydroxyethyl)-1-piperazineethanesulfonic acid (HEPES), and 10

sodium phosphocreatine at pH 7.2 with KOH and contained a low concentration (10–20 μM) of OGB1 cell impermeant (Invitrogen). All patched neurons had the typical firing of regular spiking cells. The liquid junction potential at the pipette tip was −16 mV. This value should be added to all voltages to obtain the correct value of the membrane potential in whole-cell configuration. Ca^{2+} signals were simultaneously acquired with a TCS-SP5-RS confocal microscope (Leica) equipped with a 20× objective (NA, 1.0) and a CCD camera for differential interference contrast images. Extracellular recordings were performed with an A-M System Model 1800 amplifier (>1 Hz and <1 KHz; Sequim, WA, U.S.A.) and glass pipettes filled with NaCl 0.9% (3–4 MΩ). Laser emission at 488 nm was used for stimulation of OGB-1. Time frame acquisitions from 314–491 ms (with 4–6 line averaging) were used. No background subtraction or other manipulations were applied to digitized Ca^{2+} signal images that are reported as raw data, with the exception of the difference images in Figs 1 and 3. A precise alignment of Ca^{2+} and electrophysiologic signals was achieved by using a syncronization signal produced by the confocal microscope.

Drugs

4-AP (100 μM) and kynurenic acid were obtained from Ascent Scientific (Avonmouth, Bristol, U.K.). NMDA (1 mM; Sigma-Aldrich, Milan, Italy) was pressure applied (4–10 psi for 400–600 ms) through a glass-pipette by a PDES Picospritzer (NPI, Tamm, Germany). Lamotrigine (LTG), carbamazepine (CBZ), and valproic acid (VPA) were also purchased from Sigma-Aldrich.

Data analysis

Data analysis was performed with CLAMPFIT 8, Microsoft Office 2003 (Microsoft, Seattle, WA, U.S.A.), ORIGIN 6.0 (Microcal software, Northampton, MA, U.S.A.), MATLAB (The MathWorks, Natick, MA, U.S.A.), LEICA LAS-AF (Leica), and MBF-ImageJ (NIH, Bethesda, MD, U.S.A.). The Ca^{2+} signal is reported as $\triangle F/F_0$, where $\triangle F$ is the fluorescence change and F_0 is the baseline fluorescence. Data are shown as mean ± SEM (standard error of the mean) unless otherwise stated, Student's t test was used, with p-values ≤0.05 taken as statistically significant. To evaluate the level of synchrony in large neuronal populations, MATLAB was used to calculate a mean cross-correlation function ($\overline{CC}$) in neurons (N) by averaging cross-correlations between all pairs of neurons (N_{pairs}) from the recording field, as follows:

$$\overline{CC}(\tau) = \sum_{i<j-1}^{N} \frac{CC_{ij}(\tau)}{N_{pairs}},$$

where $CC_{ij}(\tau) = \sum_{t=0}^{T} [X_i(t) - \overline{X_i(t)}][X_j(t+\tau) - \overline{X_j(t+\tau)}]$ is the cross-correlation function between the ith and jth neuron normalized so that the autocorrelations at zero lag

17
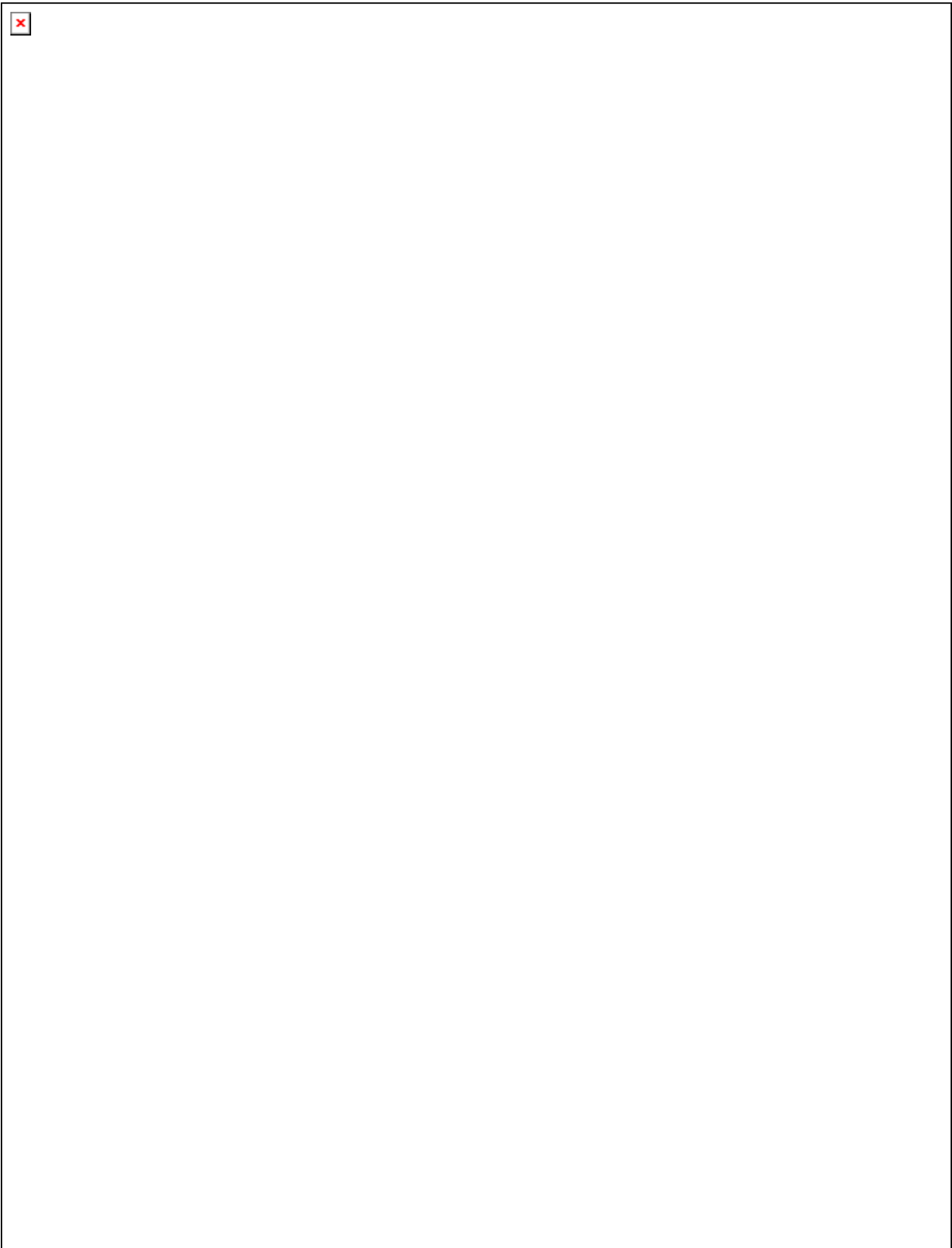
potential from a neuron located ~150 μm apart from the NMDA pipette. In the presence of 100 μM 4-AP and 0.5 mM Mg^{2+}, a single NMDA pulse (0.4–0.6 bar, 400–600 ms duration) evoked a transient Ca^{2+} elevation in the patched neuron as well as in other neurons from the region adjacent to the pipette tip, a region that we defined as "field A" (Fig. 1A, see also Movie S1). In the patched neuron, the Ca^{2+} elevation reflects a membrane depolarization with superimposed action potential (AP) firing (Fig. 1B). The transient Ca^{2+} response to NMDA is clearly illustrated by the difference images generated by subtracting the Ca^{2+} fluorescence image captured at basal conditions (t_0 or t_2) to that obtained after the NMDA stimulation (t_1; Fig. 1A). Neurons from the surrounding region, that we defined as "field B," failed to respond to the single NMDA pulse (Fig. 1A,B).

The stimulation with two NMDA pulses, applied with a 3-s interval, evoked a Ca^{2+} elevation in neurons that was initially similar (Fig. 1C, t_4–t_3), but it soon evolved into a strikingly different response (Fig. 1C, t_5–t_3). In the patched neuron, the initial transient depolarization evoked by the double NMDA pulse was followed by a more sustained depolarization and by a sequence of AP bursts that is typical of the ictal, seizure-like discharge, that is, the afterdischarges (Fig. 1D). This epileptic discharge was accompanied by a sustained Ca^{2+} increase followed by a sequence of Ca^{2+} peaks from the patched neuron as well as from other neurons in field A. In field B neurons, the initial response to NMDA was absent, but the sustained Ca^{2+} increase and the periodic Ca^{2+} elevations that we observed in field A neurons occurred simultaneously also in these neurons, suggesting that the ID involved all neurons in field A and field B (Fig. 1C,D). This sequence of events can be readily followed in the Movie S2. The difference images illustrate clearly the delayed recruitment of field B neurons into the massive Ca^{2+} rise of the ID (Fig. 1C, t_5–t_3). The activation of field B neurons was secondary to that of field A neurons, since it was totally abolished by tetrodotoxin (TTX). As shown by the cross-correlation plots, the Ca^{2+} signal of the patched neuron, both at the onset and during the afterdischarges, was highly correlated with the AP bursts of the ID (Fig. 1D, insets 1 and 2) as well as with the Ca^{2+} signal of all neurons (Fig. 1D, insets 3 and 4). These data suggest that the Ca^{2+} signal can be a useful tool to monitor the onset of epileptic discharges, the extent of the underlying synchrony, and the spread to adjacent and distant neuronal populations. These results also demonstrate that a local activation by NMDA of a group of EC neurons creates an epileptogenic focus that generated an ID, which propagated to adjacent neuronal populations.

By dual patch-clamp recordings from two, layer VI neurons, one in field A and the other in field B (Fig. 2A,B, N_1 and N_2, respectively), we next confirmed that the Ca^{2+} elevation observed in field B neurons after a double NMDA pulse reflects a propagating ID. Indeed, field A and B neurons showed a simultaneous ID onset and synchronous afterdischarges (Fig. 2B,C). These experiments (n = 9) also confirmed that NMDA stimulation failed to activate directly field B neurons (Fig. 2B). Field potential recordings through two electrodes placed in layers V–VI at different distances from the focus of ID generation showed that the NMDA-evoked ID propagated laterally in the EC with the typical pattern of a seizure-like discharge. Notably, cross-correlation analysis revealed that the Ca^{2+} signal of neurons (Fig. 2D, gray traces) and the field potential recorded from the same region were highly correlated (Fig. 2D).

Spontaneous IDs were observed occasionally in 27 of 116 slices examined. As revealed by patch-clamp and Ca^{2+} signal recordings in slices from three different animals (Fig. 3), the spontaneous (n = 12) and evoked IDs (n = 16) were indistinguishable, as they showed similar AP discharge pattern, duration (102 ± 5%; p = 0.97), and amplitude (114 ± 17%; p = 0.55).

Threshold and reproducibility of the ID evoked by local NMDA stimulations

To find the threshold for ID generation, 10–15 min after the onset of slice perfusion with 4-AP and low Mg^{2+}, we increased with small steps either the pressure or the duration of the two successive pulses applied with a 3-s interval to an NMDA-containing pipette until an ID was evoked. The application of a single NMDA pulse, even at high pressure and duration, was rarely capable of eliciting an ID, whereas a stimulation with two consecutive NMDA pulses (duration, 400–600 ms, pressure 0.4–0.6 bar), applied at a 3-s interval, effectively induced an ID. In a small percentage of slices (8 of 116), we failed to activate IDs, despite increasing the intensity and number of the NMDA pulses.

Once the parameters of the pressure pulse were established, to study the reproducibility of our stimulation a double NMDA pulse was applied repetitively with 4–5 min intervals. As shown in the examples of current- and voltage-clamp recordings from neurons of two different slices, a double NMDA pulse regularly evoked an ID and no failures were observed even after stimulations were applied repetitively to the same slice (up to 20) over a long time period (Fig. 4A,B). Quantitative analysis of 145 IDs from 24 experiments reveals a mean delay of 11 ± 1 s between the first NMDA application and the ID onset (a period that we defined as a "transition phase") and a mean ID duration of 42 ± 4 s. The ID duration from these experiments was variable (range 15–82 s; compare also the ID in Fig. 4A,B). However, within each experiment, the ID evoked by the successive NMDA stimulations had comparable durations (Fig. 4C). These results demonstrate that with the exception of a few slices in which neurons were completely refractory to ID generation, successive double NMDA pulses evoked comparable events with a high efficiency and over a long time period. IDs evoked in EC slices from mice (n = 3) were similar to those observed in rats slices, with an average

19
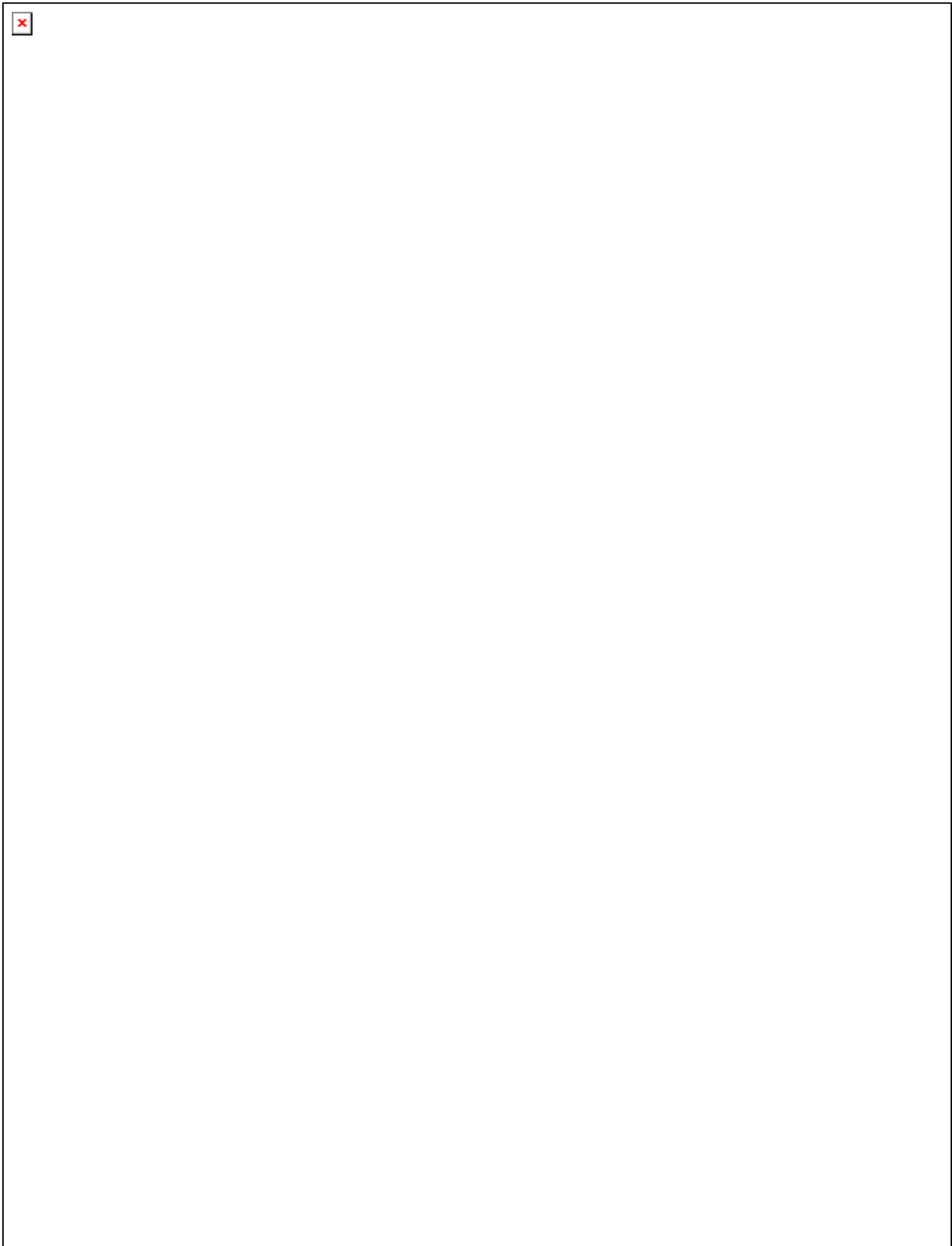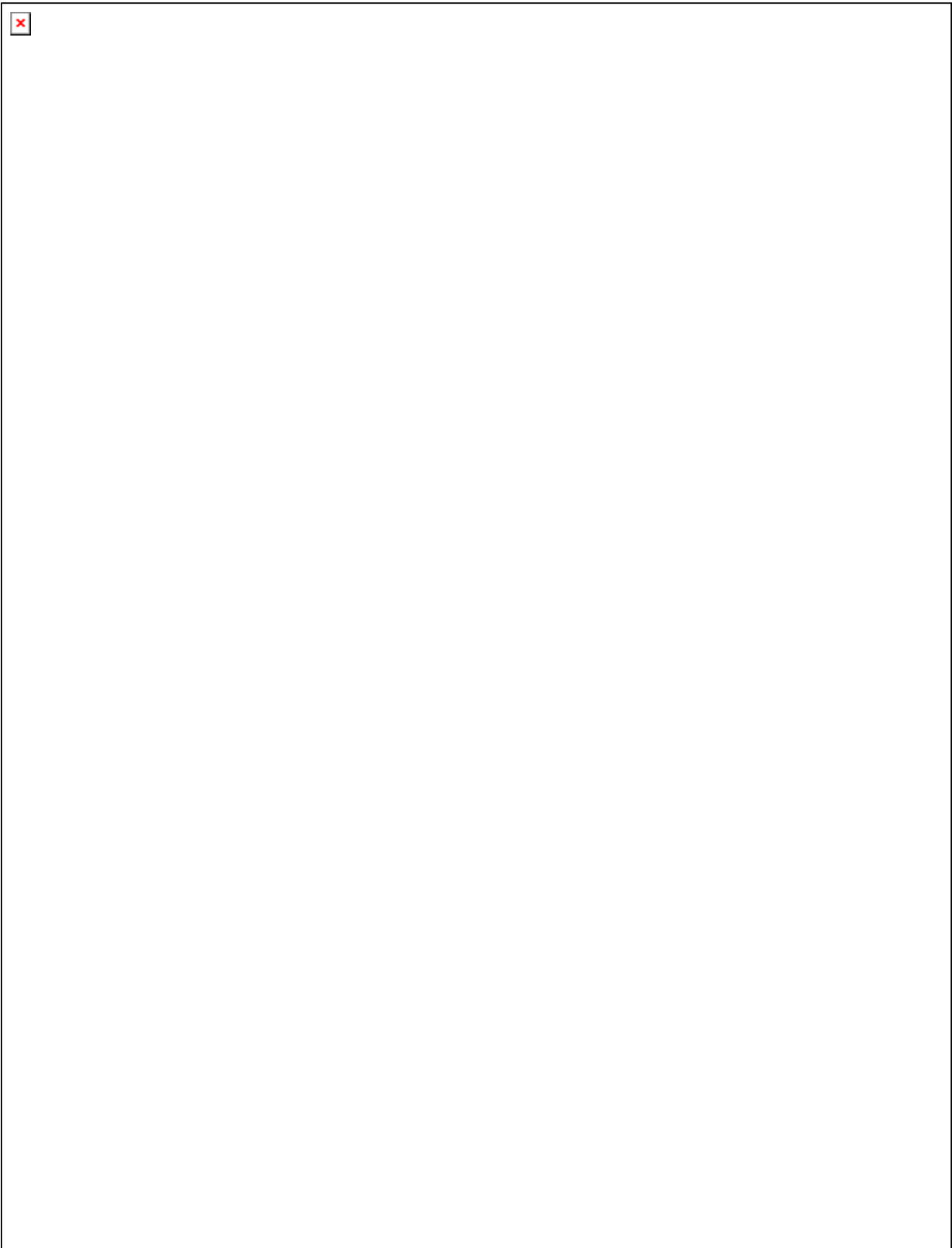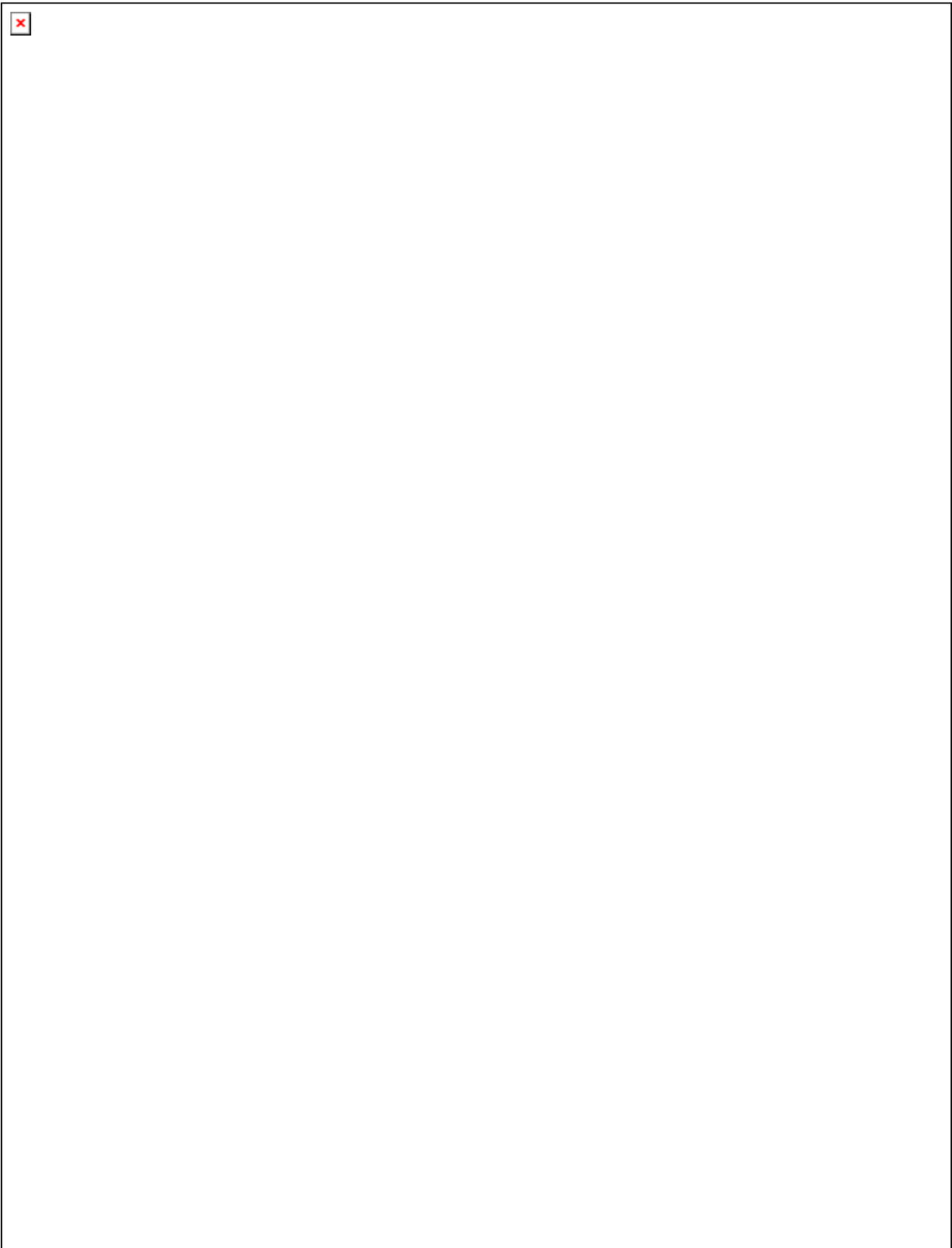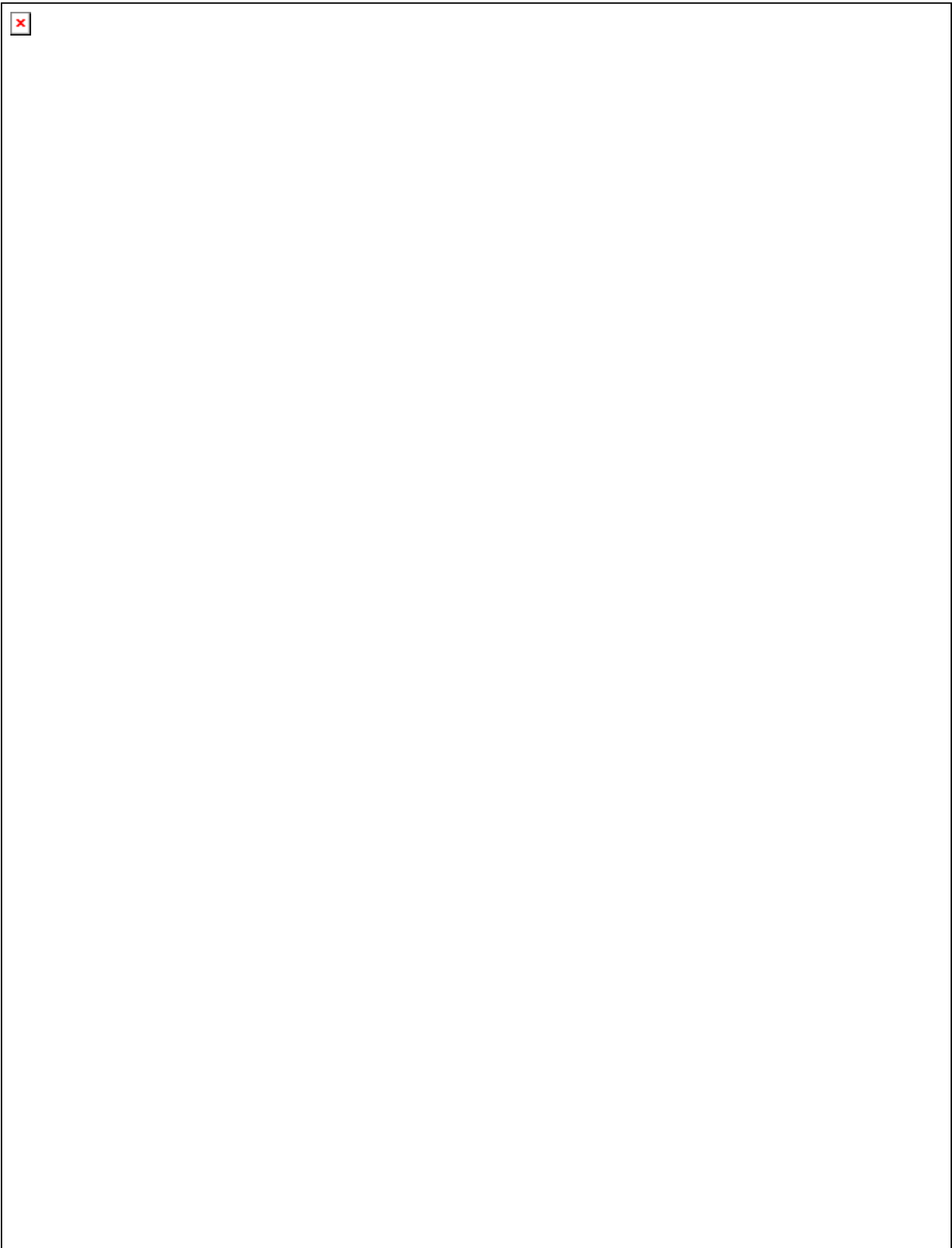
what was previously reported by Trevelyan et al. (2007). Additional, specifically designed experiments are required to clarify this issue.

Our experimental approach can be also suited to investigate the distinct role of diverse signaling pathways, such as that of inhibitory interneurons, which is highly debated in epilepsy research (Avoli et al., 1996; Trevelyan et al., 2006, 2007; Ziburkus et al., 2006; Gnatkovsky et al., 2008). Our model applied to EC slices of transgenic mice expressing the green fluorescent protein in specific subsets of interneurons, has, indeed, the potential to become a powerful approach to clarify the role of interneurons in the initiation of a focal ID.

In previous studies that used brain slices in interface chambers and 4-AP perfusion, spontaneous IDs were commonly observed to originate from EC deep layers (Avoli et al., 2002). We thus applied NMDA to layer V–VI neurons, although we obtained similar results by stimulating layer II–III neurons (data not shown). The low spontaneous epileptic activity in our model may be linked to the submerged slice chambers that we used. However, given the large number of successive IDs evoked by NMDA stimulations in our slice preparations, the generation of spontaneous IDs may have been prevented by the postictal refractory period that follows each ID. Notably, the observation that the general features of IDs evoked by local NMDA stimulations, such as the pattern of AP bursts during the tonic and the clonic phases, and ID duration, were similar to spontaneous IDs, confirms the validity of our model to study focal seizure discharges.

Effects of AEDs on focal IDs

The results that we obtained with three AEDs that are currently used in the treatment of partial and generalized seizures, that is, LTG, CBZ, and VPA, validated our model for testing the efficacy of anticonvulsants. We found that these drugs affected differently focal epileptic activities. Although both LTG and CBZ inhibited ID generation, VPA, even after 30 min of slice perfusion, failed to prevent ID generation and reduced only the synchrony of neurons during the phase of the afterdischarges. Different mechanisms in the anticonvulsant action of these compounds may account for these data. LTG and CBZ, which both prolong Na$^+$ channels inactivated state, similarly inhibited ID generation, whereas VPA, which has a different anticonvulsant mechanism, was poorly effective in our ictogenic model and affected only the late afterdischarges. VPA has been, indeed, reported to have variable effects on epileptiform activities in slice models (Loscher, 2002; Rogawski & Loscher, 2004). It will be of interest to investigate in future studies the nature of the effect of VPA on neuronal synchrony of the afterdischarges.

Limitations of our EC slice model of ictogenesis

Our experiments set the conditions for studying the generation of a focal seizure-like discharge in acute brain slice preparations. This preparation has unique advantages for investigating the cellular and molecular mechanism of epileptiform activities as well as the action of anticonvulsants. However, it also has several limitations that should be taken into account, such as the activation by slicing procedures of inflammatory signaling pathways, a reduced connectivity among neurons from the same and different regions, and the lack of blood-derived components. It will be thus important to test in future studies whether our model of ictogenesis can be replicated in chronic models of epilepsy, including genetically determined in vivo models of epilepsy, and in the close-to in vivo whole guinea pig brain preparation (de Curtis et al., 1998; Uva et al., 2005) that more closely mimics the complex feature of seizures in epileptic patients.

CONCLUSIONS

We described a simple EC slice model of ictogenesis in which an ID can be repetitively evoked at a specific site and time, and its propagation to nearby and distant neuronal populations monitored by simultaneous dual patch-clamp/field recordings and Ca^{2+} imaging. This model provides the unique opportunity to study the early events that at a restricted brain site contribute to the generation of a focal seizure-like discharge, as well as the following events that at the surrounding regions favor or restrict the ID propagation. The reliability of ID generation renders our model particularly well suited to study the anticonvulsant action of drugs. Insights into the mechanism underlying the generation of seizure provided by this new model can be thus particularly relevant for developing new therapeutic strategies for human focal epilepsies.

ACKNOWLEDGMENTS

DISCLOSURE

None of the authors has any conflict of interest to disclose. We confirm that we have read the Journal's position on issues involved in ethical publication and affirm that this report is consistent with those guidelines.

REFERENCES

Avoli M, Barbarosie M, Lucke A, Nagao T, Lopantsev V, Kohling R. (1996) Synchronous GABA-mediated potentials and epileptiform discharges in the rat limbic system in vitro. *J Neurosci* 16:3912–3924.
Avoli M, D'Antuono M, Louvel J, Kohling R, Biagini G, Pumain R, D'Arcangelo G, Tancredi V. (2002) Network and pharmacological mechanisms leading to epileptiform synchronization in the limbic system in vitro. *Prog Neurobiol* 68:167–207.
Baulac M, Pitkanen A. (2008) Research Priorities in Epilepsy for the Next Decade-A Representative View of the European Scientific Community. *Epilepsia* 50:571–583.

24

de Curtis M, Biella G, Buccellati C, Folco G. (1998) Simultaneous investigation of the neuronal and vascular compartments in the guinea pig brain isolated in vitro. *Brain Res Brain Res Protoc* 3:221–228.

Demir R, Haberly LB, Jackson MB. (1998) Voltage imaging of epileptiform activity in slices from rat piriform cortex: onset and propagation. *J Neurophysiol* 80:2727–2742.

Fellin T, Pascual O, Gobbo S, Pozzan T, Haydon PG, Carmignoto G. (2004) Neuronal synchrony mediated by astrocytic glutamate through activation of extrasynaptic NMDA receptors. *Neuron* 43:729–743.

Gnatkovsky V, Librizzi L, Trombin F, de Curtis M. (2008) Fast activity at seizure onset is mediated by inhibitory circuits in the entorhinal cortex in vitro. *Ann Neurol* 64:674–686.

Gomez-Gonzalo M, Zonta M, Losi G, Uva L, Brondi M, DeCurtis M, Ratto G, Carmignoto G (2008) *A neuron astrocyte loop contributes to epileptiform activity.* 147.23 Society for Neuroscience 38th Meeting Abstract.

Jefferys JG. (1990) Basic mechanisms of focal epilepsies. *Exp Physiol* 75:127–162.

Loscher W. (2002) Basic pharmacology of valproate: a review after 35 years of clinical use for the treatment of epilepsy. *CNS Drugs* 16:669–694.

McNamara JO, Huang YZ, Leonard AS. (2006) Molecular signaling mechanisms underlying epileptogenesis. *Sci STKE* 2006:re12.

Perreault P, Avoli M. (1989) Effects of low concentrations of 4-aminopyridine on CA1 pyramidal cells of the hippocampus. *J Neurophysiol* 61:953–970.

Pinto DJ, Patrick SL, Huang WC, Connors BW. (2005) Initiation, propagation, and termination of epileptiform activity in rodent neocortex in vitro involve distinct mechanisms. *J Neurosci* 25:8131–8140.

Pitkänen A, Schwartzkroin PA, Moshé SL. (2006) *Models of seizures and epilepsy*. Elsevier, Amsterdam.

Rogawski MA, Loscher W. (2004) The neurobiology of antiepileptic drugs. *Nat Rev Neurosci* 5:553–564.

Rutecki PA, Lebeda FJ, Johnston D. (1987) 4-Aminopyridine produces epileptiform activity in hippocampus and enhances synaptic excitation and inhibition. *J Neurophysiol* 57:1911–1924.

Traub RD, Wong RK. (1982) Cellular mechanism of neuronal synchronization in epilepsy. *Science* 216:745–747.

Trevelyan AJ, Sussillo D, Watson BO, Yuste R. (2006) Modular propagation of epileptiform activity: evidence for an inhibitory veto in neocortex. *J Neurosci* 26:12447–12455.

Trevelyan AJ, Sussillo D, Yuste R. (2007) Feedforward inhibition contributes to the control of epileptiform propagation speed. *J Neurosci* 27:3383–3387.

Tsau Y, Guan L, Wu JY. (1998) Initiation of spontaneous epileptiform activity in the neocortical slice. *J Neurophysiol* 80:978–982.

Uva L, Librizzi L, Wendling F, de Curtis M. (2005) Propagation dynamics of epileptiform activity acutely induced by bicuculline in the hippocampal-parahippocampal region of the isolated Guinea pig brain. *Epilepsia* 46:1914–1925.

Voskuyl RA, Albus H. (1985) Spontaneous epileptiform discharges in hippocampal slices induced by 4-aminopyridine. *Brain Res* 342:54–66.

Ziburkus J, Cressman JR, Barreto E, Schiff SJ. (2006) Interneuron and pyramidal cell interplay during in vitro seizure-like events. *J Neurophysiol* 95:3948–3954.

SUPPORTING INFORMATION

Additional Supporting Information may be found in the online version of this article:

Video clip S1. A single NMDA pulse evokes in EC neurons only a transient Ca^{2+} response.

Video clip S2. A double NMDA pulse evokes an ID.

Please note: Wiley-Blackwell is not responsible for the content or functionality of any supporting information supplied by the authors. Any queries (other than missing material) should be directed to the corresponding author for the article.

An Excitatory Loop with Astrocytes Contributes to Drive Neurons to Seizure Threshold

Marta Gómez-Gonzalo[1,2⑨], Gabriele Losi[1,2⑨], Angela Chiavegato[1,2], Micaela Zonta[1,2], Mario Cammarota[1,2], Marco Brondi[3,4], Francesco Vetri[4], Laura Uva[5], Tullio Pozzan[1,2,6], Marco de Curtis[5], Gian Michele Ratto[3,4], Giorgio Carmignoto[1,2]*

1 Institute of Neuroscience – Consiglio Nazionale delle Ricerche (CNR), University of Padova, Padova, Italy, 2 Department of Experimental Biomedical Sciences, University of Padova, Padova, Italy, 3 National Enterprise for nanoScience and nanoTechnology (NEST), Instituto Nanoscienze CNR, Scuola Normale Superiore, Pisa, Italy, 4 Institute of Neuroscience – CNR, Pisa, Italy, 5 Fondazione Istituto Neurologico Carlo Besta, Milano, Italy, 6 Venetian Institute of Molecular Medicine, Padova, Italy

Abstract

Seizures in focal epilepsies are sustained by a highly synchronous neuronal discharge that arises at restricted brain sites and subsequently spreads to large portions of the brain. Despite intense experimental research in this field, the earlier cellular events that initiate and sustain a focal seizure are still not well defined. Their identification is central to understand the pathophysiology of focal epilepsies and to develop new pharmacological therapies for drug-resistant forms of epilepsy. The prominent involvement of astrocytes in ictogenesis was recently proposed. We test here whether a cooperation between astrocytes and neurons is a prerequisite to support ictal (seizure-like) and interictal epileptiform events. Simultaneous patch-clamp recording and Ca^{2+} imaging techniques were performed in a new in vitro model of focal seizures induced by local applications of N-methyl-D-aspartic acid (NMDA) in rat entorhinal cortex slices. We found that a Ca^{2+} elevation in astrocytes correlates with both the initial development and the maintenance of a focal, seizure-like discharge. A delayed astrocyte activation during ictal discharges was also observed in other models (including the whole in vitro isolated guinea pig brain) in which the site of generation of seizure activity cannot be precisely monitored. In contrast, interictal discharges were not associated with Ca^{2+} changes in astrocytes. Selective inhibition or stimulation of astrocyte Ca^{2+} signalling blocked or enhanced, respectively, ictal discharges, but did not affect interictal discharge generation. Our data reveal that neurons engage astrocytes in a recurrent excitatory loop (possibly involving gliotransmission) that promotes seizure ignition and sustains the ictal discharge. This neuron–astrocyte interaction may represent a novel target to develop effective therapeutic strategies to control seizures.

Competing Interests: The authors have declared that no competing interests exist.

Abbreviations: AP, action potential; EC, entorhinal cortex; 2P-LSM, two-photon laser scanning microscopy; SE, status epilepticus; SIC, slow inward current

* E-mail: giorgio.carmignoto@bio.unipd.it

⑨ These authors contributed equally to this work.

Introduction

Focal epilepsies are characterized by a condition of neuronal hyperexcitability that is restricted to the epileptogenic region. Focal seizures originate at this region and secondarily spread to distant cortical areas [1 5]. Several factors, from ion channel mutations to brain injury, may cause neuronal hyperexcitability changes that sustain an epileptic condition [6]. Yet, the earlier cellular events that initiate a seizure in the first place are still unclear. The understanding of ictogenesis is thus central to the pathophysiology of focal epilepsies and is a requirement to develop new pharmacological therapies for drug-resistant focal epilepsies [7].

In the present study, we specifically address the hypothesis that the activation of a loop between neurons and astrocytes is an early event that contributes to focal seizure initiation. This hypothesis stems from a series of recent studies that reappraised the role of neurons in epileptogenesis and hinted at a possible, direct contribution of astrocytes to the generation of an epileptic discharge. The first clue was the observation that the release of glutamate from astrocytes, elicited by Ca^{2+} oscillations, promotes local synchronous activities in hippocampal neurons by acting on extrasynaptic N-methyl-D-aspartic acid (NMDA) receptors [8]. Studies performed both on brain slices and in vivo showed that during epileptiform activity, the frequency of Ca^{2+} oscillations in astrocytes is significantly increased [9,10], and it is reduced by anticonvulsant drugs [9]. Moreover, the expression of metabotropic glutamate receptors (mGluRs, mediators of Ca^{2+} oscillations in these cells) in hippocampal astrocytes from animal models of temporal lobe epilepsy was found to be increased [11,12]. These observations suggest that the excessive neuronal synchronization that characterizes the epileptic discharge might be sustained, at least in part, by an astrocyte hyperactivity. In support of an astrocyte role in epileptiform activities, it has been proposed that

26

Author Summary

In focal epilepsy, seizures are generated by a localized, synchronous neuronal electrical discharge that may spread to large portions of the brain. Despite intense experimental research in this field, a key question relevant to the human epilepsy condition remains completely unanswered: what are the cellular events that lead to the onset of a seizure in the first place? In various in vitro models of seizures using rodent brain slices, we simultaneously recorded neuronal firing and Ca^{2+} signals both from neurons and from astrocytes, the principal population of glial cells in the brain. We found that activation of astrocytes by neuronal activity and signalling from astrocytes back to neurons contribute to the initiation of a focal seizure. This reciprocal excitatory loop between neurons and astrocytes represents a new mechanism in the pathophysiology of epilepsy that should be considered by those aiming to develop more effective therapies for epilepsies that are not controlled by currently available treatments.

the interictal events recorded between seizures might be in some conditions tetrodotoxin (TTX)-resistant and mediated by glutamate release from astrocytes [9]. These findings fuelled a controversial debate on the role of astrocytes in focal epileptogenesis and in the generation of epileptiform discharges [13 15].

In the present study, we used different models of epileptic seizures, including a new model of focal seizures, to define the role of astrocytes in the generation of epileptiform activities. We performed simultaneous Ca^{2+} imaging and electrophysiological recordings of epileptic discharges in brain slices and in isolated intact guinea pig brains, focusing on the entorhinal cortex. This experimental approach allowed us to define the timing of astrocyte Ca^{2+} excitability in relation to interictal and ictal discharges. By using different pharmacological tools to affect selectively the Ca^{2+} signal in astrocytes, we also investigated a possible causative role of astrocyte activation in the generation of these epileptic discharges.

We demonstrate here that a recurrent excitatory loop between neurons and astrocytes involving Ca^{2+} elevations in a large number of glial cells is an early event that contributes to the initiation of a focal seizure-like discharge.

Results

A Large Number of Astrocytes Are Activated by Ictal, but Not Interictal, Discharges

Picrotoxin/zero-Mg^{2+} entorhinal cortex slice model. In a first series of experiments, we investigated neuron and astrocyte activities in entorhinal cortex (EC) slices during interictal and ictal discharges induced by the gamma-aminobutyric acid $(GABA)_A$ receptor inhibitor picrotoxin applied in Mg^{2+}-free solution. Slice incubation with the Ca^{2+} dye Oregon Green BAPTA-1 acetoxymethyl ester (OGB1-AM) allowed us to monitor Ca^{2+} signals from both neurons and astrocytes, identified according to morphological and functional criteria [16 18] (see also Materials and Methods). Patch-clamp recordings coupled to Ca^{2+} imaging revealed a clear correlation between action potential (AP) bursts and Ca^{2+} changes from the patched neuron during both the brief interictal and the prolonged ictal discharges (Figure 1A and 1B). Ca^{2+} elevations with similar onset and time course were also observed in unpatched neurons simultaneously monitored in the same field (Figure 1A, and other neurons in 1B). These observations demonstrate that the neuronal Ca^{2+} signal reflects faithfully the AP discharge during ictal and interictal discharges

and represents a useful tool to i) detect epileptic discharges; ii) mark ictal discharge initiation; and iii) evaluate the extension of underlying neuronal synchronies.

A Ca^{2+} rise was distinctly activated by ictal discharges in most astrocytes, whereas interictal discharges failed to evoke a similar astrocyte activation (Figure 1A and 1B; see also Figure 1E and Video S1), and it increased only the frequency of independent Ca^{2+} oscillations in single astrocytes (Figure S1). In a total of 15 experiments, $73.5\pm4.0\%$ of the astrocytes present in the recording field ($n=227$; Figure 1E) were activated by the ictal discharge, and in most of these (57.7%) a Ca^{2+} elevation occurred 1.8 ± 0.2 s after the ictal discharge onset. A similar distinct activation of astrocytes during the ictal event evoked by picrotoxin/zero-Mg^{2+} was observed also in CA3 region from hippocampal slices of both rats (Figure 1E) and pGFAP-EGFP transgenic mice in which astrocytes are labelled by the enhanced green fluorescent protein (EGFP) under the control of the human glial fibrillary acidic protein (GFAP) promoter (unpublished data).

Bicuculline-perfused, whole guinea pig brain model. To validate in an intact brain the findings obtained in EC slices, we used the in vitro isolated whole brain from young adult guinea pigs [19] since imaging of the EC is impracticable in vivo. In this preparation, networks responsible for focal ictogenesis in the EC hippocampus have been analyzed in detail [20,21]. We simultaneously recorded the extracellular field potential and Ca^{2+} signals by two-photon laser scanning microscopy (2P-LSM) during epileptiform activities induced by arterial application of the $GABA_A$ receptor antagonist, bicuculline methiodide. Ca^{2+} signals in neuropile were tightly correlated with the changes in the field potential observed during the seizure discharge and increased in parallel with the appearance of a fast activity at 20 30 Hz that accompanied the onset of the ictal discharge [21,22] (Figure 1D). As in brain slices, in this close to in vivo condition, seizure-like events regularly evoked Ca^{2+} elevations in astrocytes (Figure 1C and 1D), whereas interictal events failed to activate astrocyte responses (Figure S1). A bar graph summarizes the different response of astrocytes to interictal and ictal discharges in the different models (Figure 1E).

Astrocyte Activation by the Ictal Discharge Involves Glutamate and ATP

The activation of astrocytes by neuronal activity is mainly mediated by synaptic neurotransmitter release, such as glutamate [16,23] and ATP [24]. We next asked whether these neuronal signals mediate Ca^{2+} elevations triggered in astrocytes by the ictal discharge. We found that the activation of astrocytes by the ictal discharge was significantly reduced by slice perfusion with either the antagonist of mGlu receptors 2-methyl-6-(phenylethynyl)-pyridine (MPEP), or the antagonist of purinergic (P2) receptors pyridoxal phosphate-6-azophenyl-2′,4′-disulfonic acid (PPADS, Figure 2A). MPEP/PPADS co-perfusion abolished ictal discharges, thus hampering the possibility to clarify whether glutamate and ATP can entirely account for astrocyte activation by the ictal event.

We also found that after slice perfusion with either MPEP or PPADS, the duration and frequency of ictal episodes in neurons were significantly reduced with respect to controls (Figure 2B and 2C), whereas interictal discharges were either unaffected (PPADS and MPEP/PPADS) or increased in frequency (MPEP; Figure 2D). These results clearly show that Ca^{2+} elevations mediated by mGlu and P2 receptors in astrocytes (and neurons) do not have a role in the generation of interictal discharges. Given that MPEP and PPADS block receptors in both neurons and astrocytes, these

27
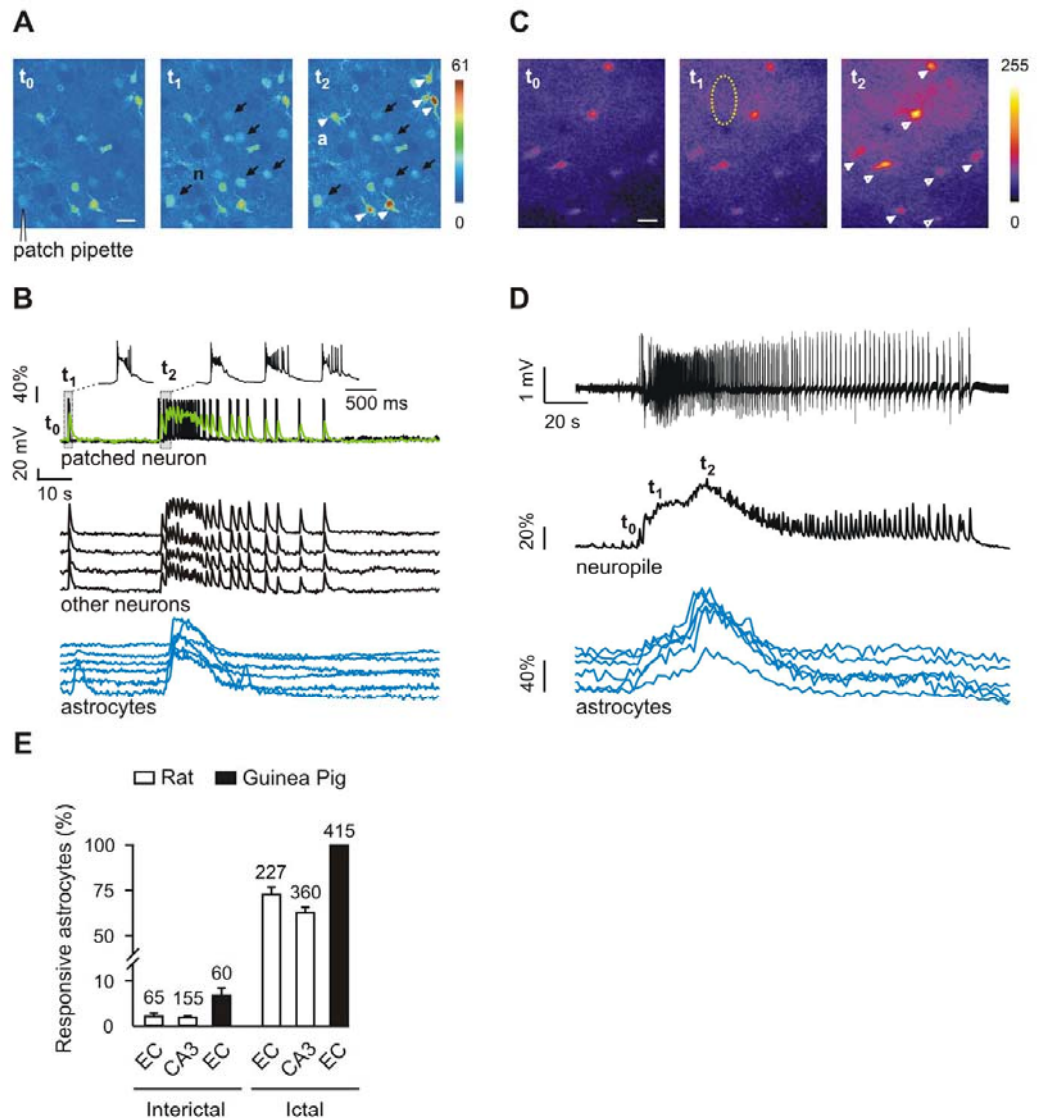
Figure 1. The large majority of astrocytes respond with a Ca^{2+} elevation to ictal, but not interictal, discharges. (A) Ca^{2+} changes, with respect to the basal level (t_0), in neurons (n, black arrows) and astrocytes (a, white arrowheads) during an interictal (t_1) or an ictal (t_2) event after EC slice perfusion with picrotoxin/zero-Mg^{2+}. Scale bar represents 20 μm. (B) AP bursts and Ca^{2+} change (green trace) from the patched neuron, and Ca^{2+} changes from other neurons and from astrocytes indicated in (A). Note the large Ca^{2+} rise evoked in astrocytes by ictal (t_2) and not by interictal (t_1) events. (C) 2P-LSM Ca^{2+} imaging in guinea pig EC before (t_0) and during the development (t_1 and t_2) of the ictal discharge induced by arterial perfusion with bicuculline. Scale bar represents 20 μm. (D) Field potential and Ca^{2+} signal changes from neuropile (dashed circle in [C]) and astrocytes (arrowheads in [C]) during the ictal discharge. (E) Mean percentage of interictal- and ictal-activated astrocytes. Numbers over each bar indicate the total number of astrocytes examined. The interictal and ictal events analyzed were, respectively, 130 and 21 in rat CA3, 69 and 15 in rat EC, 347 and 31 in guinea pig EC. Error bars in this and other figures indicate SEM.
doi:10.1371/journal.pbio.1000352.g001

28
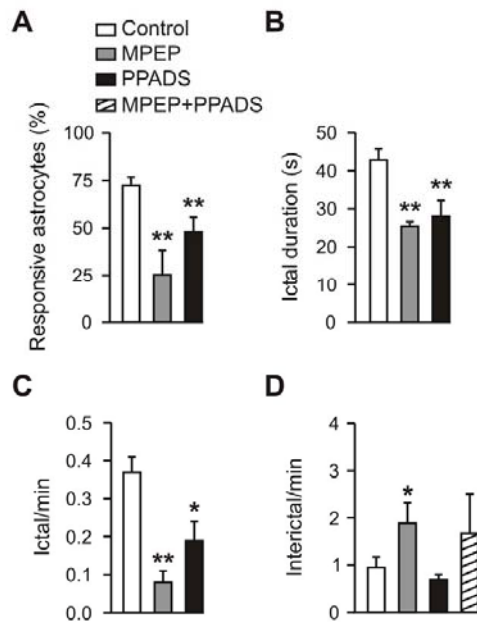
Figure 2. Astrocyte Ca^{2+} signal inhibition does not affect interictal discharges. (A–D) Mean percentage of astrocytes activated by the ictal discharges (A), mean duration (B) and frequency (C) of the ictal discharge, and mean frequency of interictal discharges (D) under different experimental conditions in EC slice preparations. Controls ($n = 16$), MPEP ($n = 7$), PPADS ($n = 9$), and MPEP+PPADS ($n = 3$). A single asterisk (*) indicates $p < 0.05$; double asterisks (**), $p < 0.01$.
doi:10.1371/journal.pbio.1000352.g002

results also suggest that Ca^{2+} signals activated by these receptors, on one or both cells, may have a role in ictal discharge generation.

Selective Activation of Astrocytes Favours Ictal Discharge Generation

We next asked whether astrocyte Ca^{2+} elevations may have a specific role in ictal discharge generation. To investigate this hypothesis, an agonist able to selectively trigger a Ca^{2+} increase in astrocytes should be used. The peptide TFLLR, a PAR-1 thrombin receptor agonist, is preferentially expressed in astrocytes and is known to activate glutamate release in astrocytes [25,26]. We found that PAR-1 immunoreactivity in the EC was largely associated with the soma and the processes of GFAP-positive astrocytes (Figure 3A). Noteworthy, GFAP-negative PAR-1 puncta appeared in continuity with distal portions of astrocyte processes, where GFAP is barely expressed [27] (Figure 3B). Following TFLLR (10 μM) bath perfusion in the presence of both TTX and D-2-amino-5-phosphonopentanoate (D-AP5), which blocks NMDAR-mediated astrocyte-to-neuron signalling [8,28], we could not detect any Ca^{2+} change in EC neurons, whereas large Ca^{2+} elevations were observed in astrocytes (Figure 3C).

We next asked whether PAR-1 receptor activation could stimulate the release of glutamate from EC astrocytes, as previously reported for hippocampal astrocytes [25,26]. We found that Ca^{2+} elevations triggered in EC astrocytes by short pressure

pulses applied to a TFLLR-containing pipette (1 mM) were followed by slow inward currents (SICs) in adjacent patched neurons (Figure 3D). Most of the SICs recorded in six of 12 neurons occurred within 10 s (mean delay ± SEM, 1.3±0.3 s) after the TFLLR-induced Ca^{2+} elevations in astrocytes (Figure 3D and 3E). Unlike fast spontaneous synaptic currents (asterisks in Figure 3D), SICs have typical slow kinetics (rise time, 83.0±36 ms, decay time, 451±171 ms; $n = 13$), are insensitive to TTX, and are sensitive to the NMDAR blocker D-AP5 (Figure 3E), as demonstrated in neurons from other brain regions [8,28–30].

In the picrotoxin/zero-Mg^{2+} entorhinal cortex slice model, we then investigated whether selective astrocyte activation enhanced ictal discharge generation. We found that Ca^{2+} elevations triggered in astrocytes by local TFLLR applications were sufficient to shift neurons towards the ictal discharge threshold (Figure 3F; Video S2). To demonstrate the causal link between the ictal discharge and the immediately preceding TFLLR-induced Ca^{2+} increase in astrocytes, we simulated the ictal occurrence by a Monte Carlo procedure. Results from this analysis revealed that in six experiments in which 30 TFLLR applications were performed, 10 of the 15 observed ictal events were correlated at the 0.05 confidence level with a preceding astrocyte Ca^{2+} increase (Figure S2).

These results suggest that when the level of basal excitability and the predisposition of neurons to generate epileptiform discharges is high, as in the picrotoxin/zero-Mg^{2+} model, activation of the NMDAR by astrocytic glutamate could trigger neuronal hyperactivity that is sufficient to generate an ictal discharge. Compelling, although indirect, support for this hypothesis derived from the observation that a short pressure-pulse application of NMDA via an NMDA-containing pipette could also evoke an ictal discharge (Figure S3).

In the Presence of 4-AP, a Local Application of NMDA Evokes a Focal Ictal Discharge

To further investigate the possible role of astrocytes in seizure initiation, we developed a model of focal seizures alternative to the picrotoxin/zero-Mg^{2+} model. In this latter model, indeed, epileptic activities arise spontaneously and at unpredictable foci [31,32], and therefore the cellular mechanism of seizure initiation cannot be analyzed accurately.

In our new model, ictal discharges are reproducibly generated at discrete sites of the EC by focal NMDA applications. Figure 4A reports schematically the positions of an NMDA-containing pipette and an OGB1-containing patch pipette in layer V of the EC. A confocal image of this region under basal conditions (t_0) is also presented. Focal episodes of neuronal hyperactivity are induced in the presence of 100 μM 4-aminopyridine (4-AP) and 0.5 mM Mg^{2+} by short pressure-pulse applications of NMDA via the NMDA-containing pipette. The effect of the NMDA pulse ejection was monitored by simultaneously recording Ca^{2+} signals from neurons and the AP firing from one of the neurons close to the NMDA pipette. Notably, in the submerged chamber experiment used in our study, no spontaneous ictal discharges were observed during 4-AP slice perfusion, whereas under different experimental conditions, such as in interface chamber experiments, epileptiform activities arise spontaneously [2]. As illustrated by the fluorescence change, a single NMDA pulse stimulated a transient Ca^{2+} increase in a limited number of layer V-VI neurons from the region close to the pipette tip, that we termed the *field A* (t_1, Figure 4B; Video S3). This local response is clearly illustrated by the difference image generated by subtracting the fluorescence image captured at basal conditions to that obtained after the NMDA stimulation ($t_1 - t_0$, Figure 4B).

29
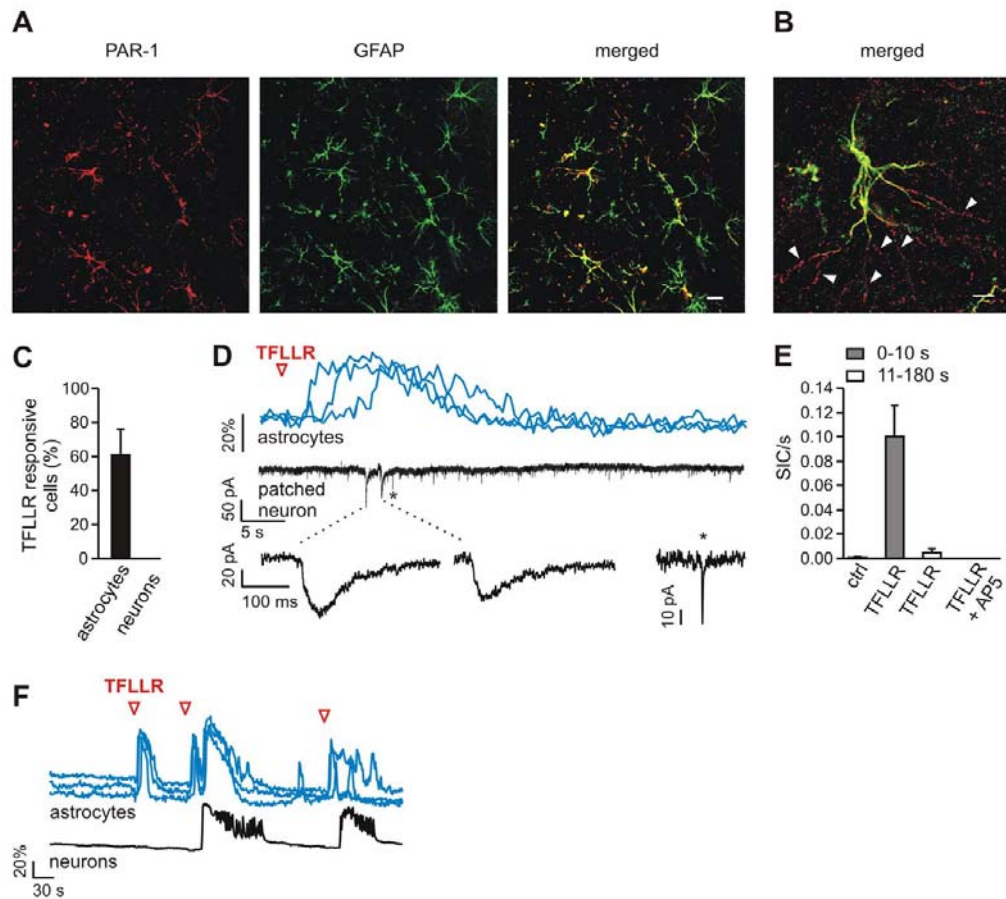
Figure 3. PAR-1 receptor activation in astrocytes favours ictal discharge generation. (A) Images showing PAR-1 (red) and GFAP (green) immunoreactivity and the merged image in EC layers V-VI; 86.7% of GFAP-positive astrocytes were PAR-1 immunopositive. Scale bar represents 20 µm. (B) High magnification of a confocal image showing a merged image of PAR-1 and GFAP immunoreactivity from EC layer V-VI. Note the continuity of PAR-1 punctate signals that are presumably associated with GFAP-negative distal portions of GFAP-positive astrocyte processes (white arrowheads). Scale bar represents 5 µm. (C) Bar graph showing that bath perfusion with TFLLR (10 µM) in the presence of D-AP5 and TTX failed to trigger any Ca^{2+} response in 70 neurons analyzed from three different experiments. (D) Ca^{2+} elevations in astrocytes (top traces) and whole-cell recording of an adjacent neuron (lower trace) after a single TFLLR pulse (indicated by an open red arrowhead) applied in the presence of TTX. The Ca^{2+} elevation in astrocytes is followed by the activation of SICs in the nearby patched neuron. Note the slower kinetics of SICs (insets) with respect to those of a spontaneously occurring fast synaptic miniature event (*). (E) Bar graph reporting the frequency of SICs before and after TFLLR pulses. The large majority of SICs (six of 11) occurred within 10 s of the TFLLR-evoked Ca^{2+} increase in astrocytes. No SICs where observed after TFLLR induced Ca^{2+} elevations in astrocytes in the presence of D-AP5. (F) In the picrotoxin/zero-Mg^{2+} model, astrocyte stimulation by TFLLR (open red arrowhead) was sufficient to evoke an ictal discharge.
doi:10.1371/journal.pbio.1000352.g003

Simultaneous patch-clamp recording and Ca^{2+} imaging revealed that the NMDA stimulus leads to AP burst firing in the patched neuron coupled with a Ca^{2+} elevation in this and the other neurons from field A, but it failed to activate neurons of the surrounding region, which we termed *field B* (Figure $4D_1$).

Two-pulse NMDA stimulation with a 3-s interval evoked a stronger activation of neurons and a transient Ca^{2+} elevation in some of the previously unresponsive neurons from the surrounding field B (t_2 and $t_2 - t_0$, Figure 4C). The response to the double NMDA pulse evolved into a sustained plateau with superimposed Ca^{2+} spikes correlated with AP bursts typical of an ictal discharge, i.e., the cellular equivalent of a seizure [2] (Figure $4D_2$, see also Figure 4C, t_3). The ictal discharge was characterized by Ca^{2+} spikes from unpatched neurons in both field A and field B, highly synchronized with the AP bursts (Figure $4D_2$; Video S4). The recruitment of neurons in field B that underlines the spreading to this region of the ictal discharge is also clearly illustrated by the difference image $t_3 - t_0$ (Figure 4C). The time window between

30

31
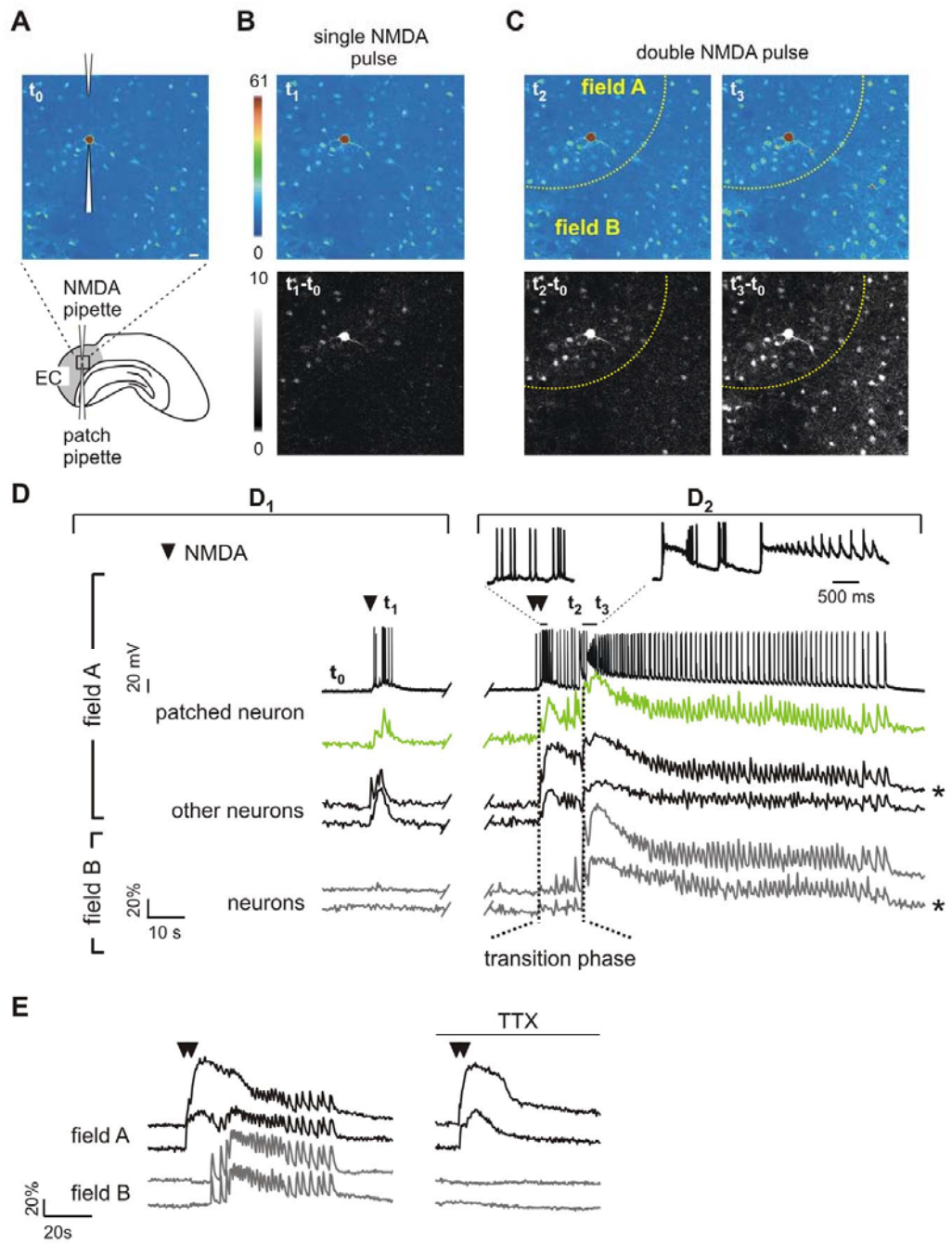
Figure 4. Local neuronal activation evokes ictal discharges. (A) Drawing and pseudocolour image of the Ca^{2+} signal at basal conditions (t_0) of an EC slice showing the NMDA-containing pipette and the patch pipette on a layer V neuron. Scale bar represents 20 μm. (B) Pseudocolour (t_1) and difference image ($t_1 - t_0$) of local Ca^{2+} changes after a single NMDA pulse. (C) Pseudocolour and difference images of the Ca^{2+} response triggered by a double NMDA pulse. t_2 and $t_2 - t_0$ illustrate the initial Ca^{2+} elevation in neurons from the region close to the NMDA pipette (field A, dashed yellow line) and in some neurons from the surrounding field B. t_3 and $t_3 - t_0$ illustrate the Ca^{2+} change in all neurons reflecting the ictal discharge. (D) (D_1) NMDA-induced AP firing from the patched neuron and Ca^{2+} changes from this (green trace) and other neurons from field A and field B after a single NMDA pulse (indicated by a black arrowhead). (D_2) AP bursts from the patched neuron (see also insets) and Ca^{2+} changes from this and other neurons from field A and field B during the ictal discharge induced by a double NMDA pulse (black arrowheads). Vertical dashed lines mark the transition phase from the onset of the direct response (left line) to the emergence of the ictal discharge in field B neurons (right line). t_{0-3} mark the timing for the images shown in (A–C). *Traces are reported also in Figure 5. (E) TTX blocked the ictal discharge in both field A and B neurons, but not the direct response of field A neurons to a double NMDA pulse (black arrowheads).
doi:10.1371/journal.pbio.1000352.g004

the double NMDA pulse and the Ca^{2+} elevation that occurs synchronously in both field A and B neurons represents a transition phase during which the ictal discharge develops in field A. In the presence of TTX, the ictal discharge in both field A and B neurons was abolished, whereas the initial response of field A neurons was unaffected (Figure 4E). The size of the cortical region occupied by neurons that respond directly with a transient Ca^{2+} rise to a double NMDA pulse applied in the presence of TTX was 369 ± 17 μm. Notably, the number of neurons in this response (56.5 ± 7.2) is underestimated since it comprises only neurons activated by NMDA in a single focal plane. These results demonstrated that i) AP-mediated events secondary to the initial activation of field A neurons are crucial for ictal discharge maturation; and ii) the activation of neurons from field B and the generation of the ictal discharge was not due to a delayed diffusion of NMDA. Paired recordings from two pyramidal neurons (one in field A and the other in field B) confirmed that similar ictal discharges were regularly evoked in field A and B by successive double NMDA pulses (Figure S4).

According to results obtained from 14 experiments, no failures were observed in a total of 101 double NMDA pulse stimulations, and the mean duration of the ictal discharge repetitively evoked by these stimulations was reproducible over long time periods (up to 60 min, Figure S4). By applying successive double NMDA pulses in the presence of TTX, no NMDA-mediated Ca^{2+} elevations were detected in field B neurons, whereas the number of field A neurons activated directly by NMDA and the amplitude of their Ca^{2+} response were found to be unchanged over the same time period (Figure S4).

Ictal discharges could be evoked also by two single NMDA pulses applied at two different sites, either simultaneously or in succession. Intervals of 3 or 5 s were successful, but not an interval of 10 s. To be effective, the two pipette tips should be positioned close enough to allow a large spatial overlapping of the two pulses. Only in this overlapping region were neurons strongly activated by the two NMDA pulses. Notably, if the distance between the two pipette tips was 172 ± 30.2 μm ($n = 5$) (a value similar to the mean radius of the field A directly activated by double NMDA pulses), the two single NMDA pulses regularly evoked an ictal discharge. If the distance of the two pipette tips was 220 ± 38.5 μm, no ictal discharges could be evoked.

Altogether, these data show that an episode of activity evoked in a group of neurons by local NMDA applications creates an initiation site for a seizure-like discharge that secondarily involves adjacent neuronal populations. They also demonstrate that our model is highly reliable since comparable ictal discharges can be evoked by repetitive stimulations applied to the same restricted site. Notably, in contrast to the picrotoxin/ zero-Mg^{2+} model, in the 4-AP model, single NMDA pulses failed to trigger focal ictal discharges, suggesting different thresholds for seizure generation in these two models (see Discussion).

The Development of the Ictal Discharge Is Accompanied by Astrocyte Activation

We next investigated astrocyte activities during the development of focal ictal discharges. We observed that shortly after the initial neuronal response to a double NMDA pulse, a large Ca^{2+} elevation occurred almost simultaneously in the large majority of field A astrocytes (Figure 5A, red traces; Video S4). Similar Ca^{2+} elevations in these astrocytes were never observed during the neuronal response to a single NMDA pulse. In 13 experiments, a mean of 17.4 ± 3.5 out of 20 ± 3.1 responsive astrocytes in field A displayed an early Ca^{2+} elevation during the transition phase. As a mean, astrocyte activation in field A occurred 4.8 ± 1.1 s before field B neurons were recruited into the ictal discharge. Most of the astrocytes in field B were activated later, i.e., after the invasion of the ictal discharge into this region (Figure 5A, blue traces; Video S4). High-magnification images in Figure 5B illustrate "early" and "late" Ca^{2+} changes of astrocytes from field A and B, respectively. The mean percentage of astrocytes from field A and B displaying "early" and "late" responses is reported in Figure 5C. Notably, when the ictal discharge was evoked by two single NMDA pulses applied at two distinct sites (Figure 5D), most astrocytes from both the field of spatial overlapping of the two pulses and the immediately surrounding regions (fields A1 and A2) displayed a similar early Ca^{2+} elevation ($85.6 \pm 5.4\%$), whereas most astrocytes from the surrounding regions (the fields B) showed a late activation ($71.6 \pm 5.4\%$). Noteworthy is that astrocytes failed to be similarly activated by each single NMDA pulse alone (Figure 5D).

We next asked whether the initial Ca^{2+} elevation in astrocytes (and neurons) from field A spread to other astrocytes (and neurons) in the surrounding regions through a concentric wave of activation centred on the NMDA pipette. We found that the Ca^{2+} response of astrocytes as well as the recruitment of neurons into the ictal discharge is more consistent with a process of modular recruitments rather than with a propagation of a concentric wave of activity (Figure S5).

Astrocyte activation was largely due to AP-mediated neurotransmitter release since $70.4 \pm 8.3\%$ ($n = 143$, 5 experiments) of the field A astrocytes, activated by a first double NMDA pulse, failed to respond to a second double NMDA pulse applied in the presence of TTX. The Ca^{2+} rise in still-responsive astrocytes displayed slow kinetics and were of small amplitude ($\Delta F/F_0$, 64.1 ± 3.6 before and 29.0 ± 2.2 after TTX; $n = 41$; $p < 0.001$). This residual astrocyte response in TTX could be due either to neurotransmitter release mediated by activation of presynaptic NMDA receptors [33] or to the direct activation by NMDA of NMDA receptors that may be present on astrocytes [34,35].

The results from these experiments indicate that the development of a focal ictal discharge is accompanied by Ca^{2+} elevations in astrocytes.

32
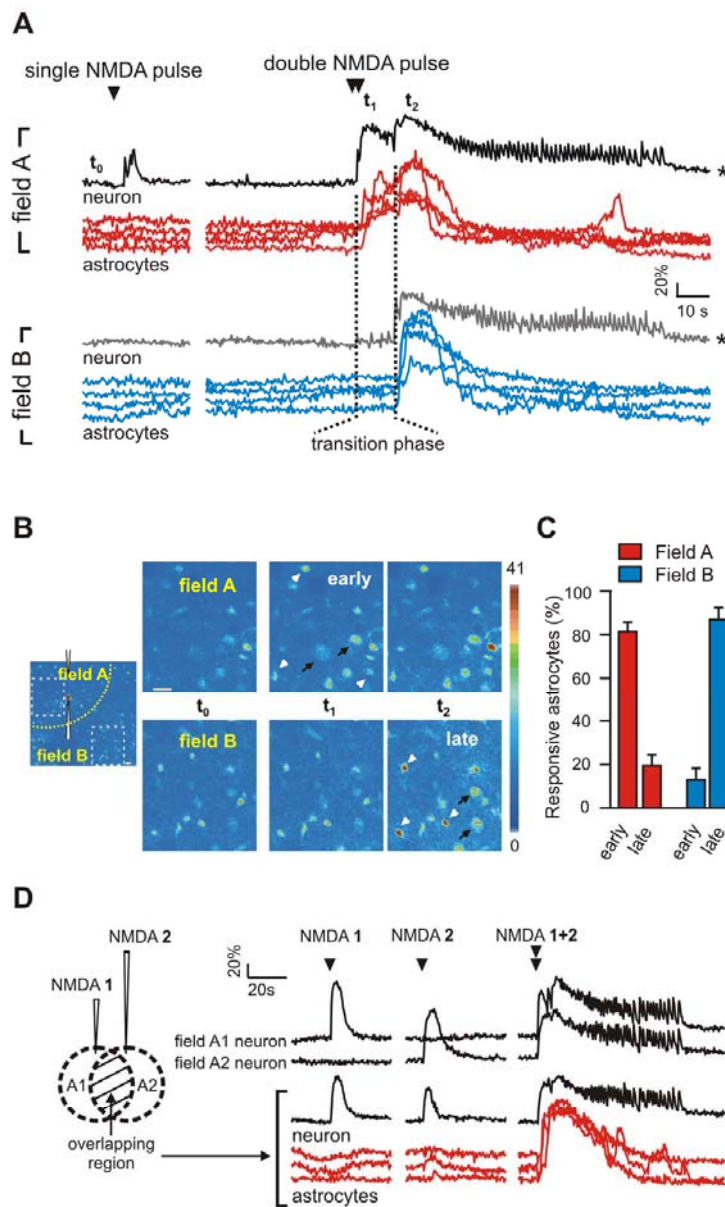
Figure 5. The ictal discharge generation is accompanied by Ca^{2+} elevations in astrocytes. (A) Ca^{2+} changes of a field A neuron, a field B neuron, and astrocytes in field A and field B from the same experiment illustrated in Figure 4A–4D. The single NMDA pulse fails to activate astrocytes (red and blue traces, left), whereas the double NMDA pulse evokes a large astrocyte Ca^{2+} rise that in field A (red traces, right) is associated with the initial development of the ictal discharge, whereas in field B (blue traces, right), the rise follows it. Vertical dashed lines mark the transition phase. *Traces from Figure 4 are shown for comparison. (B) Image at high magnifications (dashed boxes in left panel) illustrating the early Ca^{2+} increase that in field A astrocytes occurs during the transition phase (t_1) and the late Ca^{2+} increase that in field B astrocytes occurs after the ictal discharge (t_2). Arrows and arrowheads mark neurons and astrocytes, respectively. Scale bars represent 20 µm. (C) Percentage of field A astrocytes (13 experiments, 262 responsive astrocytes) and field B astrocytes (12 experiments, 187 responsive astrocytes) that displayed an early or a late Ca^{2+} increase. (D) Left,

33

Selective Inhibition of Astrocytes Impairs Ictal Discharge Generation

If this early Ca^{2+} elevation in astrocytes is not a mere consequence of neuronal activity and has, instead, a causative role in ictal discharge generation, its inhibition should reduce the ability of NMDA to trigger an ictal discharge. To address this hypothesis, we first bath applied MPEP and PPADS ($n=4$) and found that the direct activation of neurons by a double NMDA pulse was unchanged, but early activated astrocytes were reduced to $4.6\pm2.6\%$ of controls. Under these conditions, the generation of the ictal discharge in field A and the subsequent recruitment of neurons into the epileptic discharge in field B were inhibited (Figure 6A). The ictal discharge recovered after washout of the antagonists and the reappearance of the associated Ca^{2+} elevation in astrocytes. Interestingly, a stronger neuronal stimulation obtained by increasing the number of successive NMDA puffs evoked an ictal discharge, although of short duration, even in the presence of MPEP/PPADS and without a recovery of astrocyte Ca^{2+} signals (Figure 6A).

We also found that the NMDA-induced ictal discharge was blocked after inhibition of the early responsive astrocytes in field A by MPEP/PPADS applied locally to this region (Figure 6B; $n=4$). Ictal discharge recovery was regularly observed 5 10 min after cessation of the MPEP/PPADS pulses. In contrast, applications of MPEP/PPADS to a limited sector of field B failed to affect the spread to field B of the ictal discharge generated in field A ($n=4$). However, it is noteworthy that the Ca^{2+} elevations in astrocytes from this sector were poorly affected (Figure 6B).

Given that MPEP and PPADS are not selective antagonists of Ca^{2+} signals in astrocytes, to provide a direct evidence for a causal link between Ca^{2+} elevations in field A astrocytes and ictal discharge generation, we inhibited Ca^{2+} signals in these astrocytes selectively by introducing the Ca^{2+} chelator 1,2-bis(o-aminophenoxy)ethane-N,N,N',N'-tetraacetic acid (BAPTA; 50 mM) into individual astrocytes through a patch pipette [36].

First, we indirectly evaluated BAPTA spreading in the astrocyte syncytium by patching single EC astrocytes with a Texas Red-containing pipette. We counted 31 ± 7 red-labelled astrocytes in an area of 242 ± 50 µm in diameter (Figure 7A). This value is close to the size of the cortical region occupied by neurons that respond directly with a transient Ca^{2+} rise to a double NMDA pulse applied in the presence of TTX (Figure 7A). In subsequent experiments, before patching a field A astrocyte with a BAPTA-containing pipette, a double NMDA pulse was applied to trigger an ictal discharge (Figure 7B and 7C). In five out of nine BAPTA experiments, a double NMDA pulse applied 50 min after BAPTA diffusion in the astrocyte syncytium failed to activate both the Ca^{2+} elevations in astrocytes and the ictal discharge (Figure 7B and 7C). Notably, in these five experiments, the response of early activated field A astrocyte was strongly reduced with respect to that observed before BAPTA (Figure 7D). In these experiments, we addressed the contribution of astrocytes in the activation of neurons during the transition phase. In the presence of BAPTA, which specifically inhibited Ca^{2+} signals in field A astrocytes, the number of recruited neurons upon the double NMDA pulse was $33.1\pm3.2\%$ lower than in controls ($p<0.05$). Such a reduction is unlikely due to experimental variability in the intensity of the NMDA stimulation since the number of neurons activated and the

amplitude of their Ca^{2+} responses to successive double NMDA pulse stimulations (as measured in the presence of TTX) were unchanged over a 50-min period (Figure S4). These observations indicate that the recruitment of neurons into the ictal discharge is also mediated by the early activated astrocytes that signal back to neurons.

In the four experiments with BAPTA in which the ictal discharge was preserved, most of the astrocytes in field A still displayed an early Ca^{2+} response, suggesting a defective diffusion of BAPTA in the astrocyte syncytium in these experiments (Figure 7D). These data provide a plausible explanation for the lack of inhibition of the ictal discharge in these BAPTA experiments.

In a number of different control experiments, we found that i) two subsequent double NMDA pulses applied before and 50 min after patching either a neuron ($n=8$) or an astrocyte ($n=4$) with a pipette not containing BAPTA always evoked comparable ictal discharges, indicating that such a long time interval does not affect the ability of a double NMDA pulse to trigger an ictal discharge; ii) double NMDA pulses regularly evoked an ictal discharge even after 50 mM BAPTA was puffed directly over the neurons for 2 min via a pipette ($n=4$), indicating that a leakage of BAPTA, putatively occurring during astrocyte seal formation, cannot account for the ictal discharge inhibition observed in the BAPTA experiments; iii) successive double NMDA pulses applied in the presence of TTX over a period of 50 min, while patching single astrocytes with a BAPTA-containing pipette, evoked an unchanged response in neurons (Figure 7E), demonstrating that the direct response of neurons to NMDA is not affected after BAPTA-mediated inhibition of astrocyte Ca^{2+} signals.

We next asked whether the late activation of astrocytes in field B contributes to the spreading of the ictal discharge. After patching individual field B astrocytes with a BAPTA-containing pipette, we observed that the ictal discharge evoked in field A by a double NMDA pulse still invaded field B and further propagated to the adjacent region, whereas the activation of field B astrocytes was drastically affected both in terms of Ca^{2+} signal amplitude ($-56.6\pm2.4\%$, $p<0.001$) and kinetics (time to peak, 2.6 ± 0.4 s and 15.2 ± 3.3 s, before and after BAPTA, respectively; $p<0.001$; Figure S6).

As a further control for the specificity of the BAPTA effect, we demonstrated that the ictal discharge inhibition by BAPTA was spatially restricted. After the astrocyte syncytium in region 1 was loaded with BAPTA, a double NMDA pulse stimulation close to the BAPTA-loaded region failed to trigger an ictal discharge, whereas the same NMDA stimulation applied $\sim$500 µm away from region 1 readily evoked an ictal discharge (region 2, Figure 7F 7H).

The ictal discharge blocked after the BAPTA-mediated inhibition of field A astrocytes was recovered in two of three experiments by applying a stronger stimulation of neurons, such as a triple NMDA pulse (Figure 7I; white arrowheads). Notably is that under these conditions, astrocytes recovered a Ca^{2+} response that was, however, delayed and of reduced amplitude with respect to that without BAPTA. These results are consistent with the hypothesis that the astrocyte contribution to ictal discharge generation is not an absolute requirement and can be bypassed by a stronger stimulation of neurons, as already suggested by the results obtained in MPEP/PPADS experiments.

34
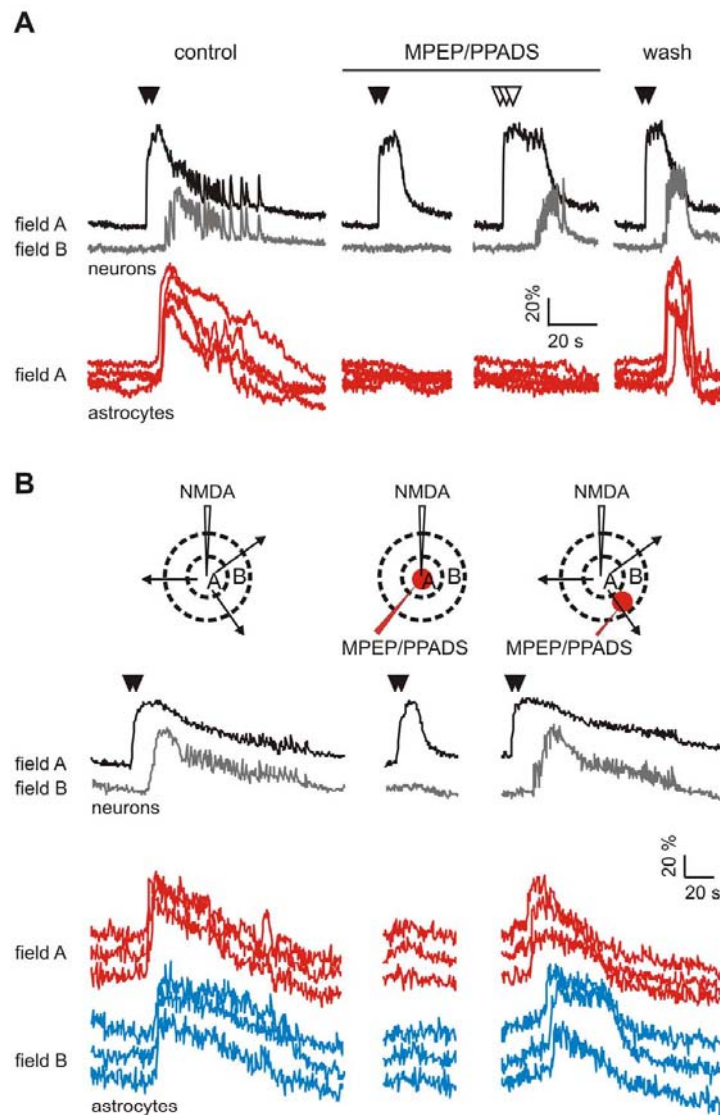
Figure 6. Inhibition of field A astrocytes by MPEP/PPADS impairs ictal discharge generation. (A) Ca²⁺ signal from a field A neuron, a field B neuron, and field A astrocytes in response to repetitive episodes of NMDA stimulation (black arrowheads). The NMDA stimulation that evoked an ictal discharge became ineffective after blocking the astrocyte response by bath perfusion with MPEP and PPADS. An ictal discharge could be recovered by increasing the number of NMDA puffs (white arrowheads). A double NMDA pulse evoked both astrocyte activation and the ictal discharge after inhibitor washout. (B) Top, drawings of field A and B illustrating different experimental conditions. The three black arrows symbolize the spreading of a focal ictal discharge. The red spots indicate the region of local MPEP/PPADS applications. Bottom, Ca²⁺ signal from a field A neuron, a field B neuron, field A astrocytes, and field B astrocytes in response to repetitive episodes of NMDA stimulation (black arrowheads). The double NMDA pulse that evoked an ictal discharge became ineffective after local MPEP/PPADS application to field A, but not to field B. Note also the absence of "early" responsive astrocytes after MPEP/PPADS applications to field A, whereas "late" responsive astrocytes are only slight changed after MPEP/PPADS applications to field B.
doi:10.1371/journal.pbio.1000352.g006

35

36
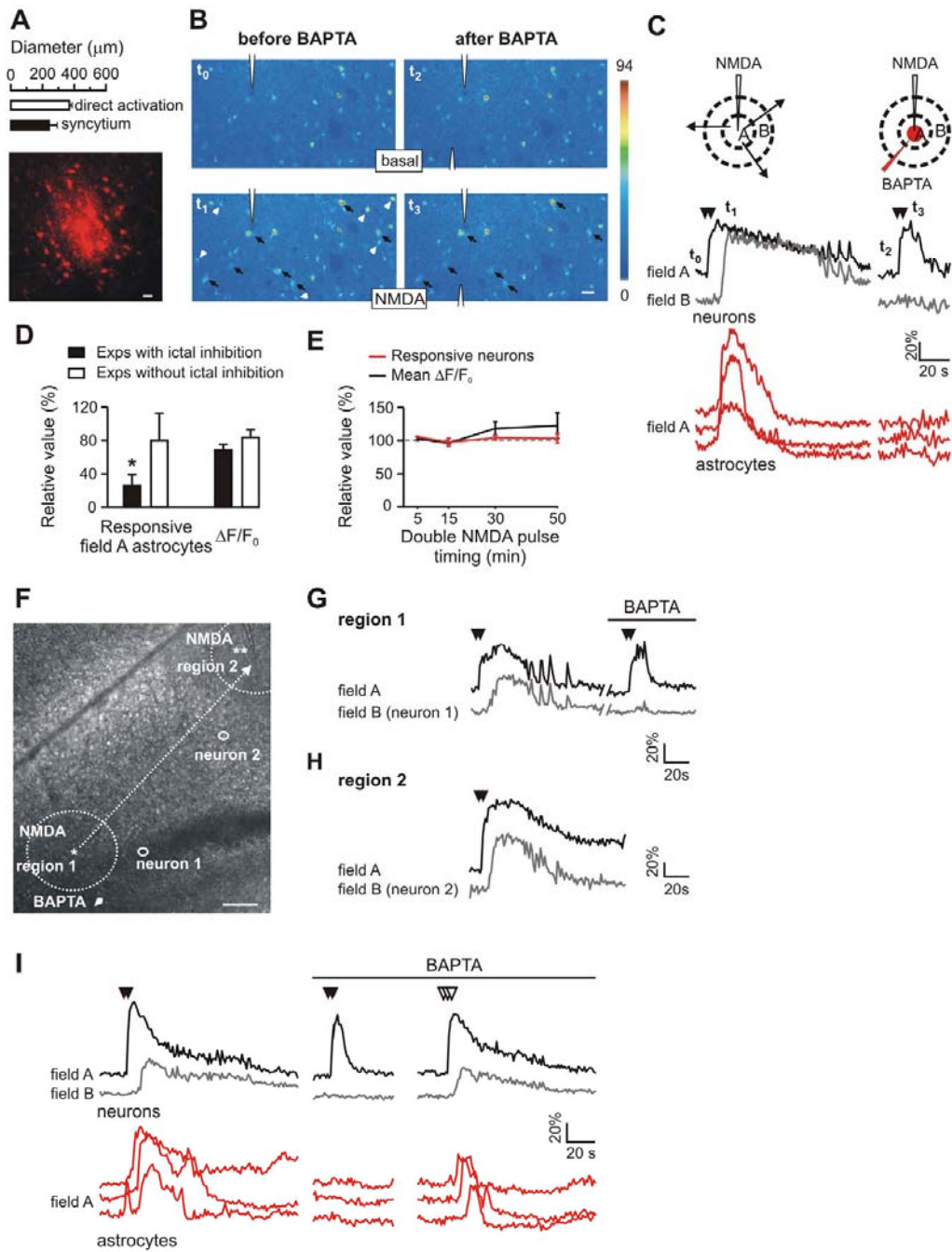
Figure 7. Selective inhibition of astrocytes impairs ictal discharge generation. (A) Maximal projection of a Texas Red–labelled astrocyte syncytium after patching a single astrocyte with a Texas Red–containing pipette in an EC slice. Top, bar graph reporting the mean size of the labelled astrocyte syncytium ($n = 5$) and of the region of neurons directly activated by NMDA ($n = 4$). Scale bar represents 20 μm. (B) Images from an EC slice illustrating the Ca^{2+} signal in neurons and astrocytes from field A before and after BAPTA spreading in the astrocyte syncytium, at rest (t_0 and t_2, respectively) and after the NMDA stimulation (t_1 and t_3, respectively). Responsive neurons (black arrows) and astrocytes (white arrowheads) are indicated. Note the absence of astrocyte responses after BAPTA (t_3). Scale bar represents 20 μm. (C) Ca^{2+} changes from some of the neurons and astrocytes indicated in (B). Also reported is the Ca^{2+} change of the ictal discharge from a field B neuron not present in the image (gray trace). The NMDA stimulation that can evoke an ictal discharge becomes ineffective after inhibition of the astrocyte Ca^{2+} signal in field A by BAPTA (red traces). (D) Change in the number of early responsive field A astrocytes and in the amplitude of the Ca^{2+} increase activated by a double NMDA pulse applied after BAPTA spreading in the astrocyte syncytium, expressed as percentage of control values, i.e., before BAPTA dialysis, in the experiments in which BAPTA inhibited, or failed to inhibit, the ictal discharge. One-sample Student t-test, an asterisk (*) indicates $p < 0.05$. (E) Number of responsive neurons and amplitude of the Ca^{2+} signal after repetitive double NMDA pulses applied in the presence of TTX during BAPTA spreading in the astrocyte syncytium ($n = 3$), expressed as relative values with respect to measurements performed before BAPTA spreading. (F) Differential interference contrast image of an EC slice showing the BAPTA-containing pipette (arrowhead) and the first location of the NMDA pipette (asterisk in region 1) that was used to trigger the first ictal discharge. The NMDA pipette was then moved to region 2 and its tip is indicated by the two asterisks. Dashed circle indicates the field A in each region. The small circles mark the position of a field B neuron in region 1 (neuron 1) and in region 2 (neuron 2). Scale bar represents 100 μm. (G) Double NMDA pulse–induced ictal discharge in field A and B neurons in region 1 and its failure 50 min after BAPTA spreading in the astrocyte syncytium. (H) Recovery of the ictal discharge evoked by a double NMDA pulse after moving the NMDA pipette to region 2. (I) Ca^{2+} changes in field A and B neurons and field A astrocytes illustrating the inhibition of the ictal discharge by BAPTA in a different EC slice and its recovery after increasing the NMDA stimulation to three pulses (white arrowheads). Note that after increasing the NMDA stimulation, astrocyte activation partially recovers, but the response is delayed and develops after the emergence of the ictal discharge in field B neurons.
doi:10.1371/journal.pbio.1000352.g007

Taken together, the results of these series of experiments confirm the reliability of the double NMDA pulse paradigm in evoking an ictal discharge over long time periods and, on the other hand, validate the selective inhibition of astrocyte Ca^{2+} signals by intracellular BAPTA application.

Selective Activation of Astrocytes Favours the Generation of Focal Ictal Discharges

If inhibition of Ca^{2+} signals in astrocytes can block the generation of a focal ictal discharge, it would be expected that direct astrocyte stimulation promotes ictal discharges. In the experiments that addressed this hypothesis, we took advantage of the finding that none of the 48 single NMDA pulses performed in the 4-AP ictogenic model could generate an ictal event. Single NMDA pulses that repetitively failed to trigger an ictal discharge became effective when they were coapplied with TFFLR (Figure 8). We found that a single NMDA pulse coupled with TFFLR, evoked an ictal event in six of nine trials from a total of three experiments. In these experiments, we also found that the number of neurons activated by the NMDA/TFLLR coapplication during the transition phase was higher than that activated by

NMDA alone (mean increase, $+119.3 \pm 16.3\%$; $n = 6$; $p < 0.001$). These data confirm that the contribution of astrocytes in the recruitment of neurons can be critical for the generation of the ictal discharge.

Discussion

In brain slice models of seizures, the ictal discharge is proposed to initiate at focal brain sites by asynchronous neuronal hyperactivities that progressively recruit adjacent neurons into a synchronous discharge [1,3 4]. In our study, we found that neuronal hyperactivities at these restricted brain sites are accompanied by Ca^{2+} elevations in a large number of astrocytes that contribute to drive neurons towards seizure threshold.

The focal ictogenesis in our model is schematically illustrated in Figure 9. This process starts with an isolated episode of local neuronal hyperactivity that triggers a large and synchronous Ca^{2+} elevation in closely associated astrocytes (N_1). These activated astrocytes signal back to neurons (A_1) favouring the recruitment of neurons into a coherent activity that underlies the hypersyn-
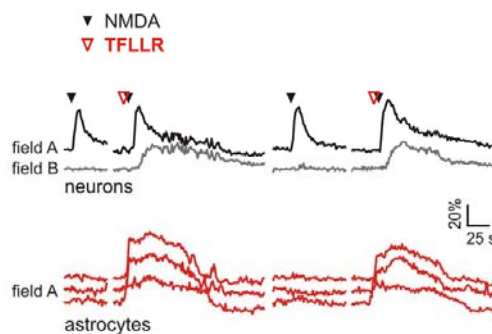
Figure 8. Selective astrocyte activation favours focal ictal discharges. In the 4-AP model, single NMDA pulses evoke the ictal discharge only when an astrocyte Ca^{2+} increase is induced by TFLLR.
doi:10.1371/journal.pbio.1000352.g008
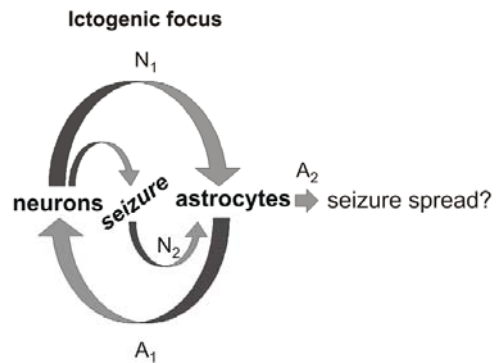
Figure 9. Neuron–astrocyte loop in ictal discharge generation. Schematic of the sequence of events in the recurrent neuron–astrocyte excitatory loop that develops at a restricted brain site to generate seizures. N_1 and N_2, neuron-to-astrocyte signalling; A_1 and A_2, astrocyte-to-neuron signalling.
doi:10.1371/journal.pbio.1000352.g009

37

chronous ictal discharge. This event, in turn, triggers a second activation of astrocytes (N_2). The secondary astrocyte activation may then contribute to sustain the ictal discharge (A_2). This sequence of events represents a recurrent neuron astrocyte excitatory loop that drives neurons towards the ictal discharge threshold.

Since our slice experiments were performed mainly in young animals, the role of astrocytes to seizure generation may be restricted to the immature brain. Although additional experiments are necessary to clarify this important issue, the ability of astrocytes to release glutamate and activate neuronal SICs in slices from young adult rats [8,28,37,38] suggests that astrocyte-to-neuron signalling may contribute to seizure initiation also in the adult brain.

The Early Ca^{2+} Elevation in Astrocytes Has a Causative Role in Ictal Discharge Initiation

In EC slices perfused with the proconvulsant agent 4-AP in low Mg^{2+} conditions, we found that a synchronous Ca^{2+} elevation in a high number of astrocytes occurred along with the development of the ictal discharge evoked by a local NMDA application. This response was largely TTX sensitive, indicating that astrocytes were activated by AP-mediated neurotransmitter release. Most importantly, the early astrocyte activation was a crucial step in the generation of ictal discharges. Indeed, when Ca^{2+} elevations in field A astrocytes were inhibited by BAPTA, the episode of neuronal hyperactivity induced by NMDA failed to generate an ictal discharge. According to results obtained from different control experiments, the effect of BAPTA on ictal discharge generation was specifically linked to the inhibition of astrocyte Ca^{2+} signals.

The Ca^{2+} elevations in astrocytes are associated with the release of gliotransmitters, such as glutamate [39 41] and D-serine [42], that modulates neurotransmitter release [24,43,44], triggers AP firing in neurons [10], and promotes local neuronal synchrony [8,28]. Ca^{2+}-dependent release of D-serine from astrocyte activated by Schaffer collateral stimulation has been also recently shown to be crucial for the potentiation of synaptic transmission in the CA1 hippocampal region [45]. As previously reported in the hippocampus [25,26], we show here that Ca^{2+} elevations stimulated in EC astrocytes by the PAR-1 receptor agonist, TFLLR, triggers glutamate release in these cells and, in turn, NMDA receptor mediated SICs in neurons. The activation of neurons by gliotransmission can thus account for the finding that a single NMDA pulse, ineffective per se, was able to trigger the ictal discharge if coupled with the direct stimulation of a Ca^{2+} rise in astrocytes by TFLLR. Data analysis of these experiments revealed that the number of neurons activated after NMDA/TFLLR coapplication was higher than that activated after NMDA alone.

These results suggest that when an episode of hyperactivity in a group of neurons consistently engages nearby astrocytes, a larger population of neurons is recruited into a coherent activity. If this feedback signal operates on a brain network prone to seizures, it contributes to drive neurons towards the ictal discharge threshold. The initiation site is thus represented, not only by the neurons activated by NMDA, but also by those that are secondarily activated in a recruitment process that involves astrocytes. Consistent with this view is our finding that when a double NMDA pulse (that successfully evoked an ictal discharge) was applied either after BAPTA was introduced in the astrocyte syncytium or after local applications of MPEP/PPADS to the site of activation, astrocytes were poorly activated, fewer neurons were recruited, and no ictal discharge was evoked. Further support for this conclusion derives from the experiments with a single NMDA

pulse delivered from two pipettes positioned at different distances. These experiments revealed that an ictal discharge could be evoked when astrocytes from the region of overlapping neuronal activation were activated. When the pipette tips were more distant, the overlapping region was reduced, astrocytes were poorly activated, and no ictal discharge was evoked.

Distinct subpopulations of astrocytes might differently contribute to modulate neuronal hyperactivity in the epileptogenic region, possibly by releasing in addition to glutamate, ATP, and other neuroactive signals, e.g., GABA, through a Ca^{2+}-dependent or -independent mechanism [46,47]. Given that inhibitory interneurons have been reported to restrain the recruitment of neurons during the development of the ictal discharge [4,48], an opposite action of astrocytes in this process might involve a distinct inhibition of interneurons by GABA released from astrocytes. Indirect support for this possible astrocyte action derives from the observation that GABA released from astrocytes can, indeed, result in a long-lasting inhibition of inhibitory granule cell activity in the olfactory bulb [37]. Whether a similar signalling between a subpopulation of GABA-releasing astrocytes and interneurons may be involved in ictal discharge initiation in the EC represents an interesting question to be addressed in future studies.

Episodes of focal seizures can arise in a nonepileptic tissue due to genetic causes or as a consequence of various brain damage. These may lead to status epilepticus (SE), a condition of persistent seizures, and evolve into chronic epilepsy after a latent period of epileptogenesis. Our results were obtained in nonepileptic brain tissue and provide evidence for the contribution of astrocytes in the initiation of seizure during SE. Therefore, whether astrocytes contribute also to seizure initiation in chronic epilepsy is, at present, unknown and should be appropriately investigated in chronic epilepsy models. However, results from a recent in vivo study showed that astrocytes, which exhibited long-lasting Ca^{2+} oscillations during SE, contributed to the neuronal death that characterizes chronic epilepsy [38]. This effect was due to astrocytic glutamate that activated neuronal NMDARs, possibly favouring seizure generation. It is also worth underlining that in the epileptic brain tissue, astrocytes undergo significant changes in their physiological properties that may result in decreased glutamate uptake, altered extracellular K^+ buffering capacities, and activation of inflammatory pathways [49,50]. All these changes may contribute to the increased neuronal network excitability that characterizes the epileptic brain.

The Astrocyte Contribution to Ictal Discharge Generation Depends on Neuronal Excitability Levels

The efficacy of astrocyte stimulation in evoking an epileptic discharge was different in the two models used in the present study, probably because of differences in their intrinsic neuronal predisposition to ictal discharge generation. As suggested by the presence of recurrent spontaneous epileptic discharges, the picrotoxin/zero-Mg^{2+} model can be considered, indeed, a model with a low-threshold for epileptic discharges. In this model, a single NMDA pulse triggered synchronous activity in a number of neurons sufficient to reach the ictal discharge threshold, and a single stimulation of astrocytes was also sufficient to trigger an ictal discharge. As suggested by the absence of spontaneous epileptic events, the 4-AP model has a higher threshold for epileptic phenomena. In this model, seizure discharges could be triggered by a more prolonged and intense episode of neuronal activity induced by a double NMDA pulse, and not by single NMDA or TFLLR pulses. An ictal discharge could be also evoked when a single NMDA application (ineffective per se) was coupled with TFLLR-mediated astrocyte activation. Furthermore, the reduc-

tion in astrocyte Ca^{2+} signals blocked the ictal discharge in the 4-AP model, but not in the picrotoxin/zero-Mg^{2+} model. These data demonstrate that experimental manipulations of the astrocyte Ca^{2+} signals can influence neuronal recruitment and thus affect, in concert with the level of neuronal activity, the likelihood of ictal events.

As revealed by results from both BAPTA and MPEP/PPADS experiments, when the astrocyte contribution was reduced by inhibiting Ca^{2+} signals in these cells and the double NMDA pulse consequently failed to evoke an ictal discharge, we could recover an ictal discharge by applying a more intense NMDA stimulation. By activating directly a larger number of neurons, this higher stimulus evokes a level of correlated activity that is sufficient for seizure-like discharge generation, bypassing the astrocyte contribution in the recruitment process. Thus, astrocyte activation is not an absolute requirement for ictal discharge generation.

However, astrocytes respond readily to synaptic activity with Ca^{2+} oscillations [16,23,51], and the frequency of these oscillations increases in parallel with an increased neuronal activity [16]. In vivo studies also revealed that sensory stimuli can evoke distinct Ca^{2+} elevations in astrocytes confirming the strict association between neuron and astrocyte activities [52 55]. Thus, pathological hyperactivities in neurons [6] should be regularly accompanied by an increased astrocyte activity. In support of this view, studies in brain slices showed that chemically induced epileptiform activity causes a sustained increase in astrocyte Ca^{2+} signalling [9,10], and in vivo studies reported a long-lasting hyperactivity of astrocytes after pilocarpine-induced SE [38]. It is conceivable that a pathological hyperexcitability that predisposes neurons to seizure discharges may originate from abnormalities in the neuron astrocyte network activity, whatever the origin of the initial dysfunction might be. As we showed here, depending on the different level of excitability in neurons, the astrocyte contribution varies, but it can even be crucial for ictal discharge generation.

Ictal, but Not Interictal, Discharges Activate a Secondary Astrocyte Ca^{2+} Elevation

In our 4-AP slice model, a second Ca^{2+} elevation even of larger amplitude than that early evoked by the double NMDA pulse, occurred in astrocytes in both field A and field B. This delayed activation of astrocytes was observed also after the spontaneously occurring ictal discharges in the picrotoxin/zero-Mg^{2+} model in both rats and pGFAP-EGFP transgenic mice, as well as in other models such as the 4-aminopyridine/picrotoxin and high-potassium models (unpublished data). Most importantly, this observation was validated in the intact guinea pig brain preparation, a well-characterized model of EC hippocampus focal ictogenesis [20,21]. In this close to in vivo preparation, the development of the ictal discharge was regularly accompanied by a Ca^{2+} elevation in virtually all astrocytes present in the recording field, whereas large-amplitude interictal discharges were never associated with a significant Ca^{2+} change in astrocytes. This Ca^{2+} elevation and the following release of gliotransmitters may contribute to the maintenance of AP bursts and to the process of neuronal recruitment that characterize seizure discharge propagation. Our finding that the duration of the ictal discharges was significantly reduced upon inhibition of the astrocyte Ca^{2+} signal by bath perfusion with MPEP or PPADS is consistent with this hypothesis, which needs, however, to be specifically addressed in future experiments.

In the present study, we also addressed a possible role of the late astrocyte response in the propagation of the ictal discharge outside the focal region. After BAPTA introduction in field B astrocyte syncytium, the ictal discharge still propagated to this region and further, suggesting that Ca^{2+} elevations in field B astrocytes may have no role in this process. Given that initiation, propagation and cessation of the ictal discharge are likely governed by distinct mechanisms [3], it would not be surprising that astrocytes have, indeed, a role in ictal discharge initiation but not in propagation. This conclusion is, however, reasonable, but it is not proven beyond all doubt. Indeed, the inhibition by BAPTA could be exerted only in astrocytes from a small sector of the large field B, whereas astrocytes outside this sector were totally unaffected. Their activation might thus be sufficient to sustain the propagation of the ictal discharge even to the small sector where astrocytes were inhibited by BAPTA. As to MPEP/PPADS, when locally applied to field B, these competitive receptor antagonists failed to inhibit the ictal discharge propagating to this region. These results, however, do not allow us to draw any conclusions since the ictal discharge invading field B still activated a significant response in astrocytes even in the presence of MPEP/PPADS. To clarify this point, another experimental approach is thus required.

It is unclear why MPEP/PPADS failed to inhibit the Ca^{2+} elevation evoked by the ictal discharge in field B astrocytes. It is likely that, with respect to the NMDA pulse, the ictal discharge represents a more powerful stimulus that triggers the release of glutamate and ATP. Accordingly, the extracellular concentration of MPEP/PPADS reached after local applications might have been insufficient to inhibit the large activation of astrocyte mGlu and P2 receptors upon the ictal discharge. However, mechanisms other than mGlu and P2 receptor activation may be also involved in this astrocyte response.

Interictal discharges failed to activate significantly a Ca^{2+} elevation in astrocytes. Recently, it has been reported that glutamate release triggered by Ca^{2+} elevations in astrocytes plays a predominant, if not obligatory role in the generation of epileptic activity in the hippocampus and, in particular, in the slow depolarization shift associated with interictal discharges [9]. This conclusion is, however, at variance with a number of studies showing that both interictal and ictal seizure-like discharges from different brain regions, including the hippocampus, are strictly linked to neuronal activity being efficiently prevented or blocked, depending on the time of application, by TTX [10,38,56 58]. In the present study, we observed that i) the interictal activity was not blocked after Ca^{2+} elevations in astrocytes were drastically reduced; and ii) synchronous astrocyte Ca^{2+} elevations were never observed to accompany an interictal discharge in the different models. We thus failed to confirm a role of astrocytic glutamate in interictal discharge generation. The reasons for this discrepancy are, at present, unknown.

Conclusions and Perspectives

The present study reveals a crucial role of neuron astrocyte interactions in sculpting activity at the epileptogenic zone. When a group of neurons is abnormally active (due to acquired or genetic causes), ictal epileptiform events may occur through the activation of astrocytes. Astrocytes can thus play a key role in seizure initiation in a nonepileptic brain tissue and, in contrast to previous observations [9], do not appear to be involved in the generation of the interictal events. This peculiarity makes the astrocyte neuron unit a primary target for novel drug development aimed at interfering selectively with ictogenesis, without affecting the interictal activity that, by preventing seizure precipitation, may have a beneficial role in focal epilepsies [59,60].

The high reproducibility in the generation of comparable ictal discharges represents an important advantage of our new EC slice model of ictogenesis. This model allowed us to investigate the early events that, at a restricted brain site, predispose neurons to seizure

39

and to obtain some insights into the mechanism of focal ictal generation that involves astrocytes. Other aspects that were not addressed in the present study, such as the neuronal recruitment process during the diffusion of the ictal discharge to regions distant from the site of ictal discharge generation, could be investigated in this model. These acute experiments set the conditions for validating the mechanisms here described in future studies in chronic models of epilepsy, including genetically determined in vivo models of epilepsy, that more closely mimic the complex feature of seizures in epileptic patients. A validation of the astrocyte role in seizures generation in these models is fundamental to provide further arguments in favour of astrocytes as targets for developing new therapeutic strategies for epilepsies.

Materials and Methods

Ethics Statement

All experimental procedures were authorized by the Italian Ministry of Health.

Brain Slice, Guinea Pig Brain Preparations, and Dye Loading

Transverse cortico-hippocampal slices were prepared from postnatal day 14 18 Wistar rats or pGFAP-EGFP transgenic mice [61], and loaded with OGB1-AM (excited at 488 nm) or Rhod-2 (excited at 543 nm), respectively, as previously described [8]. Briefly, brain was removed and transferred to ice-cold cutting solution containing (in mM): NaCl, 120; KCl, 3.2; KH_2PO_4, 1; $NaHCO_3$, 26; $MgCl_2$, 2; $CaCl_2$, 1; glucose, 10; Na-pyruvate, 2; and ascorbic acid, 0.6; at pH 7.4 (with 5% CO_2/95% O_2). Coronal slices were obtained by cutting with a Leica vibratome VT1000S in the presence of the ionotropic glutamate receptor inhibitor kynurenic acid (2 mM). Slices were recovered for 15 min at 37°C and then loaded with the Ca^{2+}-sensitive dye OGB1-AM (Invitrogen) for 60 min at 37°C. Loading was performed in the cutting solution containing sulfinpyrazone (200 μM), pluronic (0.12%), and kynurenic acid (1 mM). After loading, slices were recovered and kept at room temperature in the presence of 200 μM sulfinpyrazone. Brains from postnatal day 14 20 guinea pigs were isolated and perfused at a rate of 5.5 ml/min through the basilar artery [19,62] with a solution containing (in mM): NaCl, 126; KCl, 3; KH_2PO_4, 1.2; $MgSO_4$, 1.3; $CaCl_2$, 2.4; $NaHCO_3$, 26; glucose, 15; and 3% dextran M.W. 70.000; oxygenated with a 95% O_2/5% CO_2 gas mixture (pH 7.3). The dye OGB1-AM (50 μg) was diluted in 5 μl of standard pluronic/DMSO solution and 75 μl of saline, and filtered through a 0.2-μm microfilter (Millipore). A patch pipette (3 4 MΩ was used to pressure inject (1 2 min at 4 PSI) the Ca^{2+} dye into the EC at a depth of about 200 μm via a picospritzer (NPI Electronics). Following this procedure, the Ca^{2+} signal from astrocytes, neurons, and neuropile was monitored. All experiments were performed at 33 35°C.

Ca^{2+} Imaging

In slice experiments, we used a TCS-SP2-RS or a TCS-SP5-RS confocal microscope (Leica) equipped with a 20× objective (NA, 1.0) and a CCD camera for differential interference contrast images. For experiments on isolated guinea pig brains, we used a Fluoview 300 scanning head customized for two-photon microscopy equipped with a 5W Verdi-Mira laser (Coherent) tuned at 830 nm and external photomultipliers (Hamamatsu). Time frame acquisitions from 314 ms to 1.24 s (with one to six line averaging) were used. No background subtraction or other manipulations were applied to digitized Ca^{2+} signal images that are reported as

raw data, with the exception of the difference images in Figure 4 that were obtained by subtracting the prestimulation image from the poststimulation image. In brain slice preparations, neurons and astrocytes were distinguished on the basis of the distinct kinetics of their Ca^{2+} response to a stimulation with high K^+ extracellular solution (40 mM) obtained by isosmotic replacement of Na^+ with K^+ [16], applied at the end of the recording session in the presence of 1 μM TTX (Figure S7). Due to the lack of voltage-dependent Ca^{2+} channels in astrocytes, the Ca^{2+} elevation in these cells upon high K^+ stimulation occurs with a delay of several seconds with respect to the response in neurons, and appears to be mediated by glutamate release from depolarizing neurons [17]. In the present study, the presence of TTX was necessary to block the epileptic discharges and the underlying Ca^{2+} changes in neurons and astrocytes that would have hampered the possibility to distinguish these cells from their different responses to high K^+ stimulation. Astrocytes were identified also by their small size, low membrane potentials (-74 ± 0.4 mV without the correction for the liquid junction potential at the pipette tip, which was 15 mV; $n = 9$), and passive responses to a series of depolarizing steps. In slices from pGFAP-EGFP mice, astrocytes were identified by their green GFP fluorescence. In the guinea pig brain, astrocytes were identified using the astrocyte-specific marker sulforhodamine 101 (Invitrogen) applied at 100 μM to the cortical surface [63]. The onset of the slow Ca^{2+} elevation in astrocytes was determined on the basis of a threshold criterion. The onset was identified by the change in $\Delta F/F_0$ that should be more than two standard deviations over the average baseline and remained above this value in the successive frames for at least 2 s (two to six frames, depending on the frame acquisition rate).

Electrophysiology and NMDA Pulse Applications

Rat brain slices in a submerged chamber (Warner Instruments) were continuously perfused at a rate of 2 ml/min with (in mM): NaCl, 120; KCl, 3.2; KH_2PO_4, 1; $NaHCO_3$, 26; $MgCl_2$, 1; $CaCl_2$, 2; glucose, 10; sulfinpyrazone, 0.2; at pH 7.4 (with 95% O_2/5% CO_2). Whole-cell patch-clamp recordings in rat brain slices were performed using standard procedures and one or two Axopatch-200B amplifiers (Molecular Devices), as previously reported [8]. Typical pipette resistance was 3 4 MΩ for neurons. Data were filtered at 1 kHz and sampled at 5 kHz with a Digidata 1320 interface and pClamp8 software (Molecular Devices). Whole-cell intracellular pipette solution was (in mM): K-gluconate, 145; $MgCl_2$, 2; EGTA, 0.5; Na_2ATP, 2; Na_2GTP, 0.2; HEPES, 10; to pH 7.2 with KOH, and contained a low concentration (10 μM) of OGB1 (Invitrogen); osmolarity, 305 315 mOsm. Data analysis was performed with Clampfit 8 and Origin 6.0 (Microcal Software) software. SICs with an amplitude greater than 20 pA and a rise time slower than 10 ms are classified as SICs, as described previously. SIC rise time was calculated with the 20% 80% criterion and the decay time as the time constant of a single exponential fit. The delay of each SIC activated in neurons after astrocyte stimulation with TFLLR was calculated with respect to the peak of the immediately preceding astrocyte Ca^{2+} increase. Interictal and ictal seizure-like events resembling those recorded at the electrographic recordings from patient's brain [21], at a cellular level manifest as intense and hypersynchronous discharges that involve large neuronal population and fundamentally differ in their duration. Despite this common characteristic, they have radically different durations. Indeed, the duration of the epileptic event was an important criterion for classifying interictal and ictal events in slice and the isolated whole guinea pig brain preparations. In Ca^{2+} imaging experiments, interictal events lasted less that 3 s, whereas ictal discharges were sustained for tens of

seconds with a final pattern of highly synchronous afterdischarges. The duration of ictal events varied between 15 and 110 s in brain slices and between 21 and 152 s in the guinea pig brain. Postictal depression was also consistently observed after an ictal event, whereas it was not present after an interictal spike [21]. A pressure ejection unit (PDES, NPI Electronics) was used to apply pressure pulses (4 10 psi, 200 600 ms duration) to NMDA-containing pipettes. Pulse pressure (or duration) was increased until a double NMDA pulse evoked an ictal discharge. The stimulus parameters for successive stimulations remained unchanged over the entire recording session, except in the BAPTA experiments in which they were changed to increase the stimulation of neurons by NMDA and thus to recover the ictal discharge after inhibition of Ca^{2+} signals in astrocytes. In the double NMDA pulse, the interval between the two pulses was 3 s. NMDA pulses applied with intervals of 5 s, but not 20 s also triggered an ictal discharge (unpublished data). For BAPTA dialysis into the astrocyte syncytium, we used a patch pipette (5 6 MΩ; 310 315 mOsm) containing (in mM): K-methylsulfate, 50; ATP, 2; GTP, 0.4; HEPES, 10; BAPTA, 50. To avoid a leakage of BAPTA from the pipette during seal formation, the BAPTA solution was backfilled after loading the tip with a standard intracellular solution. Texas Red dye (excited at 543 nm) was included at 0.2 mM in a patch pipette containing standard solution and monitored 50 60 min after the whole-cell configuration. For the BAPTA and Texas Red experiments, only GluT (coupled) astrocytes were included. GluT (coupled) and GluR (uncoupled) astrocytes were distinguished according to their different responses to hyperpolarizing and depolarizing current pulses of increasing amplitude and 750 ms duration. Field potentials were recorded from the guinea pig brain with saline-filled micropipettes used to deliver OGB1-AM, via a multichannel differential amplifier (NPI Electronics). A precise allignement of Ca^{2+} and electrophysiological signals was achieved by acquiring with a syncronisation signal produced by the confocal microscope. Tip potential was measured against a ground reference placed in the recording chamber by means of a voltage follower coupled to an amplifier.

Drugs

MPEP (50 μM), PPADS (10 μM), TTX (1 μM), D-AP5 (50 μM), 4-AP (100 μM; Ascent Scientific), TFLLR (10 μM; Tocris), and picrotoxin (50 μM; Sigma-Aldrich) were bath applied. TFLLR (1 mM) and NMDA (1 mM; Sigma-Aldrich) were pressure applied. To induce local astrocyte inhibition, we applied pressure pulses of 2 s per 5 min at a frequency of 0.1 Hz to a pipette containing MPEP (500 μM) and PPADS (5 mM). Bicuculline methiodide (50 μM; Sigma-Aldrich) was applied by arterial perfusion to guinea pig brains.

Monte Carlo Simulation Procedures

The Monte Carlo simulation was designed to test whether the observed series of stimuli and ictal episodes were compatible with a random distribution. Each simulation run generated randomly distributed stimuli and ictal events based on i) recording duration; ii) number of stimuli and ictal events; iii) minimum interval between stimuli; iv) minimum interval between two successive ictal events; and v) minimum interval between a stimulus and an ictal event (ictal events seem to be followed by at least 20 s of refractory period). These rules imply that the occurrence of ictals and pulses are not completely independent. The random generator produced 30,000 temporal series for each experimental run, using experiment-specific parameters. Figure S2A shows an experiment and three simulated runs. The distance between each stimulus and the first following ictal events were computed for each simulation.

The datasets were used to compute the density probability p(t) of observing one ictal at time t after an astrocyte activation (Figure S2B). The cumulative probability CP(t) is obtained by the integration of the probability density and yields the probability of observing an ictal at a time ≤t under the hypothesis that stimuli and ictals are not causally related (Figure S2C). Each ictal event in the experiment was associated with the delay from the immediately preceding stimulus, and the probability of observing the ictal was calculated. If the cumulative probability was less than 0.05, the event was deemed as not satisfying the null hypothesis. Results are presented in Figure S2D.

Immunocytochemistry

Coronal slices (100-μm thick) of rat brains were cut with a VT 1000S vibratome (Leica) and directly fixed for 1 h in iced 4% paraformaldehyde in phosphate-buffered solution (PBS). Floating sections were first preincubated in a blocking solution (BS; 1% BSA, 2% horse serum, and 2% goat serum) containing 0.3% triton X-100 and subsequently incubated with the primary mouse anti-thrombin receptor PAR-1 antibody (1:300, Zymed Laboratories, Invitrogen) and rabbit anti-GFAP (1:500, Dako) diluted in BS. After 24 h, slices were washed at 4°C in PBS and incubated with the secondary antibodies (Cy3 conjugated donkey anti-mouse IgG, and Cy2 conjugated goat anti-rabbit F(ab')2 fragments; Chemicon International) for 2 h at room temperature. Slices were extensively washed in PBS, mounted in Elvanol, and observed with a Leica SP2 laser scanning confocal microscopy. Negative controls were performed in the absence of the primary antibodies. Images were assembled using CS Adobe Photoshop software.

Data Analysis

The Ca^{2+} signal is reported as $\Delta F/F_0$, where F_0 is the baseline fluorescence. Data are shown as mean ± standard error of the mean (S.E.M.). Unless stated otherwise, the Student t-test was used, with p values ≤0.05 taken as statistically significant.

Supporting Information

Figure S1 Interictal events activate in astrocytes only an increase in Ca^{2+} oscillation frequency. (A) Representative experiment from a rat hippocampal slice showing the Ca^{2+} elevations in CA3 neurons (black trace, averaged signal from all 20 neurons monitored) corresponding to interictal discharges in the picrotoxin/zero-Mg^{2+} model. This interictal discharge activity is accompanied by an increase in Ca^{2+} oscillation frequency in astrocytes (blue traces). (B) Bar graphs reporting the mean astrocyte Ca^{2+} oscillation frequency in controls and during interictal activity. *$p<0.05$. (C) 2P-LSM images from the EC of a guinea pig brain before (t_0), during (t_1), and after (t_2) an interictal discharge induced by arterial perfusion with bicuculline. Astrocytes (white arrowheads), neuropile (dashed circle), and a neuron (yellow arrow) are indicated. Scale bar represents 20 μm. (D) Field potential recording of two interictal discharges and correlated Ca^{2+} changes in the neuropile and the neuron indicated in (C). No correlated Ca^{2+} changes were observed from the two astrocytes (arrowheads in [C]).
Found at: doi:10.1371/journal.pbio.1000352.s001 (0.72 MB TIF)

Figure S2 Analysis by Monte Carlo simulation. (A) Diagram representing the entire length of the recording of the experiment partially reported, in terms of Ca^{2+} signal changes in neurons and astrocytes, in Figure 3F. Horizontal bar on the top marks the timing of the traces shown in Figure 3F. Black bars indicate the peak of the astrocyte Ca^{2+} response triggered by TFLLR stimuli, and the green boxes correspond to the ictal

41

events. The three underlying rows represent three results from the Monte Carlo simulation procedure (see Materials and Methods). (B and C) Density probability (B) and cumulative probability (C) computed from the Monte Carlo simulation for the depicted experiment in (A). Green arrowheads indicate the p value for the five ictal events occurring during the recording. These are the probabilities for each ictal to be independent from the astrocyte activation. The value $1 - p$ (reported in [D]) is the probability of correlation of the timing of the ictal discharge with the astrocyte Ca^{2+} increase. (D) Graph reporting the probability that the 15 ictal events (black dots) observed in six experiments are correlated positively with an astrocyte Ca^{2+} increase induced by TFLLR in the picrotoxin/zero-Mg^{2+} model.
Found at: doi:10.1371/journal.pbio.1000352.s002 (0.35 MB TIF)

Figure S3 **In the picrotoxin/zero-Mg^{2+} model, a single NMDA application is sufficient to trigger epileptiform discharges.** Representative experiment showing the effect of single local NMDA stimulation (arrowheads) on neurons from an EC slice perfused with picrotoxin/zero-Mg^{2+}. The Ca^{2+} signal from a neuron in the region close to the NMDA pipette tip (blue trace) and the current-clamp recording from a neuron located in a region distant from the NMDA pipette (black trace) revealed that NMDA puffs could induce a local response that either remained restricted (open arrowheads) or triggered a response (black arrowheads) that evolved into an interictal (second and third puffs) or an ictal event (fifth puff). Spontaneous and evoked interictal and spontaneous and evoked ictal discharges recorded from the patched neuron are undistinguishable (see lower panels). This observation validates our model since it suggests that both events i) are sustained by a similar number and subtype of active cells; and ii) rely on a common basic mechanism.
Found at: doi:10.1371/journal.pbio.1000352.s003 (0.46 MB TIF)

Figure S4 **The ictal discharge triggered by a local neuronal stimulation is highly reproducible.** (A) Pair recordings showing that successive ictal discharges occur in both field A and B neurons, whereas only field A neurons showed a direct NMDA effect. (B) Mean duration of successive ictal discharges evoked by repetitive double NMDA pulses expressed as relative values with respect to the first two ictal episodes. (C) Number of responsive neurons and mean Ca^{2+} change after repetitive double NMDA pulses applied in the presence of TTX ($n = 3$). Data are expressed as percentage of the first response.
Found at: doi:10.1371/journal.pbio.1000352.s004 (0.53 MB TIF)

Figure S5 **Spatiotemporal profile of the Ca^{2+} signal in neurons and astrocytes during a focal ictal discharge.** (A) Pseudocolour raster plots showing the time derivative of the smoothed fluorescence signal (by averaging over five points) for individual neurons and astrocytes from the region within 200 µm of the NMDA pipette tip (field A) and from the surrounding region (field B) during an ictal discharge evoked by a double NMDA pulse applied at $t = 0$. If the activation were propagating as a concentric wave originating at the focus, the time of ictal onset in each cell would increase proportionally with the distance from the focus. Therefore, the raster plots would show a diagonal band of activation. Instead, the development and spreading of the ictal discharge is more similar to a process of modular recruitments of groups of neurons (and astrocytes): cells in the field A enter in the ictal phase more or less simultaneously. Cells in field B are recruited simultaneously, but at a later time than cells at the focal site of activation. (B) Bar graphs showing the distribution of the Ca^{2+} elevation onsets in neurons and astrocytes. The onset of the Ca^{2+} signal for each neuron was defined as the time of the absolute maximum derivative value (that better reflects

the large Ca^{2+} rise of the recruitment of neurons into the ictal discharge), whereas for astrocytes, it was the time of the first local maximum derivative value (that reflects the initial Ca^{2+} rise in these cells).
Found at: doi:10.1371/journal.pbio.1000352.s005 (1.76 MB TIF)

Figure S6 **BAPTA-containing astrocyte syncytium in field B does not impair ictal discharge generation.** The introduction of BAPTA into astrocytes from a sector of field B does not impair either the generation of the ictal discharge in field A or the engagement of distant neurons from fields B and C into the ictal discharge. Note, however, that in the BAPTA-containing region, field B astrocytes are still activated by the ictal discharge, although their Ca^{2+} response have reduced amplitude and slow kinetics.
Found at: doi:10.1371/journal.pbio.1000352.s006 (0.27 MB TIF)

Figure S7 **High-potassium stimulation as a tool for cell classification in brain slices.** (A) Pseudocolour image from an EC slice loaded with OGB1-AM. Scale bar represents 20 µm. (B) Ca^{2+} signal from the eight cells indicated in (A) during an ictal event in the 4-AP model (left traces) and during the perfusion with a 40 mM K^+ solution in 1 µM TTX (right traces). TTX was perfused for 5 min to block the epileptic activity before perfusion with the high K^+ solution. Note that presumed neurons, i.e., large cells 1 4, in response to high K^+ displayed a Ca^{2+} elevation largely before that of the presumed astrocytes, i.e., small cells 5 8. This delayed Ca^{2+} elevation is due to the lack of voltage-dependent Ca^{2+} channels in these cells. (C) Pseudocolour image from an EC slice loaded with OGB1-AM from a different experiment on the picrotoxin/zero-Mg^{2+} model. Scale bar represents 20 µm. (D) Ca^{2+} signal from the eight cells indicated in (C) during an ictal event that arose spontaneously (left traces) and during the perfusion with a 40 mM K^+ solution and TTX (1 µM; right traces). Note that similar to what observed in (B), presumed astrocytes, i.e., small cells 5 8, displayed a delayed Ca^{2+} response to the high-potassium stimulation with respect to that in the large cells, presumed neurons. Note the high synchronous Ca^{2+} peaks in neurons from both experiments that reflect the afterdischarges of the seizure-like event.
Found at: doi:10.1371/journal.pbio.1000352.s007 (1.80 MB TIF)

Video S1 **Response of astrocytes to ictal and interictal discharges in EC slices.** This video shows the synchronous Ca^{2+} increase in EC neurons after slice perfusion with picrotoxin/zero-Mg^{2+} that reflects an interictal and an ictal discharge (as reported in Figure 1A and 1B). Note that at the beginning of the video there is an interictal discharge that activates only one astrocyte. A subsequent ictal discharge evokes a large and synchronous Ca^{2+} response in most astrocytes (indicated by the arrowheads in the first frame). In the final part of the video, synchronous, repetitive Ca^{2+} elevations in neurons reflect the afterdischarges typical of the late ictal phase. Time frame, 314 ms.
Found at: doi:10.1371/journal.pbio.1000352.s008 (3.34 MB MOV)

Video S2 **Selective stimulation of astrocytes with TFLLR triggers an ictal discharge.** This video shows the Ca^{2+} change in neurons and in astrocytes (indicated in the first frame by the orange arrowheads) evoked by a local application of TFLLR in an EC slice during perfusion with picrotoxin/zero-Mg^{2+} (as reported in Figure 3F). TFLLR induces a Ca^{2+} increase in astrocytes that is followed by an ictal discharge. Time frame, 1 s.
Found at: doi:10.1371/journal.pbio.1000352.s009 (5.49 MB MOV)

Video S3 A single NMDA stimulation triggers only a local Ca^{2+} response. This video shows the Ca^{2+} increase that is restricted to a group of layer V-VI EC neurons that follows a single NMDA stimulation (as reported in Figure 4). The orange circle marks the timing of the NMDA puff and the position of the NMDA pipette. Note the absence of astrocyte responses. Time frame, 356 ms.
Found at: doi:10.1371/journal.pbio.1000352.s010 (0.78 MB MOV)

Video S4 Two successive NMDA applications trigger an ictal discharge. This video shows an ictal event generated by an NMDA stimulation composed of two successive puffs (as reported in Figure 4). The orange circle in field A marks the timing of the NMDA puffs and the position of the NMDA pipette, whereas the yellow circle in field B marks the engagement of neurons from this region into the ictal discharge. The orange arrowheads indicate astrocytes in field A at the onset of their Ca^{2+} increase. Note that Ca^{2+} elevations in these astrocytes accompany the development of the ictal discharge. Yellow arrowheads indicate astrocytes in field B (at the onset of their Ca^{2+} increase) that are activated after the emergence of the ictal discharge in field B. Time frame, 356 ms. Found at: doi:10.1371/journal.pbio.1000352.s011 (2.39 MB MOV)

Author Contributions

The author(s) have made the following declarations about their contributions: Conceived and designed the experiments: MdC GMR GC. Performed the experiments: MGG GL AC MZ MB FV LU MdC GMR GC. Analyzed the data: MGG GL AC MZ MC MB MdC GMR GC. Wrote the paper: TP MdC GMR GC.

References

1. Traub RD, Wong RK (1982) Cellular mechanism of neuronal synchronization in epilepsy. Science 216: 745 747.
2. Avoli M, D'Antuono M, Louvel J, Kohling R, Biagini G, et al. (2002) Network and pharmacological mechanisms leading to epileptiform synchronization in the limbic system in vitro. Prog Neurobiol 68: 167 207.
3. Pinto DJ, Patrick SL, Huang WC, Connors BW (2005) Initiation, propagation, and termination of epileptiform activity in rodent neocortex in vitro involve distinct mechanisms. J Neurosci 25: 8131 8140.
4. Trevelyan AJ, Sussillo D, Watson BO, Yuste R (2006) Modular propagation of epileptiform activity: evidence for an inhibitory veto in neocortex. J Neurosci 26: 12447 12455.
5. Jefferys JG (1990) Basic mechanisms of focal epilepsies. Exp Physiol 75: 127 162.
6. McNamara JO, Huang YZ, Leonard AS (2006) Molecular signaling mechanisms underlying epileptogenesis. Science's STKE 2006: re12.
7. Baulac M, Pitkanen A (2008) Research priorities in epilepsy for the next decade: a representative view of the european scientific community. Epilepsia 50: 571 578.
8. Fellin T, Pascual O, Gobbo S, Pozzan T, Haydon PG, et al. (2004) Neuronal synchrony mediated by astrocytic glutamate through activation of extrasynaptic NMDA receptors. Neuron 43: 729 743.
9. Tian G-F, Azmi H, Takano T, Xu Q, Peng W, et al. (2005) An astrocytic basis of epilepsy. Nat Med 11: 973 981.
10. Fellin T, Gomez-Gonzalo M, Gobbo S, Carmignoto G, Haydon PG (2006) Astrocytic glutamate is not necessary for the generation of epileptiform neuronal activity in hippocampal slices. J Neurosci 26: 9312 9322.
11. Aronica E, van Vliet EA, Mayboroda OA, Troost D, da Silva FH, et al. (2000) Upregulation of metabotropic glutamate receptor subtype mGluR3 and mGluR5 in reactive astrocytes in a rat model of mesial temporal lobe epilepsy. Eur J Neurosci 12: 2333 2344.
12. Ulas J, Satou T, Ivins KJ, Kesslak JP, Cotman CW, et al. (2000) Expression of metabotropic glutamate receptor 5 is increased in astrocytes after kainate-induced epileptic seizures. Glia 30: 352 361.
13. D'Ambrosio R (2006) Does glutamate released by astrocytes cause focal epilepsy? Epilepsy Curr 6: 173 176.
14. Seifert G, Schilling K, Steinhauser C (2006) Astrocyte dysfunction in neurological disorders: a molecular perspective. Nat Rev Neurosci 7: 194 206.
15. Wetherington J, Serrano G, Dingledine R (2008) Astrocytes in the epileptic brain. Neuron 58: 168 178.
16. Pasti L, Volterra A, Pozzan T, Carmignoto G (1997) Intracellular calcium oscillations in astrocytes: a highly plastic, bidirectional form of communication between neurons and astrocytes in situ. J Neurosci 17: 7817 7830.
17. Carmignoto G, Pasti L, Pozzan T (1998) On the role of voltage-dependent calcium channels in calcium signaling of astrocytes in situ. J Neurosci 18: 4637 4645.
18. Steinhauser C, Jabs R, Kettenmann H (1994) Properties of GABA and glutamate responses in identified glial cells of the mouse hippocampal slice. Hippocampus 4: 19 35.
19. de Curtis M, Biella G, Buccellati C, Folco G (1998) Simultaneous investigation of the neuronal and vascular compartments in the guinea pig brain isolated in vitro. Brain Res Prot 3: 221 228.
20. Uva L, Librizzi L, Wendling F, de Curtis M (2005) Propagation dynamics of epileptiform activity acutely induced by bicuculline in the hippocampal-parahippocampal region of the isolated Guinea pig brain. Epilepsia 46: 1914 1925.
21. Gnatkovsky V, Librizzi L, Trombin F, de Curtis M (2008) Fast activity at seizure onset is mediated by inhibitory circuits in the entorhinal cortex in vitro. Ann Neurol 64: 674 686.
22. Uva L, Librizzi L, Marchi N, Noe F, Bongiovanni R, et al. (2008) Acute induction of epileptiform discharges by pilocarpine in the in vitro isolated guinea-pig brain requires enhancement of blood-brain barrier permeability. Neuroscience 151: 303 312.
23. Porter JT, McCarthy KD (1996) Hippocampal astrocytes in situ respond to glutamate released from synaptic terminals. J Neurosci 16: 5073 5081.
24. Jourdain P, Bergersen LH, Bhaukaurally K, Bezzi P, Santello M, et al. (2007) Glutamate exocytosis from astrocytes controls synaptic strength. Nat Neurosci 10: 331 339.
25. Lee CJ, Mannaioni G, Yuan H, Woo DH, Gingrich MB, et al. (2007) Astrocytic control of synaptic NMDA receptors. J Physiol 581: 1057 1081.
26. Shigetomi E, Bowser DN, Sofroniew MV, Khakh BS (2008) Two forms of astrocyte calcium excitability have distinct effects on NMDA receptor-mediated slow inward currents in pyramidal neurons. J Neurosci 28: 6659 6663.
27. Peters A, Palay SL, Webster HdF (1991) In: Press OU, ed. The fine structure of the central nervous system: neurons and their supportive cells. 3rd edition. New York (New York): Oxford University Press. pp 276 295.
28. Angulo MC, Kozlov AS, Charpak S, Audinat E (2004) Glutamate released from glial cells synchronizes neuronal activity in the hippocampus. J Neurosci 24: 6920 6927.
29. D'Ascenzo M, Fellin T, Terunuma M, Revilla-Sanchez R, Meaney DF, et al. (2007) mGluR5 stimulates gliotransmission in the nucleus accumbens. Proc Natl Acad Sci U S A 104: 1995 2000.
30. Perea G, Araque A (2005) Properties of synaptically evoked astrocyte calcium signal reveal synaptic information processing by astrocytes. J Neurosci 25: 2192 2203.
31. Demir R, Haberly LB, Jackson MB (1998) Voltage imaging of epileptiform activity in slices from rat piriform cortex: onset and propagation. J Neurophysiol 80: 2727 2742.
32. Tsau Y, Guan L, Wu JY (1998) Initiation of spontaneous epileptiform activity in the neocortical slice. J Neurophysiol 80: 978 982.
33. Woodhall G, Evans DI, Cunningham MO, Jones RS (2001) NR2B-containing NMDA autoreceptors at synapses on entorhinal cortical neurons. J Neurophysiol 86: 1644 1651.
34. Conti F, Minelli A, DeBiasi S, Melone M (1997) Neuronal and glial localization of NMDA receptors in the cerebral cortex. Mol Neurobiol 14: 1 18.
35. Lalo U, Pankratov Y, Kirchhoff F, North RA, Verkhratsky A (2006) NMDA receptors mediate neuron-to-glia signaling in mouse cortical astrocytes. J Neurosci 26: 2673 2683.
36. Serrano A, Haddjeri N, Lacaille JC, Robitaille R (2006) GABAergic network activation of glial cells underlies hippocampal heterosynaptic depression. J Neurosci 26: 5370 5382.
37. Kozlov AS, Angulo MC, Audinat E, Charpak S (2006) Target cell-specific modulation of neuronal activity by astrocytes. Proc Natl Acad Sci U S A 103: 10058 10063.
38. Ding S, Fellin T, Zhu Y, Lee SY, Auberson YP, et al. (2007) Enhanced astrocytic Ca^{2+} signals contribute to neuronal excitotoxicity after status epilepticus. J Neurosci 27: 10674 10684.
39. Parpura V, Basarsky TA, Liu F, Jeftinija K, Jeftinija S, et al. (1994) Glutamate-mediated astrocyte-neuron signalling. Nature 369: 744 747.
40. Bezzi P, Carmignoto G, Pasti L, Vesce S, Rossi D, et al. (1998) Prostaglandins stimulate calcium-dependent glutamate release in astrocytes. Nature 391: 281 285.

43

41. Pasti L, Zonta M, Pozzan T, Vicini S, Carmignoto G (2001) Cytosolic calcium oscillations in astrocytes may regulate exocytotic release of glutamate. J Neurosci 21: 477 484.
42. Mothet JP, Pollegioni L, Ouanounou G, Martineau M, Fossier P, et al. (2005) Glutamate receptor activation triggers a calcium-dependent and SNARE protein-dependent release of the gliotransmitter D-serine. Proc Natl Acad Sci U S A 102: 5606 5611.
43. Fiacco TA, McCarthy KD (2004) Intracellular astrocyte calcium waves in situ increase the frequency of spontaneous AMPA receptor currents in CA1 pyramidal neurons. J Neurosci 24: 722 732.
44. Perea G, Araque A (2007) Astrocytes potentiate transmitter release at single hippocampal synapses. Science 317: 1083 1086.
45. Henneberger C, Papouin T, Oliet SHR, Rusakov DA (2010) Long-term potentiation depends on release of D-serine from astrocytes. Nature 463: 232 236.
46. Kimelberg HK, Macvicar BA, Sontheimer H (2006) Anion channels in astrocytes: biophysics, pharmacology, and function. Glia 54: 747 757.
47. Zhang Z, Chen G, Zhou W, Song A, Xu T, et al. (2007) Regulated ATP release from astrocytes through lysosome exocytosis. Nat Cell Biol 9: 945 953.
48. Trevelyan AJ, Sussillo D, Yuste R (2007) Feedforward inhibition contributes to the control of epileptiform propagation speed. J Neurosci 27: 3383 3387.
49. Binder DK, Steinhauser C (2006) Functional changes in astroglial cells in epilepsy. Glia 54: 358 368.
50. Friedman A, Kaufer D, Heinemann U (2009) Blood-brain barrier breakdown-inducing astrocytic transformation: Novel targets for the prevention of epilepsy. Epilepsy Res 85: 142 149.
51. Araque A, Martín ED, Perea G, Arellano JI, Buño W (2002) Synaptically released acetylcholine evokes Ca^{2+} elevations in astrocytes in hippocampal slices. J Neurosci 22: 2443 2450.
52. Hirase H, Qian L, Barthó P, Buzsáki G (2004) Calcium dynamics of cortical astrocytic networks in vivo. PLoS Biol 2: e96. doi:10.1371/journal.pbio.0020096.
53. Wang X, Lou N, Xu Q, Tian GF, Peng WG, et al. (2006) Astrocytic Ca^{2+} signaling evoked by sensory stimulation in vivo. Nat Neurosci 9: 816 823.
54. Winship IR, Plaa N, Murphy TH (2007) Rapid astrocyte calcium signals correlate with neuronal activity and onset of the hemodynamic response in vivo. J Neurosci 27: 6268 6272.
55. Schummers J, Yu H, Sur M (2008) Tuned responses of astrocytes and their influence on hemodynamic signals in the visual cortex. Science 320: 1638 1643.
56. Perreault P, Avoli M (1991) Physiology and pharmacology of epileptiform activity induced by 4-aminopyridine in rat hippocampal slices. J Neurophysiol 65: 771 785.
57. Stasheff SF, Hines M, Wilson WA (1993) Axon terminal hyperexcitability associated with epileptogenesis in vitro. I. Origin of ectopic spikes. J Neurophysiol 70: 961 975.
58. Siniscalchi A, Calabresi P, Mercuri NB, Bernardi G (1997) Epileptiform discharge induced by 4-aminopyridine in magnesium-free medium in neocortical neurons: physiological and pharmacological characterization. Neuroscience 81: 189 197.
59. Barbarosie M, Avoli M (1997) CA3-driven hippocampal-entorhinal loop controls rather than sustains in vitro limbic seizures. J Neurosci 17: 9308 9314.
60. Librizzi L, de Curtis M (2003) Epileptiform ictal discharges are prevented by periodic interictal spiking in the olfactory cortex. Ann Neurol 53: 382 389.
61. Nolte C, Matyash M, Pivneva T, Schipke CG, Ohlemeyer C, et al. (2001) GFAP promoter-controlled EGFP-expressing transgenic mice: a tool to visualize astrocytes and astrogliosis in living brain tissue. Glia 33: 72 86.
62. de Curtis M, Pare D, Llinas RR (1991) The electrophysiology of the olfactory-hippocampal circuit in the isolated and perfused adult mammalian brain in vitro. Hippocampus 1: 341 354.
63. Nimmerjahn A, Kirchhoff F, Kerr JN, Helmchen F (2004) Sulforhodamine 101 as a specific marker of astroglia in the neocortex in vivo. Nat Methods 1: 31 37.

44

Computational model of neuron-astrocyte interactions during focal seizure generation

Davide Reato[1], Mario Cammarota[2], Lucas C. Parra[1] and Giorgio Carmignoto[2]*

[1] *Department of Biomedical Engineering, The City College of the City University of New York, New York, NY, USA*
[2] *Department of Experimental Biomedical Sciences, Institute of Neuroscience, Consiglio Nazionale delle Ricerche, University of Padova, Padova, Italy*

Edited by:
Vincenzo Crunelli, Cardiff University,
UK

Reviewed by:
Maxim Bazhenov, University of
California, USA
Francois David, Cardiff University,
UK

*Correspondence:
Giorgio Carmignoto, Department of
Experimental Biomedical Sciences,
Institute of Neuroscience, Consiglio
Nazionale delle Ricerche, University
of Padova, Padova, Italy.
e-mail: gcarmi@bio.unipd.it

Empirical research in the last decade revealed that astrocytes can respond to neurotransmitters with Ca^{2+} elevations and generate feedback signals to neurons which modulate synaptic transmission and neuronal excitability. This discovery changed our basic understanding of brain function and provided new perspectives for how astrocytes can participate not only to information processing, but also to the genesis of brain disorders, such as epilepsy. Epilepsy is a neurological disorder characterized by recurrent seizures that can arise focally at restricted areas and propagate throughout the brain. Studies in brain slice models suggest that astrocytes contribute to epileptiform activity by increasing neuronal excitability through a Ca^{2+}-dependent release of glutamate. The underlying mechanism remains, however, unclear. In this study, we implemented a parsimonious network model of neurons and astrocytes. The model consists of excitatory and inhibitory neurons described by Izhikevich's neuron dynamics. The experimentally observed Ca^{2+} change in astrocytes in response to neuronal activity was modeled with linear equations. We considered that glutamate is released from astrocytes above certain intracellular Ca^{2+} concentrations thus providing a non-linear positive feedback signal to neurons. Propagating seizure-like ictal discharges (IDs) were reliably evoked in our computational model by repeatedly exciting a small area of the network, which replicates experimental results in a slice model of focal ID in entorhinal cortex. We found that the threshold of focal ID generation was lowered when an excitatory feedback-loop between astrocytes and neurons was included. Simulations show that astrocytes can contribute to ID generation by directly affecting the excitatory/inhibitory balance of the neuronal network. Our model can be used to obtain mechanistic insights into the distinct contributions of the different signaling pathways to the generation and propagation of focal IDs.

Keywords: computational model, epilepsy, excitation/inhibition balance, neuron-astrocyte interaction, tripartite synapse

INTRODUCTION

The intracellular Ca^{2+} elevations occurring in cultured astrocytes in response to a glutamate challenge (Cornell-Bell et al., 1990) was the initial observation that hinted at the existence of a form of excitability in astrocytes based on cytosolic Ca^{2+} concentration changes. A few years later, Ca^{2+} elevations in astrocytes from both cell cultures (Parpura et al., 1994) and brain slices (Pasti et al., 1997) were observed to result in Ca^{2+} increases in nearby neurons mediated by astrocytic glutamate. Considering that astrocytes occupy non-overlapping spatial territories (Bushong et al., 2002; Halassa et al., 2007b) and that the processes of a single astrocyte can contact hundreds of synapses (Ventura and Harris, 1999), it was suggested that astrocyte-to-neuron communication may play a fundamental functional role in the brain. It was also found that astrocytes establish extensive contacts with cerebral blood vessels (Simard et al., 2003), which added further complexity to the functional role of neuron-to-astrocyte signaling. This neuron-astrocyte-blood-vessel signaling pathway was revealed to be central in neurovascular coupling, the process by which episodes of intense neuronal activity at restricted brain regions trigger local increases in cerebral blood flow to satisfy the energy demand of active neurons (Zonta et al., 2003; Mulligan and MacVicar, 2004; Gordon et al., 2008).

These pioneering results lead to the idea that astrocytes and neurons establish a bidirectional communication in the brain which may play fundamental roles in the modulation of synaptic transmission and plasticity (Carmignoto, 2000; Haydon, 2001).

Over the last decade numerous studies provided evidence for the ability of astrocytes to listen and talk to the synapse by exerting both excitatory and inhibitory actions on neurons (Araque et al., 1999; Brockhaus and Deitmer, 2002; Zhang et al., 2003; Pascual et al., 2005; Panatier et al., 2006; Serrano et al., 2006; Jourdain et al., 2007; Perea and Araque, 2007). These studies revolutionized our view of how the brain works. The processing of sensory information in the brain, which has been for many years considered to be based exclusively on neuronal communication, is now viewed as a product of the dynamic signals that neurons and astrocytes constantly exchange in the brain network.

Such a bidirectional communication between neurons and astrocytes was conceptualized in the tripartite synapses in which the astrocyte composes with the pre-synaptic terminal and the post-synaptic target neuron, a third functional element of the synapse (Araque et al., 1999; Carmignoto, 2000; Halassa et al., 2007a; Perea et al., 2009).

The discovery that astrocytes are crucially involved in normal brain function raised the intriguing possibility that these cells may be involved also in brain dysfunction. The observation that glutamate released by astrocytes evokes episodes of synchronous activity in small groups of nearby neurons (Fellin et al., 2004, 2006), was the first clue suggesting that gliotransmission represent a relevant non-neuronal mechanism for neuronal synchrony, which may ultimately favor the generation of focal epileptiform activity (Kang et al., 2005; Tian et al., 2005). A new experimental protocol was recently developed by our group in rat enthorinal cortex (EC) slices in order to reproduce the spatial and temporal features of focal epileptiform discharges (Gomez-Gonzalo et al., 2010; Losi et al., 2010). In this model, a pharmacological stimulation of neurons from a restricted cortical region induces a propagating seizure-like ictal discharge (ID). The ability to emulate an epileptogenic focus allows us to study the early cellular events that take place during the generation of epileptiform activity as it arises at a focal site and propagates to the surrounding brain tissue. By using this experimental protocol we recently provided evidence that neurons engage astrocytes into an excitatory loop that pushes the neuronal network toward the ID generation threshold (Gomez-Gonzalo et al., 2010).

There are currently many computational models of seizures generation, development and cessation (Pitkänen et al., 2006). The level of description ranges from mean field models (Wendling et al., 2002; Suffczynski et al., 2004) to biophysically detailed models (Destexhe, 1998; Bazhenov et al., 2004; Traub et al., 2005). We used here a simplified approach in the description of the dynamics of single neurons and astrocytes. With this simplified dynamics we implemented a computational network model that allowed us to investigate the network mechanisms of focal ID generation and the role of astrocytes at the onset of the ID.

We found that the positive feedback provided by the astrocytes influences the dynamics of the system and favors the generation of epileptiform activities. The computational model quantitatively reproduces the spatial and temporal features of ID generation and propagation and provides mechanistic insights into the astrocyte contribution.

METHODS

NEURON MODEL

The computational model aims to reproduce the behavior of a brain network that in response to NMDA pulse stimulation generates a focal ID (Losi et al., 2010). The network consists of 320 excitatory and 80 inhibitory neurons randomly disposed and synaptically connected in a 2D configuration. As in our previous work (Reato et al., 2010), we used Izhikevich's model (Izhikevich, 2003) to describe the dynamics of single neurons. Briefly, the voltage dynamics of single neurons is characterized

by four parameters: a, b, c, d as follows:

$$
\begin{aligned}
\frac{dv}{dt} &= 0.04v^2 + 5v + 140 - u + I = f(v, u) + I \\
\frac{du}{dt} &= a\,(bv - u)
\end{aligned}
\tag{1}
$$

With a reset of the dynamic variables u, v when a spike is generated:

$$
\text{if } v \geq 50 \text{ mV, then }
\begin{cases}
v \leftarrow c \\
u \leftarrow u + d
\end{cases}
\tag{2}
$$

The choice of values for the four parameters defines different spiking behaviors. The parameters were chosen to reproduce the behavior of a regular spiking neuron for excitatory neurons ($a = 0.02$, $b = 0.2$, $c = -65$, $d = 10$) and of a fast spiking neuron for inhibitory neurons ($a = 0.2$, $b = 0.26$, $c = -65$, $d = 0.5$). The variable I represents the sum of the synaptic current and the external stimulation.

The synaptic currents mimic AMPA, NMDA, $GABA_A$, and $GABA_B$ receptor activation following (Izhikevich and Edelman, 2008). Briefly, the synaptic conductances are described by first-order linear kinetics, $\frac{dg_x}{dt} = -\frac{g_x}{\tau_x} + \sum_j s_j \delta\left(t - t_f\right)$ (where $x = $ AMPA, NMDA, $GABA_A$, $GABA_B$) with, $\tau_{AMPA} = 1$ ms, $\tau_{NMDA} = 2000$ ms, $\tau_{GABA_A} = 6$ ms, $\tau_{GABA_B} = 150$ ms. Every time a pre-synaptic neuron m fires an action potential the conductance of the post-synaptic neurons increases instantaneously by $s = s_{exc}$ and $s = s_{inh}$ for pre-synaptic excitatory or inhibitory neurons respectively ($s_{exc} = 0.001$, $s_{inh} = 0.01$). The ratio of NMDA to AMPA receptors was set to be uniform at a value of 2, while $GABA_B$ to $GABA_A$ equal to 0.3 ($s_{exc} = 0.002$ for NMDA and $s_{inh} = 0.003$ for $GABA_B$). The synaptic current of a post-synaptic neuron is then given by:

$$
\begin{aligned}
I_{syn} &= I_{exc} + I_{inh} \\
I_{exc} &= g_{AMPA}\,(v_{exc} - v) \\
&\quad + g_{NMDA} \frac{[(v + 80)\,/60]^2}{1 + [(v + 80)\,/60]^2}\,(v_{exc} - v) \\
I_{inh} &= g_{GABA_A}\,(v_{inh} - v) + g_{GABA_B}\,(v_{inh} - v)
\end{aligned}
\tag{3}
$$

Where v (function of time, Equation 1) is the voltage of the post-synaptic neuron and v_{exc} and v_{inh} are the reversal potentials for excitatory and inhibitory synapses. Here we chose $v_{inh} = -90$ mV, $v_{exc} = 0$ mV. Each neuron receives excitatory inputs from a square of maximum 48 neighbors, while inhibition from maximum eight neurons. Using these parameters a single excitatory pre-synaptic spike induces a depolarization of maximum $\sim$0.1 mV, while an inhibitory pre-synaptic spike leads to maximum $\sim$0.5 mV hyperpolarization. All the main parameters of the simulations (the a, b, c, d parameters describing the dynamics of single neurons for both excitatory and inhibitory neurons and the s parameters for synaptic connections) were selected from a normal distribution with standard deviation equal to 1% of the average value. To mimic the onset of an ID, a few parameters of the network were chosen in order to place the network in a hyperexcitable state. The

46

excitability of excitatory neurons was slightly increased by injecting depolarizing currents (amplitude equal to 2), that could mimic the effects of 4-AP (a K^+ channel blocker) used in the slice preparation. The high values chosen for both the conductance and the time constant of NMDA currents aim to reproduce the low Mg^{2+} experimental conditions. Without stimulation, both excitatory and inhibitory neurons are completely silent.

The NMDA stimulation that in experimental slice preparations evoked an ID was simulated in the model by depolarizing a set of neurons within a 7×7 square area above threshold for 500 ms (49 neurons). We refer to this as a simulated pulse (SimP). Alternatively, the NMDA pulses could have been simulated by activating NMDA currents. However, since we are interested in analyzing the effects on NMDA currents during the ID onset, this would have resulted in "stimulation artifacts" (the NMDA current induced by the pulse). Since we were also interested in studying the mechanisms leading to ID generation, the intensity of the stimulation was set to a value that not necessarily induced an ID in all the simulations (see **Figure 3D**).

In each simulation, nine SimPs were applied. In unsuccessful simulations, the average firing rate in the network increases during each SimP, but it rapidly comes back to zero between successive SimPs. An ID was considered to be successfully generated when the firing rate in neurons remains sustained above 1 Hz. The ID onset was then defined as the number of SimPs which starts this process.

The cessation of the ID was obtained by a modulation of the parameter b in a firing specific way. More specifically, we assumed that an elevated spiking activity decreases the excitability of single neurons. Possible physiological correlates of this event are the inactivation of Na^+ channels (Bazhenov et al., 2004), the activation of Ca^{2+}- or Na^+-dependent K^+ channels (Alger and Nicoll, 1980; Schwindt et al., 1989; Bazhenov et al., 2004; Timofeev et al., 2004) or the exhaustion of metabolic support (Yamada et al., 2001; Kirchner et al., 2006).

The equation used is:

$$\frac{db}{dt} = -mR(t) + (b_s - b) \quad (4)$$

Where $R(t)$ is the spike train of a single neuron low-pass filtered (time constant equal to 150 s), m is the coupling constant between the spiking activity and b (chosen here to be 15), and b_s the value of b in resting conditions (no spiking activity). The second term in the equation can be thought as a driving force to recover the normal neuronal functionality of the neuron, for example the metabolic support.

Because of the hyperexcitability of the network, i.e., neurons are firing intensively at ID onset, we had to integrate Izhikevich's equations with the method proposed in Izhikevich (2010) assuming the time step to be 1 ms:

$$v(t+1) = \frac{v(t) + f(v(t), u(t)) + g(t)E(t) + I}{1 + g(t)} \quad (5)$$

Where $E(t) = \sum (g_i(t)E_i) / g(t)$ with $g(t) = \sum g_i(t)$ (the total sum of conductances) and $E_i = v_{exc}, v_{inh}$ for excitatory and inhibitory connections, respectively. This method is efficient and stable even for large synaptic currents.

"Excitation" refers to the sum of excitatory currents (AMPA and NMDA) averaged across neurons, and similarly "inhibition" refers to the average summed inhibitory currents (GABA$_A$ and GABA$_B$). Excitatory and inhibitory firing rate indicate the firing rate of excitatory and inhibitory neurons, respectively. Where otherwise indicated, excitation, inhibition and firing rates of single simulations were always filtered with a moving average filter using a 50 ms time window for better visualization. Postictal refractory period was estimated as the time between the end of the seizure (average firing rate back to zero) and the time at which the b variable recovers to the 95% of the initial value.

Under the conditions described above, our computational model is able to generate a neuronal network activity which resembles several characteristics of experimental focal IDs (see later in the "Results"):

(i) the simulated ID originates from a small number of neurons in the network and propagates outside the focal area with a delay (Traub and Wong, 1982; Avoli et al., 2002);

(ii) the simulated ID arises from an unbalance between inhibitory and excitatory activity at the focal area (Bradford, 1995; Ben-Ari, 2002);

(iii) the simulated IDs have a cessation and a similar average duration (Jefferys, 1990; Traub et al., 1993; Pinto et al., 2005);

(iv) the network enters into a period of postictal refractoriness (Jefferys, 1990);

(v) the peak in the firing rate of the excitatory and inhibitory neurons during simulated IDs is compatible with that measured in the *in vitro* experimental models.

Our model failed to reproduce the bursting behavior which characterizes the firing discharges in individual neurons and the two main phases in ID development, i.e., the initial tonic and the delayed clonic activity. However, the main focus in this computational model was to include astrocytes in the neuronal network and gain insights into how these non-neuronal cells can affect the equilibrium between excitation and inhibition in the network.

ASTROCYTE MODEL

We introduce here a simple representation of astrocytes interacting with a neuronal network. The parameters related to the ability of astrocytes to respond to neuronal activity with cytosolic Ca^{2+} elevations were captured from results obtained in experiments performed both in brain slices (Pasti et al., 1997; Porter and McCarthy, 1997) and in the living brain (Hirase et al., 2004; Wang et al., 2006; Kuga et al., 2011). To simulate the Ca^{2+} dynamics of a single astrocyte we used a framework similar to the Izhikevich neuron model. The equations represent a dynamical system of two variables [(Ca^{2+}) and φ], without non-linear action potential or reset. The set of equation describing the Ca^{2+} concentration

47

has the following form:

$$\frac{d\left[Ca^{2+}\right]}{dt} = -\varphi + \sum_j \sigma_j \delta\left(t - t_f\right)$$

$$\frac{d\varphi}{dt} = \alpha\left(\beta\left[Ca^{2+}\right] - \varphi\right) \qquad (6)$$

where φ is a recovery variable and σ_j is assumed here to be the neuronal input when an action potential is generated by the neuron j, since astrocytes respond to neuronal releases of glutamate (Pasti et al., 1997; Porter and McCarthy, 1997). Although the equations are dimensionless, the values σ_j where chosen to reproduce the pattern and amplitude of the Ca^{2+} elevations that are experimentally observed in astrocytes in response to neuronal activity (Porter and McCarthy, 1996; Pasti et al., 1997). The values of σ_j was chosen as been normally distributed with mean 0.00083 and standard deviation equal to 1% of the mean. Ca^{2+} concentration was restricted to be non-negative. Similarly to the dynamics described by the Izhikevich's single neuron, different values of α and β determine different behaviors (time constant of changes and coupling with the recovery variable). Here we chose $\alpha = 0.001$ and $\beta = 0.01$. This choice was made to reproduce the slow time course of Ca^{2+} changes in astrocytes (Kawabata et al., 1996). When astrocytes were included in the whole network, these values were chosen to be normally distributed with a standard deviation equal to 1% of the mean.

To describe the release of astrocytic glutamate triggered by Ca^{2+} elevations, we considered a first order dynamics (low pass filters), with a release of glutamate that can occur only when Ca^{2+} reach a threshold (Pasti et al., 1997; Parpura and Haydon, 2000; Pasti et al., 2001):
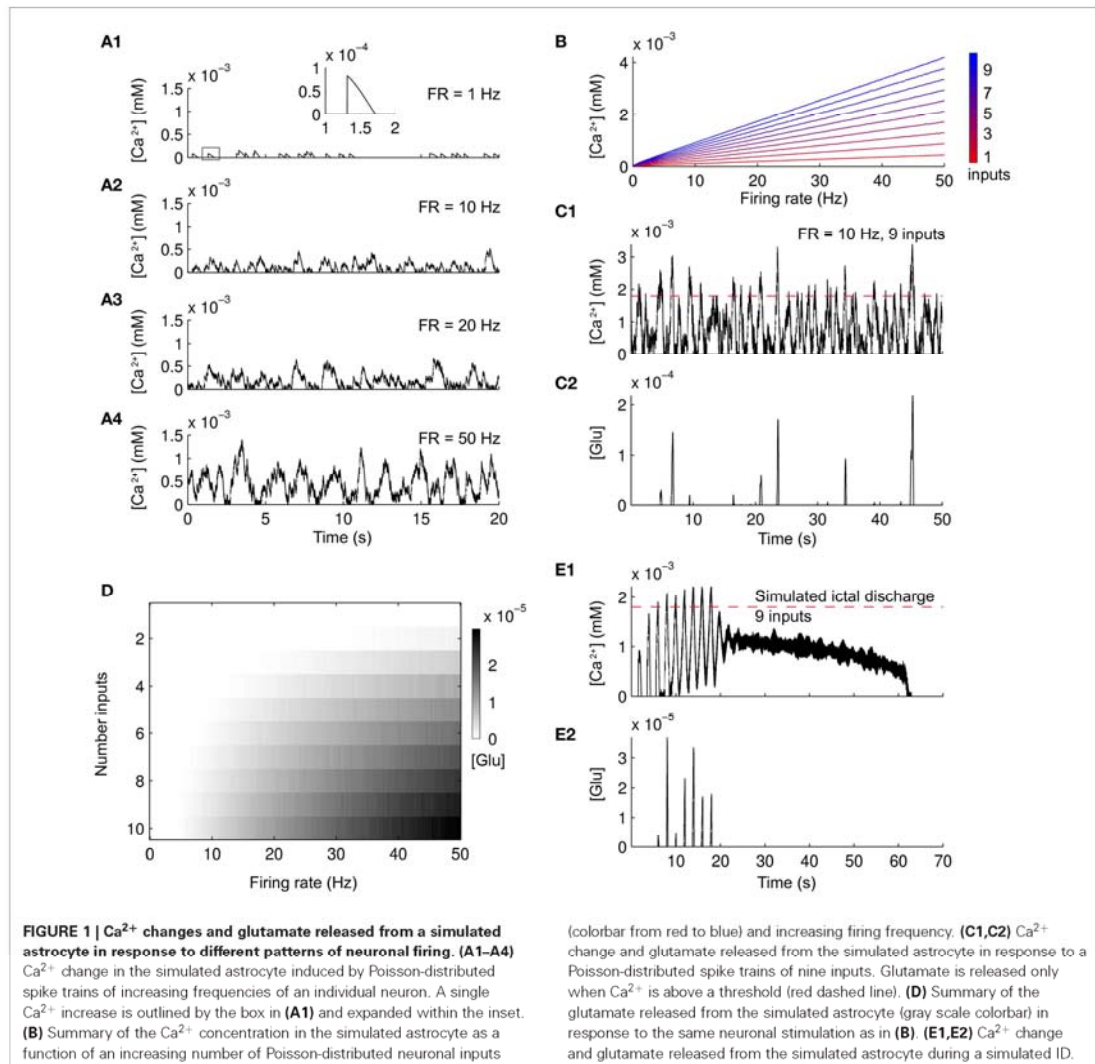
$$\mu\frac{d\left[glu\right]}{dt} = \begin{cases} -\left[glu\right] + \left(\left[Ca^{2+}\right] - \left[Ca^{2+}\right]_{th}\right) - \kappa\lambda \\ \qquad\qquad\qquad\qquad\quad \text{if } \left[Ca^{2+}\right] > \left[Ca^{2+}\right]_{th} \\ -\left[glu\right] - \kappa\lambda \qquad \text{otherwise} \end{cases} \qquad (7)$$

$$\eta\frac{d\lambda}{dt} = -\lambda + \left[glu\right]$$

Where $\left[Ca^{2+}\right]_{th} = 0.0018\,mM$ is the threshold for glutamate release, $\kappa = 200$ describes the coupling between the glutamate concentration [glu] and the recovery variable λ. Glutamate concentration was imposed to be non-negative. The time constants for the two variables were $\mu = 0.5\,s$ and $\eta = 10\,s$. The value of $\left[Ca^{2+}\right]_{th}$ was set based on available data showing that an increase in astrocytic Ca^{2+} of a few hundreds of nM was able to trigger glutamate release (Parpura and Haydon, 2000). Assuming a value of 200 nM for a single synapse (Nadkarni and Jung, 2003) and considering that astrocytes in our model receive inputs from a maximum of nine neurons, the threshold value can be determined by multiplying the value for the single synapse by the number of inputs, as considered in other studies (Wade et al., 2011).

The set of parameters used for a single astrocyte reproduces basic features of Ca^{2+} dynamics and glutamate release in astrocytes. Increasing the input to an astrocyte, simulated as

Poisson-distributed spike trains of increasing frequencies, leads to increasing Ca^{2+} concentrations (**Figures 1A1–A4**). The Ca^{2+} increase due to a single spike is less than 100 nM and lasts for about half a second (inset in **Figure 1A1**). These results are compatible with experimental evidences (Pasti et al., 1997; James et al., 2011) and previous computational models (Jefferys, 2003; Nadkarni and Jung, 2004, 2007; Wade et al., 2011). The linear dependence of Ca^{2+} increases as a function of simulated firing rate is reported in **Figure 1B**. Increasing the number of inputs by summing up Poisson-distributed spike trains (color scale from red to blue) also elevated Ca^{2+} concentrations. Since the release of glutamate due to the Ca^{2+} increases occurs only when Ca^{2+} is above a threshold, only strong activation can drive the release. As an example, nine spike trains at 10 Hz induced transient releases of glutamate (**Figures 1C1,C2**, Ca^{2+} threshold in red). **Figure 1D** summarizes the dependence of glutamate released by the astrocyte as a function of the firing rate and the number of inputs. For very low firing rates, there is no astrocytic glutamate release independently on the number of inputs. In the case of high firing rates, the release is linearly dependent on both the number of inputs and the firing rate. To further validate the parameters that we choose, we stimulated single astrocytes with a spike train from nine neurons from a simulated ID (see later in the "Results"). The neuronal activity leads to Ca^{2+} increases in the astrocyte (**Figure 1E1**) that caused a glutamate release (**Figure 1E2**) only after the second pulse (see also below). Interestingly, when the ID was fully developed, Ca^{2+} elevations reached a steady state value and glutamate was no longer released. It is known from experiments in cultures and in brain slices (Pasti et al., 1997; James et al., 2011) that upon intense stimulation the Ca^{2+} level in astrocytes increases rapidly and remains at an elevated steady-state value for tens of seconds (**Figure 1E1**). A single episode of glutamate release is experimentally observed only after the initial Ca^{2+} rise.

Astrocytes were included in the network with a 1:1 ratio with neurons. The ratio of glia to neurons increases in phylogenesis and is 1.65 in the human frontal cortex (Oberheim et al., 2006; Sherwood et al., 2006). Given that astrocytes account for about 50% of the total number of glial cells, a 1:1 ratio seems to represent an acceptable approximation. The input from neuronal activity, σ for each m astrocyte, was considered as the excitatory input from neurons firing $s_{exc}(m)$ (the excitatory component) in a 3×3 square (inputs from nine excitatory neurons). This choice was made considering that the feedback of astrocytes on neuronal activity is thought to be local with four to eight neuronal somata enveloped by a single astrocyte (Halassa et al., 2007b), but with the processes from a single astrocyte associated with up to 600 dendrites and many thousands of synapses (Bushong et al., 2002; Oberheim et al., 2006). The glutamate released by astrocytes was used as input to the same neurons to which the astrocyte is exposed. This glutamate generated NMDA currents in these neurons by activating the NMDA channel (in the same way than s_{exc}). In some simulations (see "Results") we considered the effects of inhibitory inputs from astrocytes. This was done by considering that the astrocytic response activate GABA$_A$ receptors instead of NMDA (so simulating the effect of GABA release).

48

FIGURE 1 | Ca²⁺ changes and glutamate released from a simulated astrocyte in response to different patterns of neuronal firing. (A1–A4) Ca²⁺ change in the simulated astrocyte induced by Poisson-distributed spike trains of increasing frequencies of an individual neuron. A single Ca²⁺ increase is outlined by the box in **(A1)** and expanded within the inset. **(B)** Summary of the Ca²⁺ concentration in the simulated astrocyte as a function of an increasing number of Poisson-distributed neuronal inputs (colorbar from red to blue) and increasing firing frequency. **(C1,C2)** Ca²⁺ change and glutamate released from the simulated astrocyte in response to a Poisson-distributed spike trains of nine inputs. Glutamate is released only when Ca²⁺ is above a threshold (red dashed line). **(D)** Summary of the glutamate released from the simulated astrocyte (gray scale colorbar) in response to the same neuronal stimulation as in **(B)**. **(E1,E2)** Ca²⁺ change and glutamate released from the simulated astrocyte during a simulated ID.

All the simulations were performed using MATLAB (Mathworks), and the code is available at www.neuralengr. com/code.

RESULTS

FOCAL ID GENERATION IN ENTORHINAL CORTEX SLICES

As we previously reported (Losi et al., 2010), an episode of neuronal hyperactivity can generate a focal ID in EC slices perfused with the K⁺ channel blocker 4-aminopyridine (4-AP) and low Mg²⁺. **Figure 2** illustrates a typical ID that was generated in cortical layer V-VI by a double brief pressure pulse applied to an NMDA-containing glass pipette (**Figures 2A,B**).

Dual patch-clamp recordings revealed that the firing in neurons located within the focus (**Figure 2C**, neuron 1) evolved into a focal ID with some delay after the NMDA double pulse. Following the ID generation at the focus (**Figure 2A**, gray circle), neurons outside the focus (<400 μm from the NMDA pipette tip) were also recruited and exhibited a similar pattern of action potential firing (**Figure 2C**, neuron 2). Given that the somatic Ca²⁺ change in neurons reflects faithfully the action potential firing in these cells, in slices loaded with the Ca²⁺ sensitive dye Oregon Green BAPTA1-AM (OG-B1-AM) we could monitor the activity of tens of neurons and follow how a focal ID is generated in the neuronal network. These experiments revealed that the NMDA stimulation

49

FIGURE 2 | Experimental protocol for inducing focal IDs in brain slices.
(A) Schematic of a dual voltage-clamp recording from EC deep layers
pyramidal neurons (PyNs) with indication of the NMDA pipette and the patched
neurons (1,2), one within the region directly activated by NMDA (gray circle)
and the other immediately outside (~200 and ~350 μm from the NMDA
pipette respectively). **(B)** DIC image of the area marked by the dashed box in
(A). Scale bar 100 μm. **(C)** Dual current-clamp recording from two PyNs during
a focal ID evoked by a double NMDA pulse (arrowheads). The vertical dashed
line marks the generation of ID in both cells. Note that in neuron 1 the direct
NMDA response precedes and partially masks the ID onset. **(D)** Schematic of

an experiment similar to that reported in **(A)** showing the region of Ca^{2+} signal
imaging (blue box). The image of the basal OGB1 fluorescence in the EC (t_0)
and the difference images of the fluorescence signal change captured at
different times (see lower traces) during an evoked ID (t_1-t_0; t_2-t_0) are
reported. The NMDA-pipette is visible on the left. The dashed line in the image
t_1-t_0 marks the region directly activated by NMDA. Scale bar 100 μm. Lower
traces show the Ca^{2+} signal change from two neurons that were directly
activated by NMDA (upper traces) and two other neurons, located outside the
region directly activated by NMDA, that exhibited the ID only (lower traces).
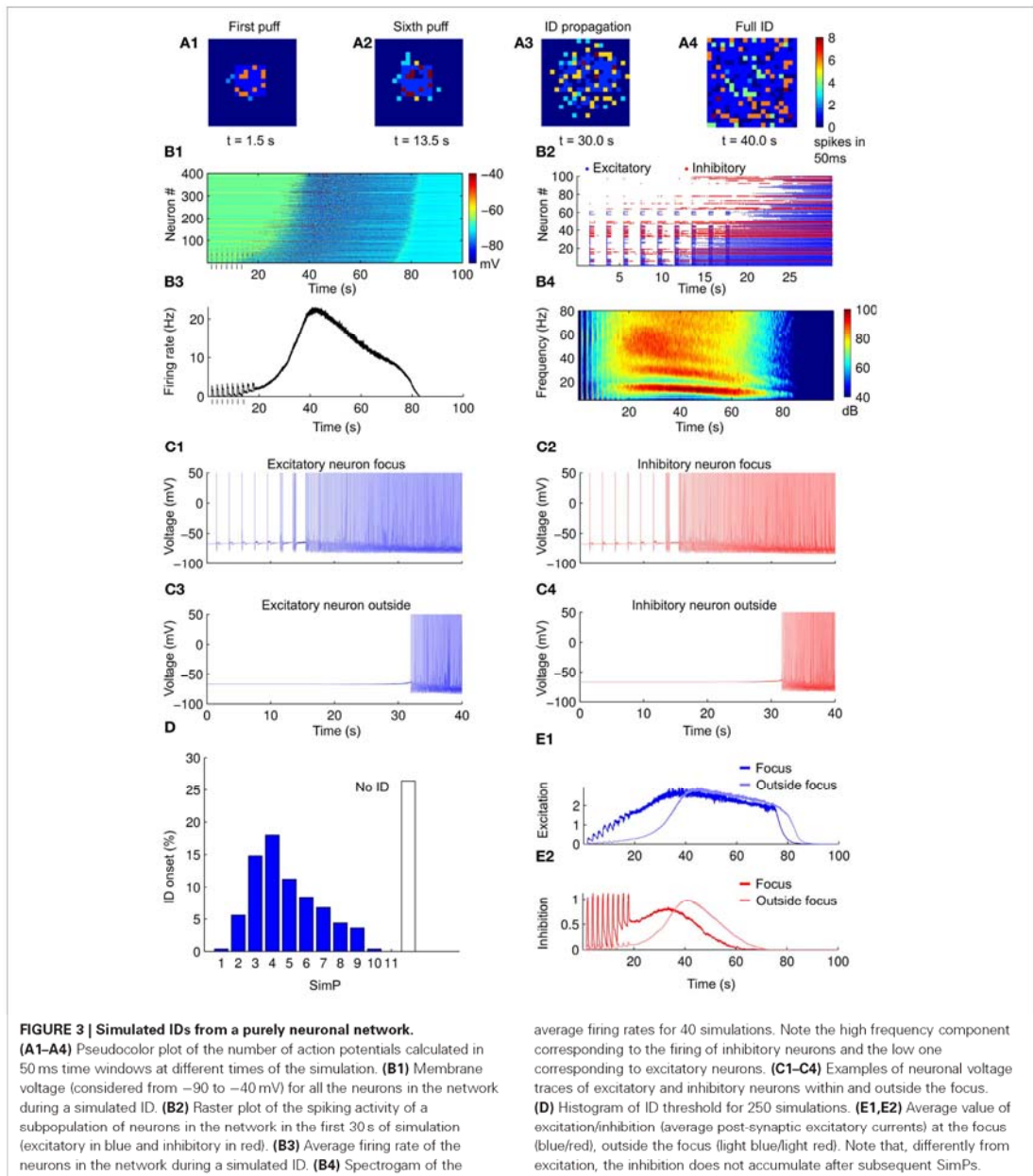The timing that corresponds to the different images (t_0, t_1, and t_2) is reported.

evoked a rapid Ca^{2+} elevation in neurons located within the focal
area, while neurons from the surrounding network were recruited
into the ID only after a delay of 10.9 ± 0.8 s (30 IDs from 15
slices).

FOCAL ID GENERATION IN THE NEURONAL NETWORK MODEL
In the model we first examined how the neuronal network
responds to a sequence of simulated NMDA pulses in the
absence of astrocytes. To mimic the NMDA pulses at the focus,
a depolarizing current pulse was injected for 500 ms in an
area of 7×7 neurons (see "Methods"). The first SimP evoked
robust spiking activity that remained restricted to neurons of the
focus (**Figure 3A1**). Upon successive SimPs the firing activity

spread from the focus to the surrounding neurons approximately
10 s after the SimP onset (**Figures 3A1–A4,B1**). The neuronal
firing discharge remained high thereafter for tens of seconds
(61 ± 2 s) before a sudden cessation (**Figure 3B1**). A postictal
refractory period was observed with an average duration of
266 ± 1 s (see "Methods"). This pattern of activity resembles
the focally evoked ID in slice preparations (see **Figure 2D**). A
raster plot of the activity in a subpopulation of excitatory and
inhibitory neurons within and outside the focus revealed that
inhibitory neurons fire more intensively as compared to excitatory
neurons during the SimPs, while the spiking activity in exci-
tatory neurons increases with successive SimPs (**Figure 3B2**).
The peak of the activity in the whole network was reached

50

FIGURE 3 | Simulated IDs from a purely neuronal network.
(A1–A4) Pseudocolor plot of the number of action potentials calculated in 50 ms time windows at different times of the simulation. (B1) Membrane voltage (considered from −90 to −40 mV) for all the neurons in the network during a simulated ID. (B2) Raster plot of the spiking activity of a subpopulation of neurons in the network in the first 30 s of simulation (excitatory in blue and inhibitory in red). (B3) Average firing rate of the neurons in the network during a simulated ID. (B4) Spectrogram of the

average firing rates for 40 simulations. Note the high frequency component corresponding to the firing of inhibitory neurons and the low one corresponding to excitatory neurons. (C1–C4) Examples of neuronal voltage traces of excitatory and inhibitory neurons within and outside the focus. (D) Histogram of ID threshold for 250 simulations. (E1,E2) Average value of excitation/inhibition (average post-synaptic excitatory currents) at the focus (blue/red), outside the focus (light blue/light red). Note that, differently from excitation, the inhibition does not accumulate after subsequent SimPs.

during the ID (**Figure 3B3**) and its spectrogram clearly revealed two main components corresponding to the different activity in excitatory and inhibitory neurons that fire at about 15 and 60 Hz, respectively (**Figure 3B4**). This pattern of activity in the two neuronal populations is consistent with experimental

observations (Ziburkus et al., 2006). While both excitatory and inhibitory neurons at the focus were activated upon the initial stimulation (representative traces in **Figures 3C1,C2**), neurons outside the focus were recruited into the propagating ID with some delay (representative traces in **Figures 3C3,C4**).

51

ID GENERATION THRESHOLD

We consider as ID threshold the number of NMDA pulses that are needed to evoke an ID. This value is constant for a given slice (Gomez-Gonzalo et al., 2010), but it can vary for different slices. Simulations with different parameters (see "Methods") showed that an ID could be generated in average by five SimPs and in more than 25% of cases no IDs could be evoked regardless the number of applied SimPs (**Figure 3D**, $n = 250$ simulations). The successive SimPs induced excitatory responses at the focus with increasing amplitude (**Figure 3E1**). The excitatory and inhibitory neurons outside the focus were not directly activated by the SimPs and increased their firing activity simultaneously, but with a marked delay (**Figures 3E1,E2**).

DYNAMICS OF EXCITATION AND INHIBITION AT THE FOCUS EXPLAIN ID GENERATION

We next investigated the interplay between excitation and inhibition in the genesis of the ID. We compared the simulations which successfully evoked an ID with those that failed to evoke an ID (in the different simulations excitatory and inhibitory neurons were randomly located within or outside the focus while maintaining their total number). For the cases in which an ID was successfully generated, we find that the ratios between the number of excitatory and inhibitory neurons, the average inhibitory and excitatory currents during the first SimP and the firing rate of inhibitory and excitatory neurons in the same time interval were lower compared to cases where an ID was not successfully generated (**Figures 4A1–A3**).

We next tested whether a different strength in either excitation or inhibition at the focus changed the efficacy of the SimP in generating an ID. We analyzed the time course of excitation and inhibition at the focus and the average firing rate in the whole network. We examined three sets of network parameters chosen at random, but leading to different ID thresholds, i.e., no ID generation, high ID threshold (five SimPs) and low ID threshold (three SimPs) (**Figures 4B–D** respectively). In all cases, excitatory and inhibitory drive increased the firing rate (**Figures 4B2,B3,C2,C3,D2,D3**). A detailed analysis of the dynamics revealed that after each SimP both excitation and inhibition were strongly but transiently activated (**Figures 4B1,C1,D1**). An important difference is that, in contrast to inhibition, excitation failed to recover the initial basal conditions, including the simulations in which no ID is generated (**Figure 4B**). An additional striking difference between the three examples is the maximal inhibition level provided by the inhibitory neurons (the dynamic range). Inhibition reached its highest value in the high ID threshold condition. These results support the view that inhibition strength is a critical factor for focal ID onset. Notably, excitation rose faster than inhibition (slope > 1) driving the growth in firing rate forward. However, the ID occurred only after inhibition reached its maximal value (all inhibitory neurons were active). Therefore the ratio of excitatory versus inhibitory drive and the limiting dynamic range of inhibition are the two critical factors in ID generation. As a summary of results obtained, we report the distribution of points in the excitation-inhibition plane at the focus during the first seven SimPs in 250 Monte-Carlo simulations for the cases that
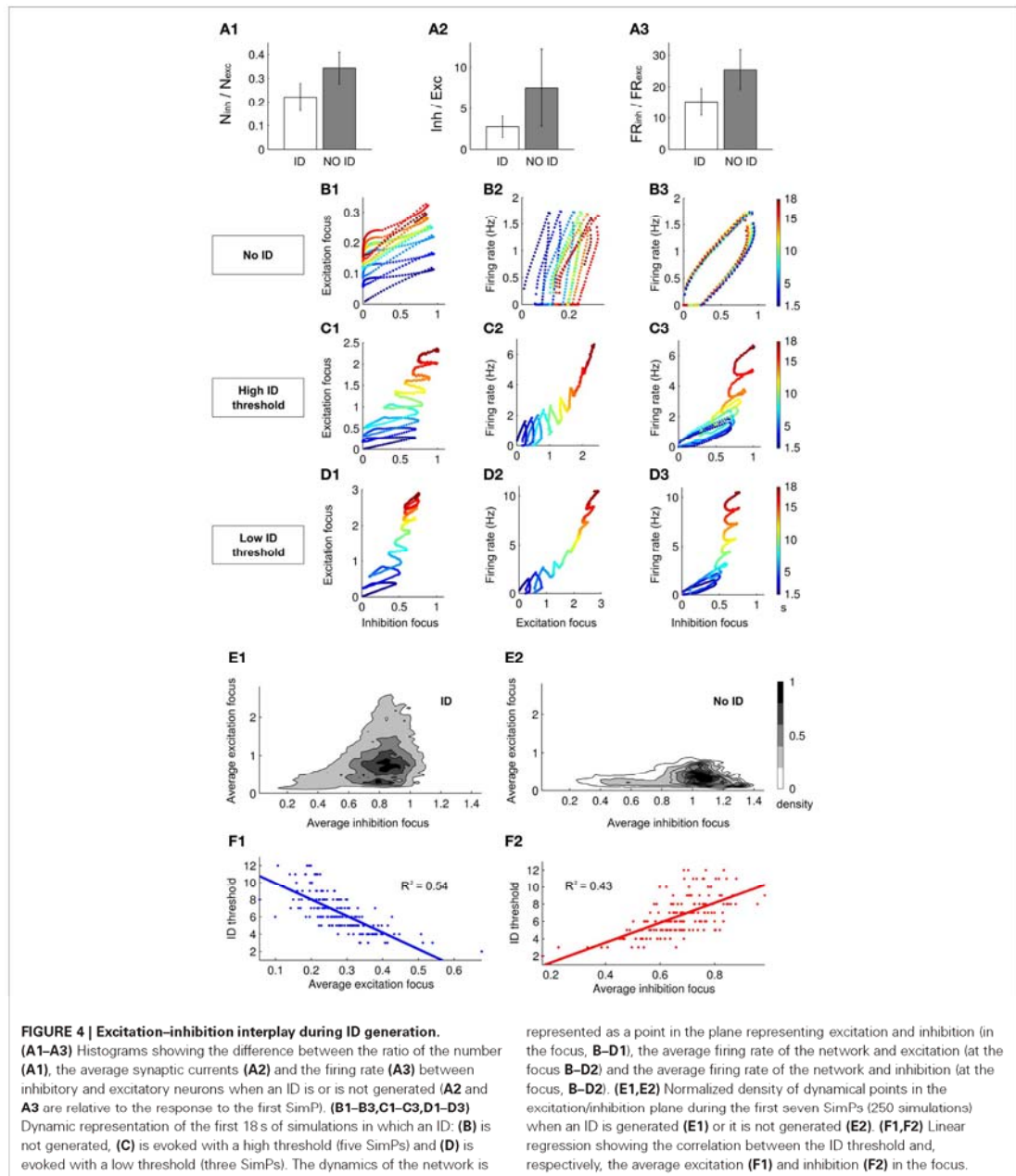
evoked or failed to evoke an ID (normalized by the total area; **Figures 4E1,E2**). When inhibition at the focus reached high values, no IDs were generated and the ratio between excitation and inhibition remained low. This stands in contrast to the cases which lead to IDs, further supporting the notion that the relationship between excitation and inhibition determines not only the threshold for ID generation, but also whether or not an ID could be evoked. Data obtained from 250 runs also showed a clear correlation between the ID threshold and the average excitation and inhibition in the network during the first SimP (**Figures 4F1,F2**). This indicates that the overall response of the network, in terms of excitation and inhibition levels, is a good predictor of ID threshold: an increased excitation results in the lowering of the ID threshold and an opposite relationship holds for inhibition.

ASTROCYTE-TO-NEURON SIGNALING DECREASES THE ID THRESHOLD

The model of the single astrocyte (see "Methods") was incorporated into the network to test how astrocytes may affect ID threshold. Specifically, 400 astrocytes were added to the network model in a parallel 2D sheet of cells (see "Methods"). Astrocytes provide an excitatory feedback to neuronal activity in a Ca^{2+}-dependent way (**Figure 5A**). As illustrated in **Figure 5B**, in the presence of the astrocyte feedback signal, the ID was evoked by two SimPs, while in its absence a more intense stimulation of neurons was necessary. As illustrated in **Figures 5F1,F2** the Ca^{2+} change from a representative astrocyte at the focus was observed to follow rapidly the spiking activity in neurons (**Figures 5C1,F1**), and astrocytic glutamate release occurred upon the second SimP (**Figure 5C2**). The average astrocytic Ca^{2+} follow the neuronal activity (example in **Figure 5D1**) while the average glutamate release occurs transiently (**Figure 5D2**). The Ca^{2+} change and the release of glutamate from astrocytes outside the focus failed to affect focal ID threshold. The results from 250 Monte-Carlo runs show that the ID threshold was lowered after including the astrocytic feedback signal to neurons (**Figure 5E**). Once the ID was fully evolved, both the Ca^{2+} change and the release of glutamate from astrocytes within and outside of the focus did not differ significantly (**Figures 5F1,F2**). However, the initially dominant activity of astrocytes at the focus was followed by an activity of the astrocytes outside the focus that became dominant immediately after the ID onset. These results are consistent with those from slice experiments which showed that when Ca^{2+} elevation in astrocytes from the focus were selectively blocked (by the Ca^{2+} chelator BAPTA) or stimulated (by TFLLR, a peptide agonist of thrombin PAR-1 receptors), the threshold of ID generation increased or decreased, respectively (Gomez-Gonzalo et al., 2010).
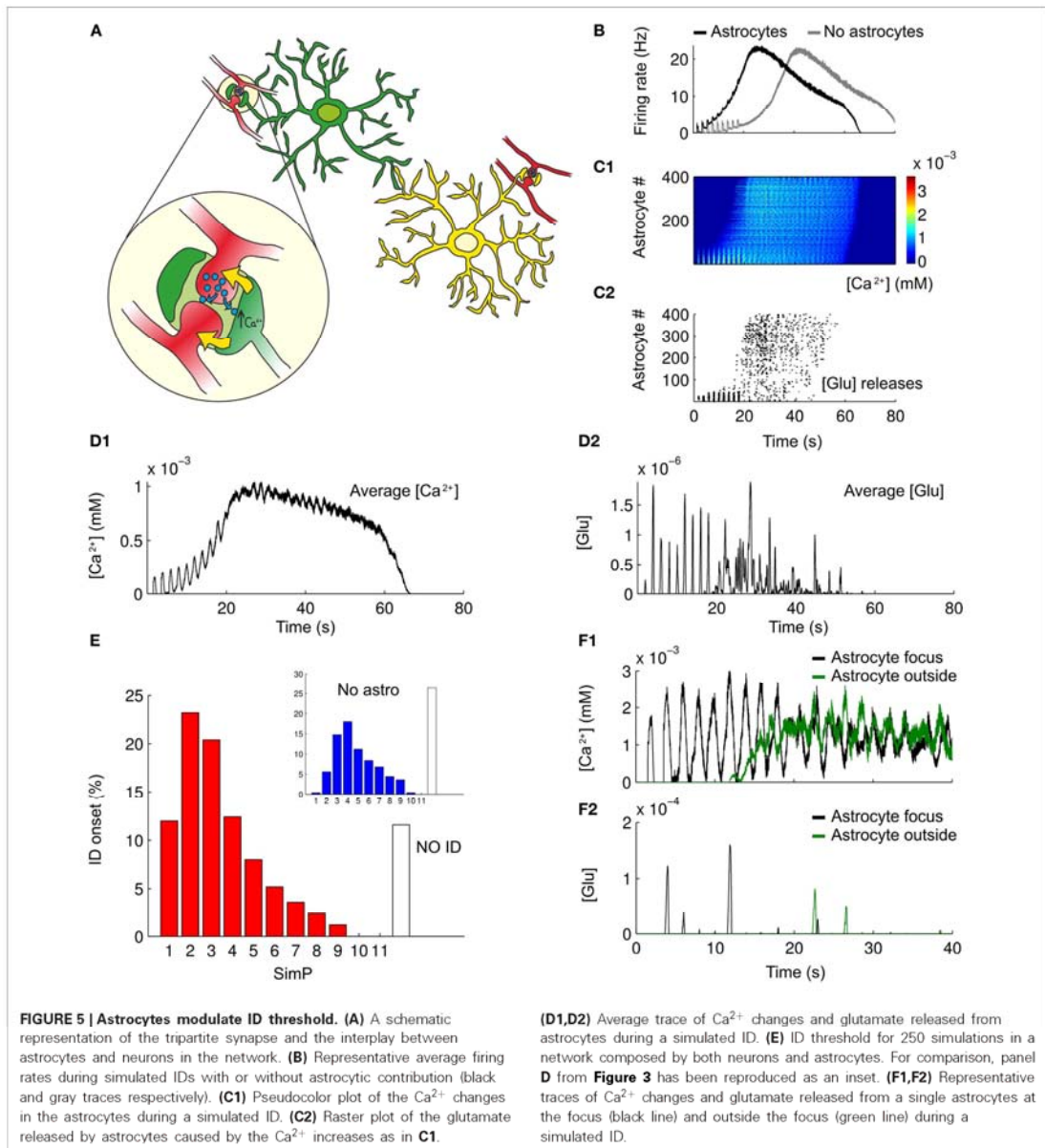
DOES AN ASTROCYTE INHIBITORY FEEDBACK SIGNAL TO NEURONS AFFECT ID THRESHOLD?

The ID threshold is mainly affected by the interplay between excitation and inhibition. Indeed, as we reported above, ID threshold can be increased by increasing the overall value of the inhibitory activity. The bar graph in **Figure 6A** reports the results from 250 simulations in different simulation settings, with and without an astrocytic contribution (mean and errors represent the results of a Poisson fit to the ID threshold distributions), while **Figure 6B**

52

FIGURE 4 | Excitation–inhibition interplay during ID generation.
(A1–A3) Histograms showing the difference between the ratio of the number (A1), the average synaptic currents (A2) and the firing rate (A3) between inhibitory and excitatory neurons when an ID is or is not generated (A2 and A3 are relative to the response to the first SimP). (B1–B3,C1–C3,D1–D3) Dynamic representation of the first 18 s of simulations in which an ID: (B) is not generated, (C) is evoked with a high threshold (five SimPs) and (D) is evoked with a low threshold (three SimPs). The dynamics of the network is represented as a point in the plane representing excitation and inhibition (in the focus, B–D1), the average firing rate of the network and excitation (at the focus, B–D2) and the average firing rate of the network and inhibition (at the focus, B–D2). (E1,E2) Normalized density of dynamical points in the excitation/inhibition plane during the first seven SimPs (250 simulations) when an ID is generated (E1) or it is not generated (E2). (F1,F2) Linear regression showing the correlation between the ID threshold and, respectively, the average excitation (F1) and inhibition (F2) in the focus.

is the cumulative sum of the ID threshold distributions corresponding to the analyzed cases. Blue and red bars show that the ID threshold can be increased by increasing the overall strength of inhibitory connect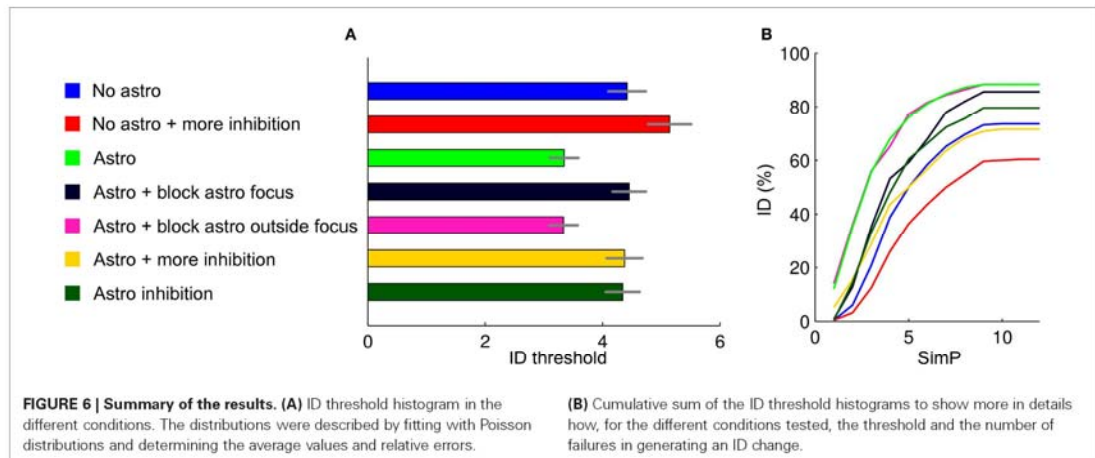ions (in this case from 0.01 to 0.015) in a purely neuronal network (no astrocytes). With higher inhibition, the simulated stimulation failed to induce an ID in 40% of simulations (**Figure 6B**). As already shown, the introduction of an astrocytic excitatory feedback lowers the ID threshold (green

53

FIGURE 5 | Astrocytes modulate ID threshold. (A) A schematic representation of the tripartite synapse and the interplay between astrocytes and neurons in the network. **(B)** Representative average firing rates during simulated IDs with or without astrocytic contribution (black and gray traces respectively). **(C1)** Pseudocolor plot of the Ca^{2+} changes in the astrocytes during a simulated ID. **(C2)** Raster plot of the glutamate released by astrocytes caused by the Ca^{2+} increases as in **C1**. **(D1,D2)** Average trace of Ca^{2+} changes and glutamate released from astrocytes during a simulated ID. **(E)** ID threshold for 250 simulations in a network composed by both neurons and astrocytes. For comparison, panel **D** from **Figure 3** has been reproduced as an inset. **(F1,F2)** Representative traces of Ca^{2+} changes and glutamate released from a single astrocytes at the focus (black line) and outside the focus (green line) during a simulated ID.

bar) and decreases the number of failures to about 10%. In slice experiments we observed that the inhibition of Ca^{2+} signals in astrocytes at the focus, but not outside the focus, increased the threshold of ID generation. These observations were fully reproduced in the computational model (dark blue and magenta bars) without further manipulations of the model over the results from the previous section. Astrocytic excitatory feedback in a network

with stronger inhibitory connections (0.015 as for the red bar) brings back to baseline the ID threshold (yellow).

To explore other factors that may affect ID threshold, we considered the possibility that the activation of astrocytes, or of a subpopulation of astrocytes, results in a release of GABA that can lead to an overall increase of the inhibition strength in the neuronal network. Astrocytes can, indeed, release GABA

54

FIGURE 6 | Summary of the results. (A) ID threshold histogram in the different conditions. The distributions were described by fitting with Poisson distributions and determining the average values and relative errors. **(B)** Cumulative sum of the ID threshold histograms to show more in details how, for the different conditions tested, the threshold and the number of failures in generating an ID change.

(Kozlov et al., 2006; Lee et al., 2011; Le Meur et al., 2012). As expected, when we included an astrocytic GABA release in the model, the threshold for ID generation increased (**Figure 6**, dark green). Note that this was an inhibitory-only feedback involving only GABA release and no glutamate. Surprisingly, however, the threshold for ID generation did not rise over the baseline condition with no astrocytic feedback (blue). A possible explanation for this could be the synchronizing action of an inhibitory GABA signal. Alternatively, the inhibitory feedback signal from astrocytes could be more effective in suppressing inhibitory than excitatory neurons. This action may ultimately generate a new level of complexity in the mechanism that governs the inhibition/excitation balance in the neuron-astrocyte network.

DISCUSSION
Increasing experimental evidence highlights the physiological significance of the tripartite synapse in which the astrocyte senses neurotransmitter release and, in turn, releases through a Ca^{2+}-dependent mechanism gliotransmitters that have feedback modulatory actions on neurons. A number of recent studies *in vitro* and *in vivo* showed that the release of glutamate from astrocytes can, indeed, control both the basal excitability of neurons and some forms of long-term potentiation of synaptic strength (Serrano et al., 2006; Jourdain et al., 2007; Navarrete and Araque, 2010; Santello et al., 2011; Min and Nevian, 2012) and long-term depression (Zhang et al., 2003; Serrano et al., 2006; Han et al., 2012; Min and Nevian, 2012). The contribution of gliotransmission to brain dysfunctions remains, however, poorly understood. A model composed of a network of interacting neurons and astrocytes represents a useful tool in which the spatial-temporal features of focal seizure generation observed in slice models can be replicated and new mechanistic hypotheses can be tested.

Over the last 10 years, different models have been advanced to describe the Ca^{2+} dynamics of astrocytes in response to neuronal signals (Nadkarni and Jung, 2003, 2007; Silchenko and Tass, 2008; Di Garbo, 2009). These biophysical approaches described not only the astrocytic Ca^{2+} response (Li and Rinzel, 1994), but

also the possible feedback to neurons. More recently, the possible contribution of astrocytes in events related to the plasticity of synaptic transmission were also included in models (Nadkarni et al., 2008; De Pittà et al., 2011; Wade et al., 2011). While biophysical models are very useful to simulate basic units, like the tripartite synapse, they are hardly suitable for large scale simulations. In contrast, simplified models that include only the basic features of neuron-astrocyte interactions (Postnov et al., 2009) appear more appropriate to describe network dynamics and to investigate the role of astrocytes in epilepsy (Amiri et al., 2012). In our model we did not include any distinct biophysical features that characterize the physiological actions of either neurons or astrocytes. We rather describe the activity of a single astrocyte in terms of the specific input-output signals with which astrocyte and neurons interact. This simplified astrocyte model was then embed in a neuronal network model of IDs based on the Izhikevich's single neuron model.

The slow kinetics of the astrocyte Ca^{2+} response to neuronal activity in the model reflect those of the mGluR-mediated Ca^{2+} elevations that were evoked in astrocytes by axonal afferent stimulation in young rat hippocampal slices (Porter and McCarthy, 1995; Pasti et al., 1997; Perea and Araque, 2005). Indeed, the intracellular Ca^{2+} variations in astrocytes depend primarily, although not exclusively, on activation of metabotropic receptors, phospholipase C-dependent inositol(1,4,5)-trisphosphate (IP3) production and, finally, stimulation of Ca^{2+} release from IP3-sensitive internal Ca^{2+} stores (Kawabata et al., 1996). Glutamate release at the synapse triggers a Ca^{2+} response in astrocytes that increases in both amplitude and frequency of oscillations according to increased levels of the neuronal activity (Pasti et al., 1997). These Ca^{2+} changes trigger a SNARE-dependent exocytosis of glutamate that signals back to affect the excitability of neurons (Araque et al., 2000; Pasti et al., 2001; Parpura et al., 2004). Accordingly, in the model we reproduced the most essential features of glutamate release in response to Ca^{2+} elevations in astrocytes. The release of glutamate is pulsatile and depends on the frequency of Ca^{2+} oscillations (Pasti et al., 2001), while its

55

efficacy is controlled by the amplitude of the Ca^{2+} increase (Parpura and Haydon, 2000). In addition, a steady state Ca^{2+} elevation may trigger only a single episode of release (Pasti et al., 2001).

Some approximations were applied to describe two features that characterize astrocyte signaling in our model. Firstly, we restricted our analysis to somatic Ca^{2+} signals. These Ca^{2+} increases can not be intended to fully represent the synapse-to-astrocyte signaling occurring fundamentally at the proximal and the distal processes that are in contact with the synapse. Indeed, somatic Ca^{2+} increases exhibit a lower frequency and slower kinetics with respect to those at the processes (Di Castro et al., 2011; Panatier et al., 2011). While these recent studies also showed that Ca^{2+} elevations at the astrocytic processes can have a distinct functional role, it is noteworthy that the Ca^{2+} elevation at the soma may represent a response that integrates the signals from the processes where astrocytes sense neurotransmitter release. Accordingly, Ca^{2+} signals at the soma may adequately reflect the overall firing activity of surrounding neurons. Amplitude, frequency and general pattern of somatic Ca^{2+} changes are, indeed, observed to vary according to different levels of neuronal activity (Pasti et al., 1997; Porter and McCarthy, 1997). Secondly, while glutamate (Parpura et al., 1994; Pasti et al., 1997; Bezzi et al., 1998), D-serine (Mothet et al., 2005; Henneberger et al., 2010), ATP (Arcuino et al., 2002; Serrano et al., 2006; Bowser and Khakh, 2007), and GABA (Kozlov et al., 2006; Lee et al., 2011) [for a review see Haydon and Carmignoto (2006)] are the main gliotransmitters mediating astrocyte-to-neuron signaling, in our model we fundamentally focused on glutamate because a large body of information is available about its modulatory action on both basal synaptic transmission (Fellin et al., 2004; Di Castro et al., 2011; Panatier et al., 2011) and long-term plasticity (Zhang et al., 2003; Panatier et al., 2006; Serrano et al., 2006; Jourdain et al., 2007; Navarrete and Araque, 2010; Santello et al., 2011; Han et al., 2012; Min and Nevian, 2012). In addition, the contribution of astrocytic glutamate in some forms of long-term potentiation of synaptic transmission has been recently confirmed in *in vivo* experiments (Takata et al., 2011; Navarrete et al., 2012). The potential role in focal seizure generation of ATP, D-serine and GABA will be the subject of future investigations. It is worth mentioning here that D-serine, and not glycine, is most likely the physiological co-agonist of the synaptic NMDA receptor in the brain (Mothet et al., 2000; Panatier et al., 2006; Fossat et al., 2012; Papouin et al., 2012). Given that D-serine is mainly, although not exclusively (Ding et al., 2011), synthesized in astrocytes and

released through a Ca^{2+}-dependent mechanism (Wolosker et al., 1999; Wolosker, 2011), astrocytic D-serine may cooperate with glutamate to enhance NMDA receptor openings and through this action favor neuronal excitability ultimately promoting epileptic discharges.

The pathological increase in brain network excitability that eventually leads to focal seizure generation is believed to derive from the activity of excitatory and inhibitory neurons as well as of astrocytes. The cellular events that favor or oppose seizure initiation and propagation remain, however, poorly defined. Our model offers the opportunity to study ID generation in simulated networks composed by either only neurons or interactive astrocytes and neurons. The results that we obtained are summarized in **Figure 6** and can be, in our opinion, useful to understand how distinct signaling pathways may govern focal ID generation. **Figure 6** plots the average threshold for ID generation in the different conditions (mean ± SD, **Figure 6A**) and the cumulative sum of the threshold histograms (**Figure 6B**) showing failures. We found that in a network composed exclusively of neurons an ID can be generated by applying an intense stimulation of a group of neurons. The introduction of astrocytes into the network lowered ID threshold, while the inhibition of astrocyte signaling to neurons within, but not outside the focus, increased ID threshold. These results are fully consistent with those obtained in slice experiments (Gomez-Gonzalo et al., 2010) and demonstrate that focal IDs can be faithfully reproduced in our computational model. Accordingly, our model can be used to make predictions on the distinct contribution of different signaling pathways to ID generation. We present here some results regarding inhibitory signaling pathways. The ID threshold was observed to increase upon procedures that increase the strength of inhibition onto the principal neurons. This was achieved by either increasing the strength of the inhibitory transmission or by including in the model a distinct inhibitory feedback signal from astrocytes to neurons via $GABA_A$ receptors. These observations will be useful when addressing in future slice experiments the role of inhibitory signaling in ID generation.

REFERENCES

Alger, B. E., and Nicoll, R. A. (1980). Epileptiform burst afterhyperolarization: calcium-dependent potassium potential in hippocampal CA1 pyramidal cells. *Science* 210, 1122–1124.

Amiri, M., Bahrami, F., and Janahmadi, M. (2012). On the role of astrocytes in epilepsy: a functional modeling approach. *Neurosci. Res.* 72, 172–180.

Araque, A., Li, N., Doyle, R. T., and Haydon, P. G. (2000). SNARE protein-dependent glutamate release from astrocytes. *J. Neurosci.* 20, 666–673.

Araque, A., Parpura, V., Sanzgiri, R. P., and Haydon, P. G. (1999). Tripartite synapses: glia, the unacknowledged partner. *Trends Neurosci.* 22, 208–215.

Arcuino, G., Lin, J. H.-C., Takano, T., Liu, C., Jiang, L., Gao, Q.,

et al. (2002). Intercellular calcium signaling mediated by point-source burst release of ATP. *Proc. Natl. Acad. Sci. U.S.A.* 99, 9840–9845.

Avoli, M., D'Antuono, M., Louvel, J., Kohling, R., Biagini, G., Pumain, R., et al. (2002). Network and pharmacological mechanisms leading to epileptiform synchronization in the limbic system *in vitro*. *Prog. Neurobiol.* 68, 167–207.

Bazhenov, M., Timofeev, I., Steriade, M., and Sejnowski, T. J. (2004). Potassium model for slow (2-3 Hz) *in vivo* neocortical paroxysmal oscillations. *J. Neurophysiol.* 92, 1116–1132.

Ben-Ari, Y. (2002). Excitatory actions of GABA during development: the nature of the nurture. *Nat. Rev. Neurosci.* 3, 728–739.

Bezzi, P., Carmignoto, G., Pasti, L., Vesce, S., Rossi, D., Rizzini, B. L.,

56

et al. (1998). Prostaglandins stimulate calcium-dependent glutamate release in astrocytes. *Nature* 391, 281–285.

Bowser, D. N., and Khakh, B. S. (2007). Vesicular ATP is the predominant cause of intercellular calcium waves in astrocytes. *J. Gen. Physiol.* 129, 485–491.

Bradford, H. F. (1995). Glutamate, GABA and epilepsy. *Prog. Neurobiol.* 47, 477–511.

Brockhaus, J., and Deitmer, J. W. (2002). Long-lasting modulation of synaptic input to Purkinje neurons by Bergmann glia stimulation in rat brain slices. *J. Physiol.* 545, 581–593.

Bushong, E. A., Martone, M. E., Jones, Y. Z., and Ellisman, M. H. (2002). Protoplasmic astrocytes in CA1 stratum radiatum occupy separate anatomical domains. *J. Neurosci.* 22, 183–192.

Carmignoto, G. (2000). Reciprocal communication systems between astrocytes and neurones. *Prog. Neurobiol.* 62, 561–581.

Cornell-Bell, A. H., Finkbeiner, S. M., Cooper, M. S., and Smith, S. J. (1990). Glutamate induces calcium waves in cultured astrocytes: long-range glial signaling. *Science* 247, 470–473.

De Pittà, M., Volman, V., Berry, H., and Ben-Jacob, E. (2011). A tale of two stories: astrocyte regulation of synaptic depression and facilitation. *PLoS Comput. Biol.* 7:e1002293. doi: 10.1371/journal.pcbi.1002293

Destexhe, A. (1998). Spike-and-wave oscillations based on the properties of GABA$_B$ receptors. *J. Neurosci.* 18, 9099–9111.

Di Castro, M. A., Chuquet, J., Liaudet, N., Bhaukaurally, K., Santello, M., Bouvier, D., et al. (2011). Local Ca^{2+} detection and modulation of synaptic release by astrocytes. *Nat. Neurosci.* 14, 1276–1284.

Di Garbo, A. (2009). Dynamics of a minimal neural model consisting of an astrocyte, a neuron, and an interneuron. *J. Biol. Phys.* 35, 361–382.

Ding, X., Ma, N., Nagahama, M., Yamada, K., and Semba, R. (2011). Localization of D-serine and serine racemase in neurons and neuroglias in mouse brain. *Neurol. Sci.* 32, 263–267.

Fellin, T., Gomez-Gonzalo, M., Gobbo, S., Carmignoto, G., and Haydon, P. G. (2006). Astrocytic glutamate is not necessary for the generation of epileptiform neuronal activity in hippocampal slices. *J. Neurosci.* 26, 9312–9322.

Fellin, T., Pascual, O., Gobbo, S., Pozzan, T., Haydon, P. G., and Carmignoto, G. (2004). Neuronal synchrony mediated by astrocytic glutamate through activation of extrasynaptic NMDA receptors. *Neuron* 43, 729–743.

Fossat, P., Turpin, F. R., Sacchi, S., Dulong, J., Shi, T., Rivet, J. M., et al. (2012). Glial D-serine gates NMDA receptors at excitatory synapses in prefrontal cortex. *Cereb. Cortex* 22, 595–606.

Gomez-Gonzalo, M., Losi, G., Chiavegato, A., Zonta, M., Cammarota, M., Brondi, M., et al. (2010). An excitatory loop with astrocytes contributes to drive neurons to seizure threshold. *PLoS Biol.* 8:e1000352. doi: 10.1371/journal.pbio.1000352

Gordon, G. R., Choi, H. B., Rungta, R. L., Ellis-Davies, G. C., and Macvicar, B. A. (2008). Brain metabolism dictates the polarity of astrocyte control over arterioles. *Nature* 456, 745–749.

Halassa, M. M., Fellin, T., and Haydon, P. G. (2007a). The tripartite synapse: roles for gliotransmission in health and disease. *Trends Mol. Med.* 13, 54–63.

Halassa, M. M., Fellin, T., Takano, H., Dong, J. H., and Haydon, P. G. (2007b). Synaptic islands defined by the territory of a single astrocyte. *J. Neurosci.* 27, 6473–6477.

Han, J., Kesner, P., Metna-Laurent, M., Duan, T., Xu, L., Georges, F., et al. (2012). Acute cannabinoids impair working memory through astroglial CB$_1$ receptor modulation of hippocampal LTD. *Cell* 148, 1039–1050.

Haydon, P. G. (2001). GLIA: listening and talking to the synapse. *Nat. Rev. Neurosci.* 2, 185–193.

Haydon, P. G., and Carmignoto, G. (2006). Astrocyte control of synaptic transmission and neurovascular coupling. *Physiol. Rev.* 86, 1009–1031.

Henneberger, C., Papouin, T., Oliet, S. H., and Rusakov, D. A. (2010). Long-term potentiation depends on release of D-serine from astrocytes. *Nature* 463, 232–236.

Hirase, H., Qian, L., Barthó, P., and Buzsáki, G. (2004). Calcium dynamics of cortical astrocytic networks *in vivo*. *PLoS Biol.* 2:e96. doi: 10.1371/journal.pbio.0020096

Izhikevich, E. M. (2003). Simple model of spiking neurons. *IEEE Trans. Neural Netw.* 14, 1569–1572.

Izhikevich, E. M. (2010). Hybrid spiking models. *Philos. Transact. A Math. Phys. Eng. Sci.* 368, 5061–5070.

Izhikevich, E. M., and Edelman, G. M. (2008). Large-scale model of mammalian thalamocortical systems. *Proc. Natl. Acad. Sci. U.S.A.* 105, 3593–3598.

James, L. R., Andrews, S., Walker, S., De Sousa, P. R., Ray, A., Russell, N. A., et al. (2011). High-throughput analysis of calcium signalling kinetics in astrocytes stimulated with different neurotransmitters. *PLoS ONE* 6:e26889. doi: 10.1371/journal.pone.0026889

Jefferys, J. G. (1990). Basic mechanisms of focal epilepsies. *Exp. Physiol.* 75, 127–162.

Jefferys, J. G. R. (2003). Models and mechanisms of experimental epilepsies. *Epilepsia* 44(Suppl. 12), 44–50.

Jourdain, P., Bergersen, L. H., Bhaukaurally, K., Bezzi, P., Santello, M., Domercq, M., et al. (2007). Glutamate exocytosis from astrocytes controls synaptic strength. *Nat. Neurosci.* 10, 331–339.

Kang, N., Xu, J., Xu, Q., Nedergaard, M., and Kang, J. (2005). Astrocytic glutamate release-induced transient depolarization and epileptiform discharges in hippocampal CA1 pyramidal neurons. *J. Neurophysiol.* 94, 4121–4130.

Kawabata, S., Tsutsumi, R., Kohara, A., Yamaguchi, T., Nakanishi, S., and Okada, M. (1996). Control of calcium oscillations by phosphorylation of metabotropic glutamate receptors. *Nature* 383, 89–92.

Kirchner, A., Veliskova, J., and Velisek, L. (2006). Differential effects of low glucose concentrations on seizures and epileptiform activity *in vivo* and *in vitro*. *Eur. J. Neurosci.* 23, 1512–1522.

Kozlov, A. S., Angulo, M. C., Audinat, E., and Charpak, S. (2006). Target cell-specific modulation of neuronal activity by astrocytes. *Proc. Natl. Acad. Sci. U.S.A.* 103, 10058–10063.

Kuga, N., Sasaki, T., Takahara, Y., Matsuki, N., and Ikegaya, Y. (2011). Large-scale calcium waves traveling through astrocytic networks *in vivo*. *J. Neurosci.* 31, 2607–2614.

Le Meur, K., Mendizabal-Zubiaga, J., Grandes, P., and Audinat, E. (2012). GABA release by hippocampal astrocytes. *Front. Comput. Neurosci.* 6:59. doi: 10.3389/fncom.2012.00059

Lee, M., McGeer, E. G., and McGeer, P. L. (2011). Mechanisms of GABA release from human astrocytes. *Glia* 59, 1600–1611.

Li, Y. X., and Rinzel, J. (1994). Equations for InsP$_3$ receptor-mediated [Ca^{2+}]$_i$ oscillations derived from a detailed kinetic model: a Hodgkin-Huxley like formalism. *J. Theor. Biol.* 166, 461–473.

Losi, G., Cammarota, M., Chiavegato, A., Gomez-Gonzalo, M., and Carmignoto, G. (2010). A new experimental model of focal seizures in the entorhinal cortex. *Epilepsia* 51, 1493–1502.

Min, R., and Nevian, T. (2012). Astrocyte signaling controls spike timing-dependent depression at neocortical synapses. *Nat. Neurosci.* 15, 746–753.

Mothet, J. P., Parent, A. T., Wolosker, H., Brady, R. O. Jr., Linden, D. J., Ferris, C. D., et al. (2000). D-serine is an endogenous ligand for the glycine site of the N-methyl-D-aspartate receptor. *Proc. Natl. Acad. Sci. U.S.A.* 97, 4926–4931.

Mothet, J. P., Pollegioni, L., Ouanounou, G., Martineau, M., Fossier, P., and Baux, G. (2005). Glutamate receptor activation triggers a calcium-dependent and SNARE protein-dependent release of the gliotransmitter D-serine. *Proc. Natl. Acad. Sci. U.S.A.* 102, 5606–5611.

Mulligan, S. J., and MacVicar, B. A. (2004). Calcium transients in astrocyte endfeet cause cerebrovascular constrictions. *Nature* 431, 195–199.

Nadkarni, S., and Jung, P. (2003). Spontaneous oscillations of dressed neurons: a new mechanism for epilepsy? *Phys. Rev. Lett.* 91, 268101.

Nadkarni, S., and Jung, P. (2004). Dressed neurons: modeling neural-glial interactions. *Phys. Biol.* 1, 35–41.

Nadkarni, S., and Jung, P. (2007). Modeling synaptic transmission of the tripartite synapse. *Phys. Biol.* 4, 1–9.

Nadkarni, S., Jung, P., and Levine, H. (2008). Astrocytes optimize the synaptic transmission of information. *PLoS Comput. Biol.* 4:e1000088. doi: 10.1371/journal.pcbi.1000088

Navarrete, M., and Araque, A. (2010). Endocannabinoids potentiate synaptic transmission through stimulation of astrocytes. *Neuron* 68, 113–126.

Navarrete, M., Perea, G., De Sevilla, D. F., Gomez-Gonzalo, M., Nunez, A., Martin, E., et al. (2012). Astrocytes mediate *in vivo* cholinergic-induced synaptic plasticity. *PLoS Biol.* 10:e1001259. doi: 10.1371/journal.pbio.1001259

Oberheim, N. A., Wang, X., Goldman, S., and Nedergaard, M. (2006). Astrocytic complexity distinguishes the human brain. *Trends Neurosci.* 29, 547–553.

Panatier, A., Theodosis, D. T., Mothet, J.-P., Toquet, B., Pollegioni, L., Poulain, D. A., et al. (2006).

57

1

Neuroscience

The Journal of Physiology

Fast spiking interneuron control of seizure propagation in a cortical slice model of focal epilepsy

Mario Cammarota, Gabriele Losi, Angela Chiavegato, Micaela Zonta and Giorgio Carmignoto

Institute of Neuroscience, National Research Council (CNR) and Department of Biomedical Sciences, University of Padova, Padova, Italy

Key points

- In focal epilepsy the propagation of seizure discharges arising at restricted brain sites is opposed by feedforward inhibition. Failure of this inhibition marks focal seizure propagation to distant neurons.
- The cellular source of inhibition and the mechanism of inhibition failure are, however, undefined.
- Here we reveal that a subclass of GABAergic interneurons, i.e. the parvalbumin-expressing, fast-spiking interneurons, are a main source of the inhibitory signal that locally restrains seizures. Furthermore, a firing impairment in these interneurons, probably due to a drastic membrane depolarization, is an important event that by reducing the overall strength of local inhibition allows seizures to propagate across the cortex.
- Our data suggest that modulation of fast-spiking interneuron activity may represent a new therapeutic strategy to prevent generalization of focal epilepsies.

Abstract In different animal models of focal epilepsy, seizure-like ictal discharge propagation is transiently opposed by feedforward inhibition. The specific cellular source of this signal and the mechanism by which inhibition ultimately becomes ineffective are, however, undefined. We used a brain slice model to study how focal ictal discharges that were repetitively evoked from the same site, and at precise times, propagate across the cortex. We used Ca^{2+} imaging and simultaneous single/dual cell recordings from pyramidal neurons (PyNs) and different classes of interneurons in rodents, including G42 and GIN transgenic mice expressing the green fluorescence protein in parvalbumin (Pv)-fast spiking (FS) and somatostatin (Som) interneurons, respectively. We found that these two classes of interneurons fired intensively shortly after ictal discharge generation at the focus. The inhibitory barrages that were recorded in PyNs occurred in coincidence with Pv-FS, but not with Som interneuron burst discharges. Furthermore, the strength of inhibitory barrages increased or decreased in parallel with increased or decreased firing in Pv-FS interneurons but not in Som interneurons. A firing impairment of Pv-FS interneurons caused by a membrane depolarization was found to precede ictal discharge onset in neighbouring pyramidal neurons. This event may account for the collapse of local inhibition that allows spatially defined clusters of PyNs to be recruited into propagating ictal discharges. Our study demonstrates that Pv-FS interneurons are a major source of the inhibitory barrages that oppose ictal discharge propagation and raises the possibility that targeting Pv-FS interneurons represents a new therapeutic strategy to prevent the generalization of human focal seizures.

M. Cammarota and G. Losi contributed equally to this work.

Corresponding author G. Carmignoto: Institute of Neuroscience, National Research Council and Department of Biomedical Sciences, University of Padova, Viale G. Colombo 3, 35121, Italy.   Email: giorgio.carmignoto@bio.unipd.it

Abbreviations ANP, adapting non-pyramidal; EC, entorhinal cortex; FS, fast-spiking; f_w, weighted frequency; GFP, green florescence protein; IS, irregular spiking; LTS, low-threshold spiking; OG-B1-AM, Oregon Green BAPTA1-AM; Pv, parvalbumin; PB, phosphate buffer; PyN, pyramidal neuron; Som, somatostatin; TC, temporal cortex; t_{IE}, transition from inhibition to excitation.

Introduction

Focal epilepsies arise at restricted brain sites of abnormally high neuronal network activities and secondarily involve adjacent regions, eventually spreading to distant neuronal populations (Jefferys, 1990; Traub *et al.* 1993). Over the last decade, experimental research in this field has made significant advances. We know now that various synaptic and non-synaptic factors contribute to form a hyperactive network that, in turn, promotes seizure initiation and favours seizure propagation (Stanton *et al.* 1987; Jones & Lambert, 1990; Pare *et al.* 1992; McNamara, 1999, 2006; Avoli *et al.* 2002). Among the synaptic factors, GABA-mediated inhibitory synaptic transmission is proposed to control the pathogenesis and propagation of epileptic discharges by regulating the general excitability in the neuronal network. Consistent with this hypothesis, recent studies in occipital cortex slice preparations revealed that a powerful feedforward inhibition controls the propagation speed of epileptic discharges arising spontaneously in the low-Mg^{2+} model (Trevelyan *et al.* 2006, 2007). Inhibition ultimately fails and surrenders to the wave of excitation of the propagating seizure-like, ictal discharge (Trevelyan *et al.* 2006). The mechanism at the basis of this failure is, however, unclear.

The paucity of adequate experimental models in which we can specifically investigate how a focal ictal discharge propagates across the neuronal network accounts, at least in part, for our defective knowledge. We recently developed in rat entorhinal cortex (EC) slices a new model of focal ictal discharge in which we can control when and where a focal epileptic discharge will occur (Gomez-Gonzalo *et al.* 2010; Losi *et al.* 2010). The precise information on the timing and site of ictal discharge generation gives us the unique opportunity to study in this model the delay in the propagation of focal ictal discharges to regions that are at increasing distances from the focus as well as the local cellular events that govern this delay by favouring or opposing the progression of the ictal discharge. Our most relevant aims were (i) to identify the cellular source of the inhibitory signal that transiently opposes focal ictal discharge propagation and (ii) to gain insights into the cellular events that, by reducing the strength of inhibition (Trevelyan *et al.* 2007; Derchansky *et al.* 2008), cause the neuronal network to give up their resistance to the propagating focal seizure.

We used single and dual cell patch-clamp recordings from pyramidal neurons (PyNs) and interneurons coupled with simultaneous fast-laser scanning microscope imaging of the Ca^{2+} signal from tens of cells. By using, in addition, transgenic mice in which distinct subsets of interneurons are distinguished by the enhanced green fluorescence protein (GFP), we found that the inhibitory barrages opposing focal ictal discharge propagation were largely generated by local parvalbumin (Pv)-fast spiking (FS) interneurons and not by somatostatin (Som) interneurons. After Pv-FS interneurons entered into a depolarization block phase, the local inhibitory barrier collapsed and spatially distinct groups of neurons were recruited into the epileptiform discharge.

Methods

All experimental procedures were in strict accordance with the Italian and EU regulations on animal welfare and had prior authorization from the Italian Ministry of Health. The experiments included in these studies comply with the policies and regulations described by Drummond (2009). The number of animals used in our study was reduced to the minimum necessary to allow an adequate statistical analysis.

Brain slice preparations and dye loading

Coronal cortico-hippocampal slices were prepared from postnatal day 14–20 Wistar rats or mice, i.e. G42 (Chattopadhyaya *et al.* 2004) and GIN mice (Oliva *et al.* 2000). Briefly, mice were deeply anaesthetized with intraperitoneal-injected Zoletil (40 mg kg^{-1}; Virbac, Milan, Italy), a combination of a benzodiazepine-like molecule (zolazepam) and a dissociative anaesthetic (tiletamine). After decapitation, the brain was removed and transferred to ice-cold cutting solution containing (in mM): NaCl, 120; KCl, 3.2; KH$_2$PO$_4$, 1; NaHCO$_3$, 26; MgCl$_2$, 2; CaCl$_2$, 1; glucose, 10; sodium pyruvate, 2; and ascorbic acid, 0.6; at pH 7.4 (with 5% CO$_2$–95% O$_2$). Coronal slices were obtained by using a Leica vibratome VT1000S in the presence of the ionotropic glutamate receptor inhibitor kynurenic acid (2 mM). Slices were recovered for 15 min at 34°C and then loaded with either a green fluorescence dye (OGB1-AM or Fluo-4, 10 μM, excited at 488 nm) or a

red dye (Rhod-2, 10 μM; excited at 543 nm) for 50–60 min at 34°C, as previously described (Gomez-Gonzalo *et al.* 2010).

Although Rhod-2 is known to accumulate in mitochondria (Kovacs *et al.* 2005) with this loading protocol, it was highly present in the cytosol. Dye loading was performed in the cutting solution containing sulfinpyrazone (200 μM), pluronic (0.12%) and kynurenic acid (1 mM). After loading, slices were recovered and kept at room temperature and experiments performed at 32°C.

Ca^{2+} imaging

Images were acquired with a single- (TCS-SP5-RS, Leica) and two-photon (UltimaIV, Prairie Technologies) laser scanning microscope with a time frame acquisition from 351 ms to 491 ms (five to seven line averaging), and from 300 to 900 ms, respectively. Both systems were equipped with a CCD camera for differential interference contrast images. All experiments were performed in layer V–VI. With two-photon excitation we could easily distinguish GFP-expressing cells in Fluo-4-loaded slices from G42 mice because two-photon excitation spectra of GFP and Fluo-4 differ significantly. The wavelengths used for Fluo-4 and GFP were 750 and 920 nm, respectively.

Electrophysiology and induction of focal ictal discharges

Brain slices were continuously perfused in a submerged chamber (Warner Instruments) at a rate of 3–4 ml min^{-1} with (in mM): NaCl, 120; KCl, 3.2; KH$_2$PO$_4$, 1; NaHCO$_3$, 26; MgCl$_2$, 1; CaCl$_2$, 2; glucose, 10; at pH 7.4 (with 95% O$_2$–5% CO$_2$). Whole-cell patch-clamp recordings were performed using standard procedures and one or two Axopatch-200B amplifiers or Multiclamp-700B (Molecular Devices, USA), as previously reported (Fellin & Carmignoto, 2004). Typical pipette resistance was 3–4 MΩ. Data were filtered at 1–2 kHz and sampled at 5–10 kHz with a Digidata 1320 or 1440 interface and pCLAMP10 software (Molecular Devices). The whole-cell intracellular pipette solution was (in mM): potassium gluconate, 145; MgCl$_2$, 2; EGTA, 0.5; Na$_2$ATP, 2; Na$_2$GTP, 0.2; Hepes, 10; to pH 7.2 with KOH, and, when needed, contained a low concentration (10 μM) of OGB1 (Invitrogen); osmolarity, 305–315 mosmol l^{-1}. Liquid junction potentials for all solutions were measured, and all voltages reported are corrected values. Experiments were performed in the presence of 4-AP (50–100 μM) unless otherwise specified. Patched neurons were classified according to their response to hyperpolarizing and depolarizing 750 ms current steps. Neurons with no spike amplitude accommodation (except for the second action potential

in some cells), small after-hyperpolarization (AHP) and low steady-state frequency (15–23 Hz with 200 pA current injection) were considered as regular spiking pyramidal neurons (PyN). Cells with high steady-state frequency (39–60 Hz with 200 pA current injection), no spike amplitude accommodation or frequency adaptation and large AHPs were considered as FS interneurons; cells with strong spike amplitude accommodation and spike frequency adaptation were considered as adapting non-pyramidal (ANP) interneurons; cells with clear sag, one or more rebound action potentials, spike amplitude accommodation and frequency adaptation were considered as low-threshold (LTS) interneurons; cells with bursts of spikes with irregular frequency were considered as irregular spiking (IS) interneurons. In GIN mice we discarded cells that did not show the typical features of LTS interneurons. All patched neurons in rat and mouse slices, i.e. principal PyNs and different classes of interneurons, were from cortical layer V–VI. Juxtaposed recordings were performed in cell-attached mode, without rupture of the membrane patch, with pipettes filled with the bath perfusing solution. A pressure ejection unit (PDES, NPI Electronics) was used to apply a double pulse to NMDA (1 mM)-containing pipettes with a 3 s interval, a pressure of 4–10 p.s.i., and a duration of 200–600 ms. In the bicuculline experiments, three pressure pulses (4 p.s.i., 200 ms duration) with a 5 s time interval were applied to a 1 mM bicuculline-containing pipette before the NMDA stimulation. To test for a possible inhibitory synaptic connection between a Pv-FS interneuron and PyN, action potential firing at 50–70 Hz was stimulated in the Pv-FS interneuron by current injections. In the pairs in which we applied this test (4 of 11 pairs) we failed to find evidence of a direct synaptic connection.

Q3

Neuron reconstruction

Pv-FS interneurons and PyNs were patched with a biocytin-containing (0.5%) pipette (Sigma-Aldrich, Italy). Potassium gluconate was reduced to achieve a final osmolarity of 275 mosmol l^{-1}. Patched neurons were kept in whole-cell configuration for 20–30 min before gently detaching the pipette tip to preserve membrane integrity. Slices were then maintained in the standard oxygenated extracellular solution for 1 h to allow biocytin intracellular diffusion and then fixed in 4% paraformaldehyde and 0.15 M phosphate buffer (PB) at 4°C for 1–4 days. Slices were then rinsed in PB and incubated in 1% hydrogen peroxide in PB for 5 min, permeabilized in 2% Triton X-100 for 1 h and kept overnight at 4°C in the avidin–biotin–peroxidase complex solution (R.T.U. Vectastain kit PK-7100, Vector Laboratories, CA, USA). Slice were then placed in DAB-enhanced liquid substrate solution 1× (Sigma Aldrich, D3939) for a few minutes

Q4

until the slice turned light brown and then immediately transferred again to fresh PB to block the reaction. Each slice was mounted (Elvanol mounting medium) and viewed with ×20 to ×40 objectives on a DMR light microscope (Leica, Wetzlar, Germany). Images at different focal planes were acquired by a Leica DC300 digital photocamera and then reconstructed using Neurolucida software (MicroBrightField). Single ×10 optical images of pyramidal and fast-spiking neurons were reconstructed by Adobe Photoshop CS5.

Data analysis

Data analysis was performed with Clampfit 10, Origin 8.0 (Microcal Software), Microsoft Office and MATLAB 7.6.0 (R2008A). In paired recording experiments the increase in interneuron spiking activity was considered statistically significant when the instantaneous frequency, defined as the reciprocal of the interspike interval, exceeded by three standard deviations the mean of the instantaneous frequency after 4-AP slice perfusion. The relationship between inhibitory events in PyNs and the firing activity in Pv-FS and Som-LTS interneurons reported in Figs 6 and 7 was studied comparing the charge transferred to a weighted frequency (f_w) in all the inhibitory barrages before transition from inhibition to excitation (t_{IE}). The charge transferred was computed as the area of each inhibitory event and f_w was defined as: $f_w = \sum_{i=1}^{N} \frac{A_i/A}{\Delta t}$ where N is the number of action potentials within each inhibitory burst, Δt is the duration of the burst, A_i is the amplitude of each action potential and A is the mean amplitude of the action potentials of the same neuron before NMDA stimulation. f_w was calculated taking into account both action potential frequency and amplitude because a reduced action potential amplitude can affect neurotransmitter release by causing a failure in propagation through axonal branch points (Streit *et al.* 1992; Brody & Yue, 2000) and by reducing Ca^{2+} influx at synaptic terminals (Katz & Miledi, 1970; Neher & Sakaba, 2008). Data were normalized from each experiment to the maximal values. A burst was classified as a train of action potentials superimposed on a depolarization with an instant frequency higher than the basal one. To estimate the timing of the period of depolarization block in Pv-FS interneurons, we considered the first time in which, after NMDA stimulation, Pv-FS interneuron firing activity was abolished for at least 400 ms in the presence of marked membrane depolarization.

Ca^{2+} imaging experiments. The Ca^{2+} signal is reported as $\Delta F/F_0$, where F_0 is the baseline fluorescence. Each row of the recruitment diagrams in Figs 1, 2 and 5 is the pseudocolour plot of the temporal derivative of the Ca^{2+} signals in neurons ordered by the time of the maximum time derivative which marked the recruitment of neurons into ictal discharges. No background subtraction or other manipulations were applied to digitized Ca^{2+} signal images that are reported as raw data. Ca^{2+} signals from neurons were obtained after the semi-automatic detection of regions of interest (ROIs) performed using a home-made algorithm written in MATLAB.

Definition of the timing of recruitment into propagating ictal discharges. We defined the timing of recruitment of each neuron as the timing of the maximum temporal derivative of the Ca^{2+} signal. In voltage-clamp recordings, illustrated in Figs 2, 6, 7 and 8, the recruitment of a neuron into ictal discharge is marked by the transition from predominantly inhibitory to the predominantly excitatory phase (t_{IE}), which is defined as the timing in which the ratio between the *inhibition* and the *excitation index* is for the first time less than 0.1. The inhibition and the excitation indices were calculated, respectively, as the part of the positive and the negative component of the time derivative of the trace which exceeded 5 times the mean SD value evaluated during the baseline. Finally, the timing for the propagating ictal discharge in the current-clamp recordings was defined as the time of occurrence of the first excitatory burst with a duration of at least 400 ms. In Ca^{2+} imaging experiments performed in G42 mice, we compared the timing of the activation of each GFP-expressing Pv-FS interneuron (or GFP-negative, early activated neurons) and the timing of the recruitment of PyNs belonging to the cluster in which each Pv-FS interneuron was localized. In this way, we provide an average measurement of the delay between Pv-FS interneuron activation and the recruitment of the surrounding PyNs.

Cluster size measurements. The radius of the clusters defined in Ca^{2+} imaging experiments was calculated as the maximum Euclidean distance between the cells belonging to the same subgroup and the centre of gravity of each group calculated as $(x_{CG}, y_{CG}) = \sum_{\text{neurons}} (x_i, y_i)/N$, where x_i and y_i are, respectively, the coordinates of each neuron in the cluster and N is the number of neurons in the cluster.

Drugs

4-Aminopyridine (4-AP; Ascent Scientific) was bath applied. NMDA (Sigma-Aldrich) and bicuculline methiodide (Sigma-Aldrich) were pressure applied.

Q5

61

Statistical analysis

Data are shown as mean ± standard error of the mean (SEM). We analysed quantitative results by Student's t test, setting the statistical significance at $P < 0.05$. To statistically compare the distributions of the latencies between the timing of depolarization block in the different classes of interneurons and that of t_{IE} in PyNs, we applied the Fischer's exact test to data binned into 300 ms groups (Fig. 6).

Results

Propagation of ictal discharges from the focus to distant regions

Current-clamp recordings from layer V–VI PyNs in rat EC slices revealed that in the presence of the proconvulsant 4-AP (50–100 μM) (Rutecki *et al.* 1987; Perreault & Avoli, 1989, 1991; but see Streit *et al.* 2011; Zahn *et al.* 2012) and 0.5 mM Mg^{2+}, a local NMDA stimulation evokes a focal ictal discharge (mean duration, 32.9 ± 0.2 s, $n = 89$; Fig. 1*A*; Gomez-Gonzalo *et al.* 2010; Losi *et al.* 2010). As previously reported (Losi *et al.* 2010), spontaneous ictal discharges were only occasionally observed. The ictal discharge propagated to neurons surrounding the site of NMDA applications (Fig. 1*A* and *B*, grey circle) with a delay that increased significantly with distance from the focus (Fig. 1*B* and *C*). Previous studies reported a much faster propagation of seizure-like discharges upon 4-AP (Weissinger *et al.* 2005) or low Mg^{2+} slice perfusion (Buchheim *et al.* 2000). These were, however, spontaneously occurring seizures and they were observed under experimental conditions that may guarantee a better preservation of synaptic connectivity (horizontal *vs.* coronal slices and interface chambers *vs.* submerged). The ictal discharge in neurons from regions located >700 μm from the focus was regularly preceded by a series of hyperpolarizing events (Fig. 1*B*). As revealed by the recruitment diagram (Fig. 1*D*, see also Methods) derived from the analysis of the Ca^{2+} change in slices loaded with the Ca^{2+}-sensitive dye Oregon Green BAPTA1-AM (OG-B1-AM; blue box in Fig. 1*A*), neurons from the region immediately surrounding the site of NMDA application were homogeneously recruited into the ictal discharge. In contrast, more distant neurons were recruited in spatially distinct domains at different times (Fig. 1*E* and *F*). These data suggest that ictal discharges spread across the EC through neither a rapid homogeneous process nor an avalanche-like wave, but rather through a process in which clusters of neurons are intermittently recruited.
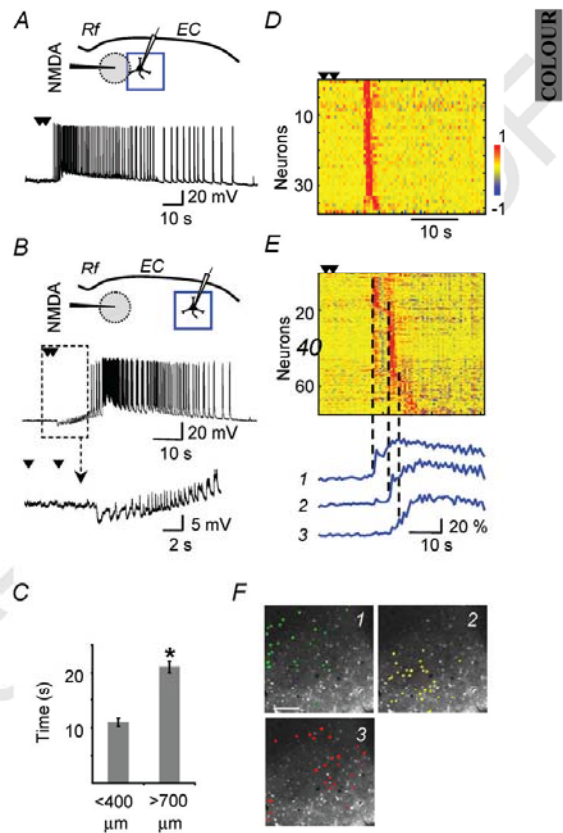

Figure 1. Modular propagation of focally evoked ictal discharges

A and *B*, current-clamp recordings from a PyN close (*A*) or distant (*B*) from the site where NMDA was applied to evoke an ictal discharge. In this and the other figures the black arrowheads mark the timing of the double NMDA pulse. The drawing reports the patch and the NMDA-containing pipettes, the epileptogenic focus (grey circle) and the region of neuronal Ca^{2+} imaging (blue box). Rf, rhinal fissure. The lower trace in *B* illustrates at expanded time scale the hyperpolarizing events that preceded ictal discharge propagation to this PyN. *C*, mean delays after the NMDA pulse of ictal discharge propagation to PyNs located close (<400 μm, 16 ictal discharges from 6 experiments) or distant (>700 μm, 19 ictal discharges from 10 experiments; *$P < 0.001$ from the focus. *D* and *E*, recruitment diagrams reporting in a pseudocolour scale the temporal derivative of the Ca^{2+} signal in each neuron (see Methods) from two different regions (<400 μm in *D*, >700 μm in *E*) outlined by the blue boxes in *A* and *B*. Lower traces in *E* show average Ca^{2+} changes from the three main clusters of neurons. *F*, OGB1 fluorescence image illustrating in different colours the three main clusters. Scale bar, 100 μm

A GABAergic inhibitory signal restrains and shapes ictal discharge propagation to PyNs distant from the focus

To investigate the role of the hyperpolarizing events in ictal discharge propagation to distant regions, in rat EC slices we next performed voltage-clamp recordings from layer V–VI PyNs. A holding potential of –50 mV was applied to monitor both excitatory and inhibitory currents. We confirmed previous observations (Trevelyan *et al.* 2006, 2007) that in propagating ictal discharges, PyNs faced an initial phase dominated by inhibitory currents before entering into a phase dominated by excitatory currents (Fig. 2A, black trace). In the majority of PyNs the inhibitory barrages initiated at the time of ictal discharge generation at the focus (Supplemental Fig. S1, available online only) and lasted for a mean of 10.5 ± 0.9 s ($n = 20$). The transition from inhibition to excitation (t_{IE}; see Methods) occurred 20.9 ± 2.3 s ($n = 12$) after the NMDA pulse, at a time similar to that of the ictal discharge onset as measured in current-clamp recordings from neurons of the same region (Fig. 1C). Simultaneous recordings of the Ca^{2+} signal also revealed that in a number of neurons the Ca^{2+} level remained unchanged during the phase of dominant inhibition and increased at the time of t_{IE} in the patched neuron (Fig. 2A, blue trace). These neurons were grouped in clusters with a mean radius of 190 ± 14 μm ($n = 67$ from 6 experiments; see Methods), and represented $75 \pm 2\%$ of the total number of responsive neurons in the clusters (Fig. 2B). The patched PyN was always localized within the cluster. These data suggest that groups of neurons share a common inhibitory signal that locally opposes the recruitment of neurons into propagating ictal discharges. In dual recordings from two PyNs located at different distances from the focus we occasionally observed that in the distant neuron only inhibitory barrages were observed, suggesting an effective block of ictal discharge propagation (Fig. 2C).

The inhibitory currents in patched PyNs were blocked by a local application of the $GABA_A$ receptor antagonist bicuculline. Consequently, the t_{IE} was reduced significantly (Fig. 2D; mean t_{IE}, 7.5 ± 0.8 s, $n = 7$; $P < 0.001$) and 90% of the total number of the neurons present in the field of view were more rapidly and homogeneously recruited into the propagating ictal discharge (Fig. 2E). In controls and after bicuculline applications neurons were recruited in a time interval of 11.62 ± 0.83 s ($n = 8$) and 3.57 ± 0.44 s ($n = 5$, $P < 0.001$), respectively. These results demonstrate that the delay in the recruitment of PyNs into the propagating ictal discharge was due to local inhibitory GABAergic events in PyNs. Notably,
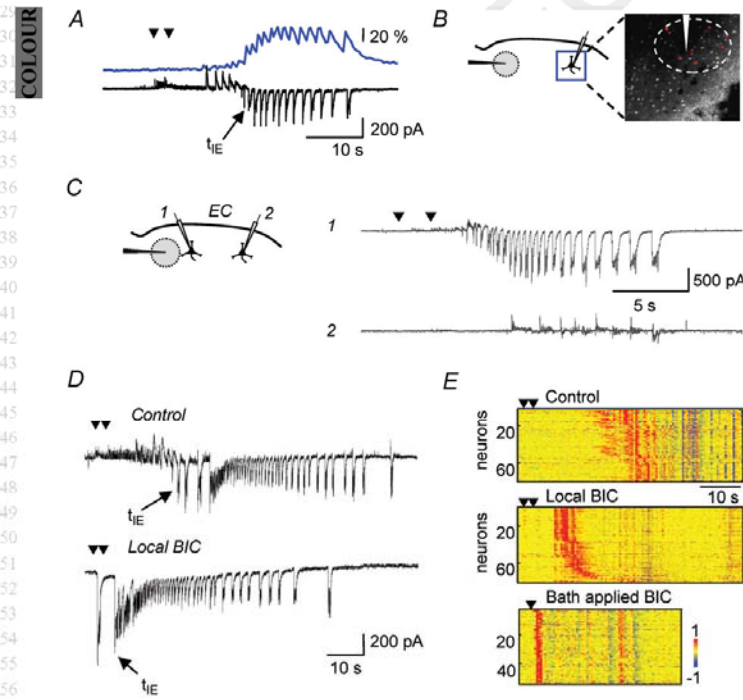

Figure 2. GABAergic inhibitory barrages restrain propagating ictal discharges
A, voltage-clamp recording in a PyN (black trace; $V_h = -50$ mV) and averaged Ca^{2+} signal (blue trace) from the putative PyNs of the same region (also shown in B). B, schematic diagram of the experiment and OGB1 fluorescence image from the same experiment showing in red the cluster of neurons recruited at the time of t_{IE} in the patched neuron. Scale bar, 100 μm. C, voltage-clamp recordings from a PyN pair showing a full ictal discharge in the PyN close to the focus and only inhibitory barrages in the more distant neuron. D, voltage-clamp recordings from a distant PyN before and after bicuculline applied locally before the NMDA pulses. E, recruitment diagrams from a region distant from the focus before (upper panel) and after bicuculline applications (lower panels).

Q6

after inhibition was massively blocked by bath-applied bicuculline, ictal discharges could be evoked by a single NMDA pulse and the modular recruitment was totally abolished (Fig. 2E).

Source of the GABAergic inhibitory barrages

To identify among the large variety of interneurons (Markram et al. 2004; Ascoli et al. 2008) the distinct type(s) that generate the inhibitory events in PyNs during ictal discharge propagation in rat EC, we monitored the activity of different classes of interneurons while evoking an ictal discharge. We found that interneurons classified as fast spiking (FS) interneurons, but not the other interneurons recorded (see Methods), fired at low-frequency during 4-AP slice perfusion. After the NMDA pulse all the FS interneurons recorded ($n = 7$) fired high frequency action potential bursts (Fig. 3A) before entering into a depolarization block phase of spike generation. The increase in spiking discharge occurred at the same time as the inhibitory barrages recorded from PyNs (Fig. 3B). We also monitored the activity in a number of non-FS interneurons subtypes ($n = 14$). Three of four low threshold (LTS) interneurons showed a firing increase soon after the NMDA stimulation, while putative adapting non-pyramidal (ANP interneurons; $n = 7$) and irregular spiking interneurons (IS interneurons; $n = 3$) fired at about the same time as PyN recruitment (Fig. 3A and B) and they never exhibited a spiking activity at the time of the inhibitory barrages in PyNs.

Pv-FS interneuron hyperactivity and block in propagating ictal discharges

To provide further evidence for the increased activity in FS interneurons after focal ictal discharge generation, we next took advantage of a transgenic mouse line (G42 mice) (Chattopadhyaya et al. 2004) expressing the enhanced GFP in a Pv-positive subset of FS interneurons. Similarly to putative FS interneurons from rat slices, Pv-FS interneurons from the EC of G42 mouse slices ($n = 5$) exhibited an early activation after ictal discharge generation (Fig. 4A) followed by a depolarization block of spike generation (white arrowhead). Cells that co-expressed Pv and GFP were only rarely found in EC, so instead, further experiments were performed in the temporal cortex (TC) where these cells were more numerous (Fig. 4B and C). We first confirmed that GFP-expressing Pv-FS interneurons from TC slices also showed an early increase in firing activity after ictal discharge generation followed by a depolarization block ($n = 29$, Fig. 4D). In Ca^{2+} imaging experiments we then observed that after the spiking impairment in the patched Pv-FS interneurons, a number of surrounding neurons exhibited Ca^{2+} elevations

typical of the ictal discharge (Fig. 4D, blue trace). These neurons were grouped in clusters with a mean radius of $205 \pm 19\,\mu m$ ($n = 32$ neurons from 3 experiments; see Methods) and they represented an average of $73 \pm 5\%$ of the total number of responsive neurons in the cluster.
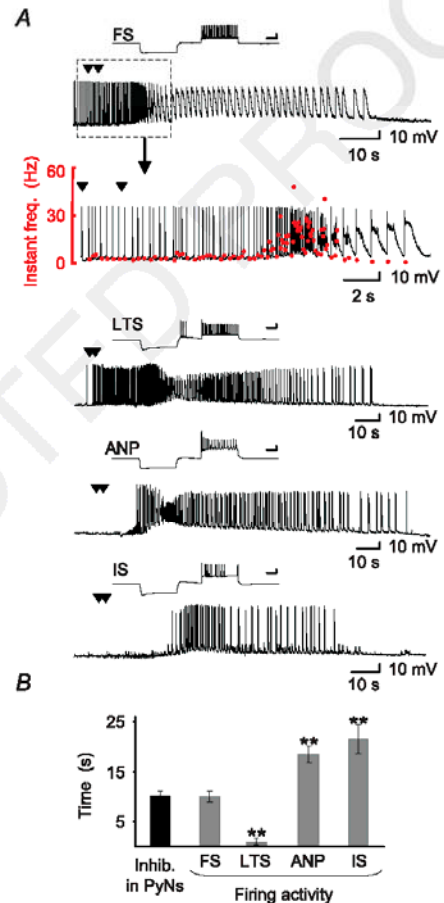

Figure 3. Activity of different classes of interneurons during propagating ictal discharges
A, representative response to hyperpolarizing and depolarizing current steps (scale bars, 20 mV and 200 ms) and current-clamp recordings from different classes of layer V–VI interneurons during propagating ictal discharges in the EC. The enlarged trace also reports the firing instant frequency (IF, red dots) of the FS interneuron. B, bar histogram reporting the mean delay of the inhibitory barrages in PyNs and of the increase in firing activity from the different interneuron types after the NMDA pulse (22 ictal discharges from 12 PyNs; 11 ictal discharges from 7 FS interneurons; 14 ictal discharges from 7 ANP interneurons; 4 ictal discharges from 3 IS interneurons and 6 ictal discharges from 3 LTS interneurons; **$P < 0.001$).

Q7

Notably, the size of these clusters is comparable to that of the clusters recruited into ictal discharges in rat EC slices. Biocytin-filled GFP-expressing Pv-FS interneurons in layer V–VI of the TC in G42 mouse slices show the typical morphology of basket cells with distinct axonal arborizations on and around the soma of target neurons (Kawaguchi & Kondo, 2002; Fig. 4E). Axon projections are mainly confined to their layer of origin and display
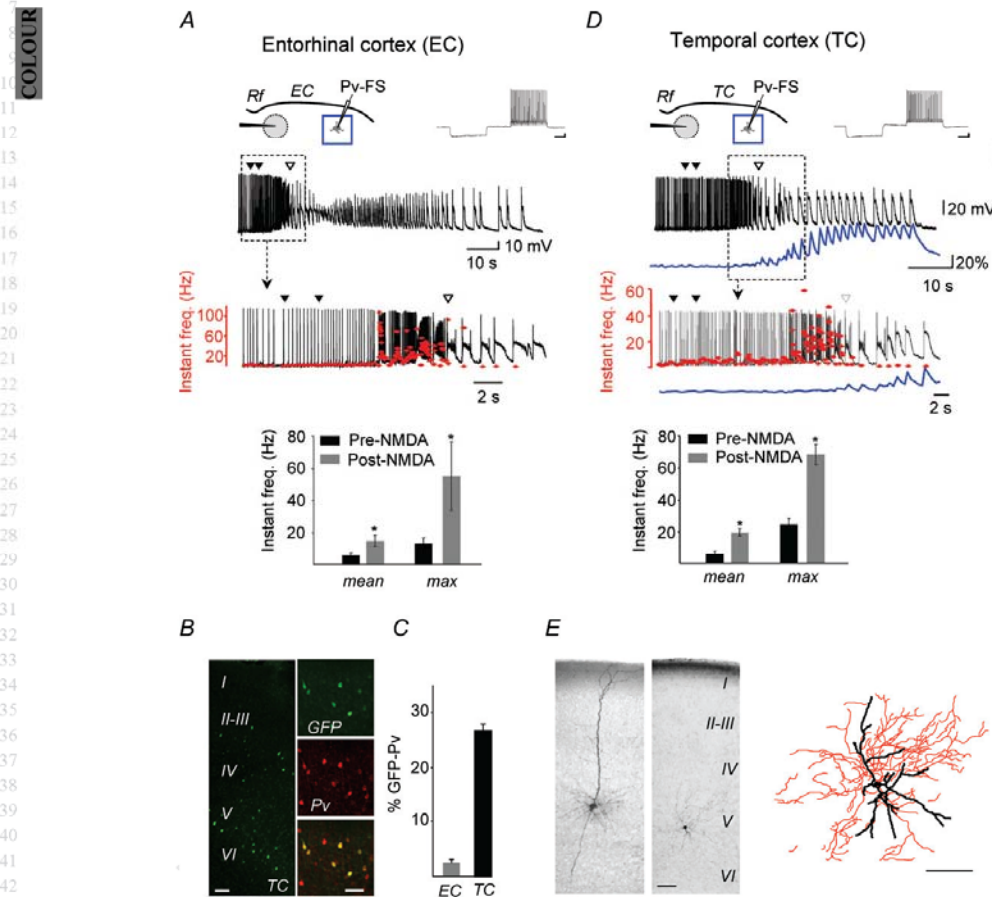

Figure 4. GFP-expressing Pv-FS interneurons during ictal discharge propagation in G42 mice
A and *D*, upper panels: schematic diagrams of the experiments in EC (*A*) and TC (*D*), current-clamp recording from Pv-FS interneurons (black traces) and simultaneous average Ca^{2+} signal (*D*, blue trace) from putative PyNs surrounding the patched Pv-FS interneuron. Superimposed is the instant frequency (red dots) of the Pv-FS interneuron firing activity. The response of the interneurons to current injections is also reported (insets; scale bars, 10 mV and 200 ms). Lower panels: bar histogram of the mean and maximal instant frequency in Pv-FS interneurons before (black bars) and after (grey bars) the NMDA pulse in EC (*A*; $n = 4$, *$P = 0.012$ and $P = 0.017$ for the mean and the maximum values, respectively) and in TC (*D*, $n = 6$, *$P = 0.011$ and $P = 0.019$ for the mean and the maximum values, respectively). *B*, left panel: confocal image of the GFP expression pattern in the TC of a G42 mouse in the different cortical layers. Scale bar, 100 μm. Right panels: double immunostaining showing that the GFP-expressing cells (green) are Pv immunopositive (red). Scale bar, 50 μm. *C*, bar histogram summarizing GFP-expressing cells in layer V–VI of the TC and the EC expressed as a percentage of the total number of Pv-immunopositive cells in G42 mice (10 and 11 slices from 3 mice, and 144 and 406 confocal sections, respectively). *E*, light microscope images of biocytin-filled PyN and GFP-expressing Pv-FS interneuron from layer V of a TC slice (left) and reconstruction of dendritic (black) and axonal (red) arborization of the latter cell (right). Scale bars, 100 μm.

65

an extensive arborization around the soma (mean radius, $268 \pm 39\,\mu m$, $n = 7$).

As Pv-FS interneurons exhibited an early increase in their bursting discharge after the NMDA pulse, they should exhibit a Ca^{2+} increase before that of nearby PyNs. However, due to the low frequency firing activity evoked in these cells by 4-AP, the Ca^{2+} signal in Pv-FS interneurons is already high before the application of the NMDA pulse. To circumvent this caveat we perfused slices with a low Mg^{2+} solution (0–0.2 mM) without 4-AP. Also under these conditions NMDA pulses reliably evoked a propagating ictal discharge (see Fig. 6A, middle traces). Figure 5 illustrates a representative experiment in a Rhod-2-loaded slice in which four GFP-expressing Pv-FS interneurons in TC from a region distant >700 μm from the focus were early activated after the NMDA pulse (Fig. 5A). The Ca^{2+} signal reveals that the GFP-expressing cells (Fig. 5B, green cells in panel 1 and green traces) and two GFP-negative cells (orange labelled cells in panel 1 and orange traces) increased their Ca^{2+} before two clusters of putative PyNs were recruited into the propagating ictal discharge (Fig. 5B, cyan-labelled cells in panels 2 and 3 and blue traces; see also online Supplemental Movie 1). Early activated GFP-negative cells may belong either to the subset of Pv-positive, GFP-negative cells, that are present in the TC of G42 mice, or to a different class of interneurons, such as the LTS interneurons that in rat slice experiments

increased their firing discharge soon after the NMDA pulse. The early Ca^{2+} elevation in GFP-positive Pv-FS interneurons and in a subset of GFP-negative neurons preceded the recruitment of PyN clusters into the propagating ictal discharge with a similar average interval (Fig. 5C, see Methods). In the five experiments performed in TC with the low Mg^{2+} solution, these neurons were $9.8 \pm 1.5\%$ of the total number of neurons present in the field of view, and the GFP-positive Pv-FS interneurons ($n = 32$) were $61.6 \pm 3.7\%$ of the early activated neurons. These data provide further evidence for the early activation of Pv-FS interneurons during ictal discharge propagation.

Relationship between FS interneuron firing activity and PyN recruitment into propagating ictal discharges

We next performed a series of paired recordings from a Pv-FS interneuron and a nearby PyN in TC slices from G42 mice. The inhibitory barrages in the PyN of the pair occurred in coincidence with a burst in the Pv-FS interneuron in both the 4-AP (Fig. 6A, upper trace) and the low Mg^{2+} model (Fig. 6A, middle trace). The analysis of the relationship between the amplitude of the inhibitory barrages and the spiking discharge intensity in Pv-FS interneurons revealed that the strength of the inhibitory barrages onto PyNs, as measured by the charge
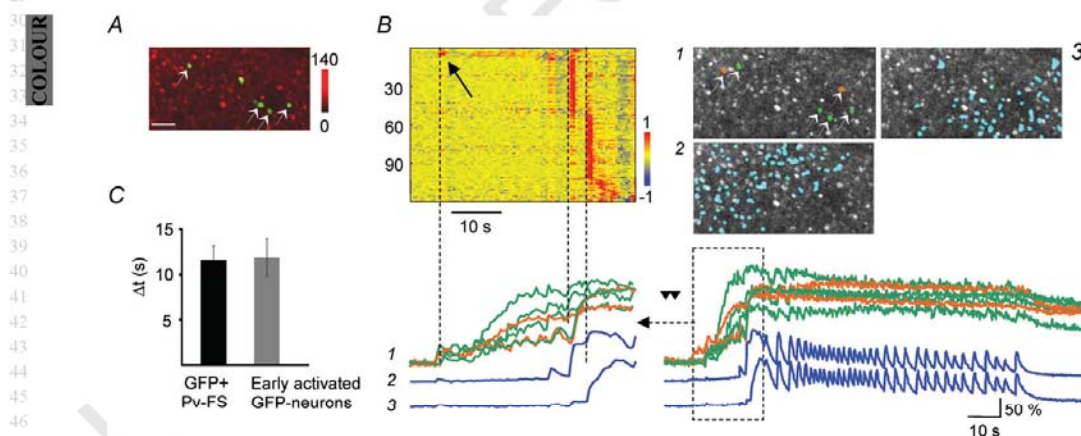

Figure 5. Early recruitment into propagating ictal discharges of GFP-expressing Pv-FS interneurons in G42 mice
A, fluorescence image of a layer V–VI region distant from the focus in a slice loaded with Rhod-2 showing GFP-expressing cells (white arrows; bar, 50 μm). A fifth GFP-expressing Pv-FS interneuron present in the field of view was not considered because it was not loaded with the Ca^{2+} dye. B, recruitment diagram from the region imaged in A. Lower traces: four GFP-expressing neurons (green traces and green cells in panel 1) and two GFP-negative neurons (orange traces and orange cells in panel 1) exhibited a Ca^{2+} increase soon after NMDA stimulation and before two different clusters of putative PyNs were recruited (blue traces and cyan cells in panels 2 and 3). The lower right traces show the Ca^{2+} change in these cells during the whole ictal discharge. C, bar histogram of the mean interval (Δt) between the timing of PyN recruitment ($n = 135$) and the Ca^{2+} increase in GFP-expressing Pv-FS interneurons ($n = 32$, from 5 experiments) and GFP-negative neurons ($n = 20$).
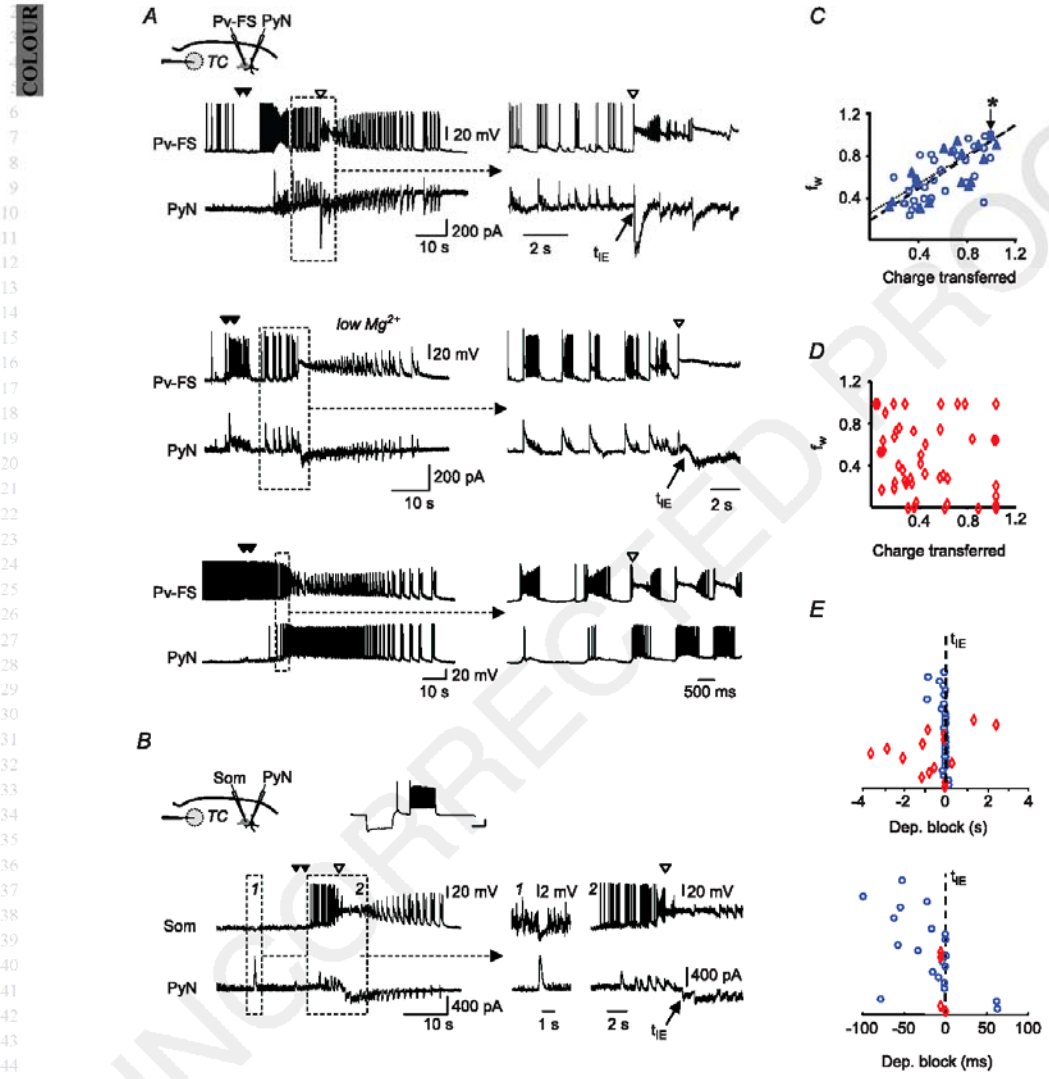
Figure 6. Hyperactivity and block in Pv-Fs interneurons precede the transition to ictal discharge
Pv-FS interneurons are a main source of the inhibitory barrages. A and B, dual current-clamp recordings from a Pv-FS (A) or a Som-IN (B) interneuron and voltage-clamp recording from a neighbouring PyN in a TC slice from a G42 mouse in the 4-AP or low Mg^{2+} model (A, middle panel). Dual recording from a Pv-FS and a PyN (both in current-clamp mode) is also reported (A, lower panel). Response of the LTS-Som interneuron to current injections is also reported (B, inset, scale bars, 20 mV and 500 ms). C, linear regression showing the correlation between the f_w of Pv-FS interneuron firing and the normalized inhibitory charge transferred in the PyNs in the 4-AP model (circles; $R = 0.79$; $P < 0.001$; 39 inhibitory barrages from 9 ictal discharges, 5 pairs) and in the low Mg^{2+} model (triangles; $R = 0.81$; $P < 0.001$; 23 inhibitory barrages from 6 ictal discharges, 3 pairs). Asterisk marks the presence of 8 circles and 5 overlapping triangles. D, linear regression showing the absence of correlation between the f_w of Som interneuron firing and the normalized inhibition ($R = -0.25$; $P = 0.08$; $n = 50$ inhibitory barrages from 9 ictal discharges in 3 pairs). E, distribution of the latency of depolarization block in the Pv-FS interneurons (blue circles; 25 ictal discharges, 10 pairs) and in the Som interneurons (red diamonds; 15 ictal discharges, 3 pairs) with respect to the t_{IE} in the PyNs. Distribution of values in a time window of ±100 ms are also reported.

Q8

67

transferred, were linearly correlated with the change in the firing intensity of Pv-FS interneurons in both the 4-AP (Fig. 6C; circles, 39 inhibitory barrages in 9 ictal discharges from five pairs) and the low Mg^{2+} model (Fig. 6C; triangles, 23 inhibitory barrages in six ictal discharges from three pairs). Furthermore, the t_{IE} in the PyN (Fig. 6A, black arrows) occurred when the Pv-FS interneuron entered into a depolarization block phase (Fig. 6A; white arrowheads). Detailed quantitative analysis from paired recordings confirmed that in 23 of 25 events the depolarization block in Pv-FS interneurons occurred *before* (mean $\pm$ SEM, 105 ± 48 ms; $n = 25$; Fig. 6E, blue circles; 25 ictal discharges from ten pairs, pooled data from 4-AP and low Mg^{2+} experiments) the PyN recruitment (i.e. the time 0 in Fig. 6E corresponding to the t_{IE}). Similar results were obtained in rat EC slices (online Supplemental Fig. S2). Paired recordings in current-clamp configuration from Pv-FS interneurons and PyNs in close proximity to each other and at a similar distance from the focus confirmed that the PyN exhibited the intense firing of the ictal discharge during the depolarization block phase in the Pv-FS interneuron (Fig. 6A, lower traces).

While results described above suggest that the inhibitory barrages which oppose ictal discharge propagation are generated by Pv-FS interneurons, an additional putative source of the inhibitory barrages in PyNs are the LTS interneurons. In rat slices these cells were, indeed, observed to fire shortly after the double NMDA pulse. To address this hypothesis, we performed paired recordings in EC slices from GIN mice in which the enhanced GFP is selectively expressed in a subset of Som interneurons (Oliva *et al.* 2000). Only cells that exhibited the typical firing pattern of LTS interneurons were selected (see Methods) (Oliva *et al.* 2000; McGarry *et al.* 2010). In the 4-AP model we confirmed that layer V–VI Som-LTS interneurons fired intensively before the recruitment of PyNs into the ictal discharge (Fig. 6B). However, the inhibitory currents in PyNs were poorly correlated with a bursting discharge in Som-LTS interneurons (Fig. 6D; 50 inhibitory barrages from 9 ictal discharges, three pairs) and some events (11 of 50) rather coincided with a hyperpolarization in Som-LTS interneurons (Fig. 6B, dashed line box 1). Indeed, recordings from three PyN/Som interneuron pairs, with both cells in voltage-clamp configuration, revealed that 29 of 41 inhibitory events recorded in the PyN during five ictal discharges also occurred synchronously in the Som-LTS interneurons (online Supplemental Fig. S3). The depolarization block in the Som-LTS interneurons was poorly associated with the t_{IE} in the PyN of the pairs (Fig. 6E, red diamonds; 15 ictal discharges from three pairs). Altogether, these results are consistent with the hypothesis that Pv-FS interneurons are a main source of the inhibitory barrages recorded in PyNs.

To rule out the possibility that the depolarization block in Pv-FS interneurons was an artifact of the whole-cell recording mode, we recorded the firing discharges in cell-attached mode. Paired recordings confirmed that the firing activity in GFP-expressing Pv-FS interneurons was strictly correlated with the inhibitory barrages in the PyN of the pairs (Fig. 7A and B) and that in 7 of 9 events the impairment of the firing discharges in Pv-FS interneurons preceded (32.6 ± 30.7 ms; $n = 9$) the ictal discharge onset in the PyNs (Fig. 7C).

Single and dual cell recordings from Pv-FS interneuron pairs (Fig. 8A and B) confirmed that with respect to the NMDA stimulation, the depolarization block in Pv-FS interneurons close to the focus ($<400 \mu$m) occurred with a significantly shorter delay (10.9 ± 1.3 s; $n = 6$) than that in Pv-FS interneurons distant from the focus ($>700 \mu$m, 23.0 ± 1.6 s; $n = 15$; $P < 0.001$). Notably, these delays are comparable to those of the ictal discharge propagation to PyNs of these regions. In PyN–Pv-FS interneuron pairs (Fig. 8C) the depolarization block in the Pv-FS interneuron close to the focus occurred largely before the recruitment into the ictal discharge of the more distant PyN.

Discussion

In the present study, we gained two fundamental insights into the events that govern focal ictal discharge propagation. First, that the inhibitory barrages which temporarily oppose the spreading of focal ictal discharges are largely generated by local Pv-FS interneurons, and second, that a functional impairment in these interneurons contributes to the collapse of the local inhibition that allows focal ictal discharges to propagate further across the cortex.

The conclusions summarized above are based on the results that we obtained in a number of different experiments. We first found that electrophysiologically classified FS interneurons from rat slices exhibited an early bursting activity during ictal discharge propagation. We then found that GFP-expressing Pv-FS interneurons in G42 mice exhibited intense bursting discharges and correlated Ca^{2+} elevations before nearby PyNs were recruited into propagating ictal discharges. In addition, dual recordings from a PyN and a nearby Pv-FS interneuron revealed that the inhibitory barrages in PyNs (i) occurred in strict coincidence with the firing discharge in Pv-FS interneurons, (ii) their strength was determined by the firing discharge intensity in Pv-FS interneurons, and (iii) they ceased after a depolarization block impaired the firing activity in Pv-FS interneurons. In our paired recordings from a PyN and a nearby Pv-FS interneuron, the latter being in either whole-cell or cell-attached mode, we also found that the depolarization block in the Pv-FS

Q9

interneuron preceded the recruitment of the PyNs into the ictal discharge. This conclusion was confirmed in recordings from Pv-FS interneuron pairs and PyN/Pv-FS interneuron pairs located at different distances from the focus as well as in Ca^{2+} imaging experiments. Results from these latter experiments revealed that clusters of PyNs surrounding the patched Pv-FS interneuron were recruited into the propagating ictal discharge after the depolarization block in the Pv-FS interneuron. Neurons from a cluster may share a common inhibitory input that, while it is fully operative, allows these cells to resist the incoming excitatory wave of the propagating ictal discharge. Our results support the view that the recruitment of neurons can be a local process governed mainly by Pv-FS interneurons from the same local network, although they cannot rule out the possibility that different classes of interneurons may also provide a significant contribution (see below).

Previous findings described an important role of the feedforward inhibition in the spreading of epileptiform discharges (Prince & Wilder, 1967; Schwartz & Bonhoeffer, 2001; Trevelyan et al. 2006, 2007). In occipital cortex slices a reduction in the strength of inhibition was also described as a crucial step in the recruitment process during ictal discharge propagation (Trevelyan et al. 2006, 2007). Our study provides evidence that a presynaptic block of Pv-FS interneuron activity is an important factor in this process. However, we cannot rule out that different events, such as a depletion of GABA vesicular stores (Liang et al.

2006; Ortinski et al. 2010; Zhang et al. 2012), a reduced release probability (Bear, 2005), modifications of GABA receptors (Thompson & Gahwiler, 1989; Whittington et al. 1995; Naylor et al. 2005) and a depolarizing GABA action (Staley et al. 1995) resulting from a Cl^- intracellular accumulation during an intense activity at GABAergic synapses (Fujiwara-Tsukamoto et al. 2004; Rivera et al. 2004) may contribute. A recent study reported, however, that intensively active Pv-FS interneuron synapses onto PyNs can be protected from a Cl^- accumulation since an efficient mechanism of Cl^- extrusion, based on voltage- and intracellular Cl^--dependent Cl^- channels, appears to be expressed specifically at these synapses (Foldy et al. 2010).

Non-FS spiking interneurons, such as putative ANP and IS interneurons (Ascoli et al. 2008) that we patched in our recordings from rat EC slices, appeared not to contribute to the inhibitory barrages since they were all quiescent while this inhibitory activity was recorded in PyNs. In contrast, Som-LTS interneurons in GIN mice (and also putative LTS interneurons in rats) fired intensively prior to the ictal discharge, but significant correlation was found neither between the firing discharges in Som-LTS interneurons and the inhibitory currents in PyNs nor between the depolarization block in these interneurons and the t_{IE} in PyNs. However, due to defective space clamp at distal dendrites, the inhibition by Som inter-neurons on distal synapses may be poorly visible in our PyN soma recordings. Therefore, we cannot rule
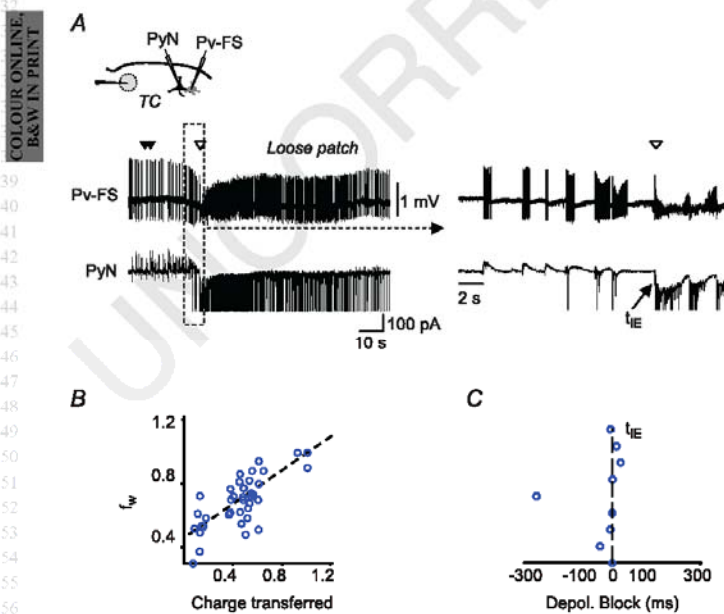

Figure 7. Hyperactivity and block in Pv-FS interneurons precede the transition to ictal discharge (cell-attached mode)
A, dual patch-clamp recordings from a GFP-expressing Pv-FS interneuron firing activity (in the cell-attached mode) and a neighbouring PyN (in whole-cell, voltage-clamp mode) in a TC slice from a G42 mouse in the 4-AP model. B, linear regression showing the correlation between the f_w of GFP-expressing Pv-FS interneuron firing and the normalized inhibitory charge transferred in the PyNs in the 4-AP model (circles; $R = 0.83$; $P < 0.001$; 44 inhibitory barrages from 7 ictal discharges, 3 pairs). C, distribution of the latency of depolarization block in the Pv-FS interneurons (9 ictal discharges, 3 pairs) with respect to the t_{IE} in the PyNs.

out the possibility that dendrites targeting Som interneurons contribute to reduce the overall excitation onto PyNs during propagating ictal discharges. Consistent with this view, a recent study showed that the inhibition by Som interneurons contributes to control the burst spiking response of hippocampal CA1 PyNs to Schaffer collateral stimulation (Lovett-Barron *et al.* 2012).

An interplay similar to that investigated here between PyNs and Pv-FS interneurons has been previously observed between hippocampal CA1 PyNs and unidentified interneurons during spontaneous seizure-like events (Ziburkus *et al.* 2006). Our results extend this observation to a different brain region, such as the EC and the TC, and to a different epileptic activity, such as focally evoked seizures, and they also provide evidence that Pv-FS interneurons are the specific interneuron subset involved. Because FS interneurons, and in particular Pv-FS interneurons, represent a major source of perisomatic inhibition onto PyNs, they are ideally positioned to exert a strict control on the output and synchrony of these neurons (Cobb *et al.* 1995; Freund & Buzsaki, 1996; Miles *et al.* 1996; Freund, 2003; Freund & Katona, 2007). The efficiency of Pv-FS interneurons in opposing

ictal discharge propagation may rely also on their intrinsic properties that promote high frequency of action potential firing, a highly synchronous release (Bacci *et al.* 2005; Hefft & Jonas, 2005) and a fast recruitment by glutamatergic input (Aradi & Maccaferri, 2004).

Our data also provide a plausible cellular mechanism for the enhanced susceptibility to epileptic seizures observed in mice in which firing activity in FS interneurons was affected due to a loss in these interneurons of either K3.2 channels (Lau *et al.* 2000) or $Na_v1.1$ channels (Ogiwara *et al.* 2007). Consistent with an important role of Pv-FS interneurons in seizure generation are also recent data showing that Pv-FS interneuron excitability, modulated by NRG1–ErbB4 signalling, contributes to limbic seizure activity (Li *et al.* 2011; Tan *et al.* 2011).

In our study we have not addressed the mechanism of the depolarization block in Pv-FS interneurons. This may rely on the extracellular K^+ increase that is recognized to accompany seizure discharges in different *in vitro* and *in vivo* models (Lux *et al.* 1986; Dreier & Heinemann, 1991; Perreault & Avoli, 1992; Durand *et al.* 2010; Frohlich *et al.* 2010), and to represent a possible causal factor for epileptic seizures (Gnatkovsky *et al.* 2008; Ullah & Schiff,
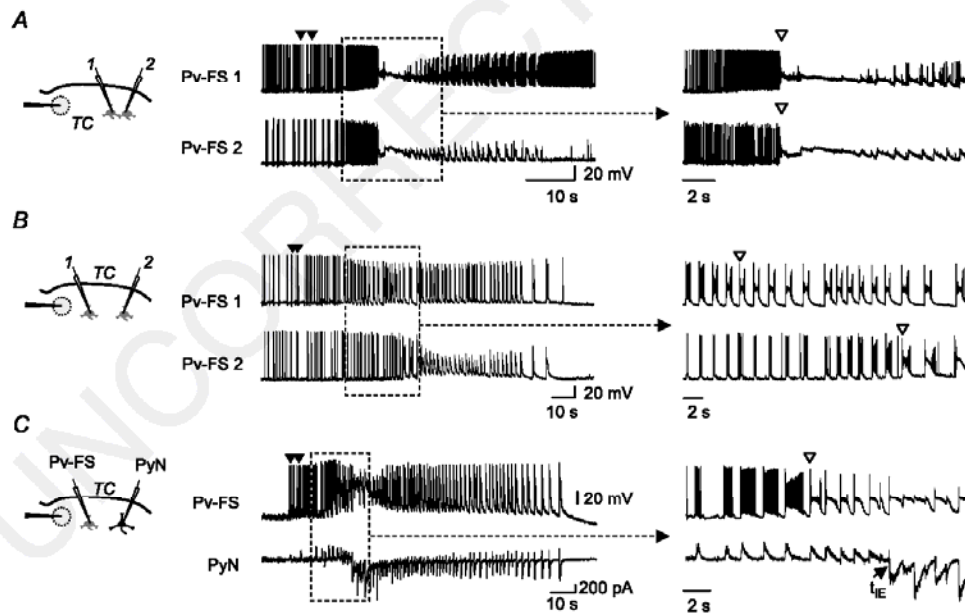

Figure 8. The timing of the depolarization block in Pv-FS interneurons depends on the distance of these cells from the focus
A, dual current-clamp recording from two adjacent Pv-FS interneurons showing simultaneous depolarization block. *B*, two Pv-FS interneurons located at different distances from the focus entered into the depolarization block at different times. *C*, dual recording from a PyN and a Pv-FS interneuron located in TC layer V–VI at different distances from the focus. The depolarization block in the Pv-FS interneuron closer to the focus occurred several seconds before the t_{IE} in the PyN. The recording periods outlined by the dashed boxes are expanded on the right.

2010). Consistent with this hypothesis, an extracellular K^+ increase to 12.5 mM was reported to result in a depolarization block in hippocampal CA3 interneurons (Shin *et al.* 2010). Additional, specifically designed experiments are necessary to clarify this important issue.

Our data on the intense activity of Pv-FS interneurons and Som-LTS interneurons during seizure propagation are consistent with the intense firing described in interneurons *in vivo* just ahead of seizure discharges during the paroxysmal depolarizing shifts (Timofeev *et al.* 2002) and in different experimental models *in vitro* (Avoli *et al.* 2002; Derchansky *et al.* 2008; Gnatkovsky *et al.* 2008). High frequency EEG activities, possibly reflecting interneuron discharges (Trevelyan, 2009), are also recorded in patients at the initiation of temporal lobe seizures (Fisher *et al.* 1992; de Curtis & Gnatkovsky, 2009; Engel *et al.* 2009). Interestingly, multiunit activity aligned with standard EEG recordings from seizure-onset areas in patients revealed that seizure spread was either delayed for several seconds, or in some cases failed to take hold, providing further evidence for an inhibitory restraint mechanism in naturally occurring chronic epilepsy (Schevon *et al.* 2012).

In conclusion, our data point to Pv-FS interneurons as a major source of the feedforward inhibitory activity that locally restrains focal ictal discharge propagation. Although our results do not rule out the possibility that other classes of interneurons, such as Som interneurons, can contribute, they suggest that an initial drastic increase and a subsequent block of the firing discharge are two opposing events in the activity of local Pv-FS interneurons that shape ictal discharge propagation. Additional experiments are, however, necessary to provide direct evidence for a causal relationship between the collapse of inhibition and the depolarization block in the Pv-FS interneurons. Our study suggests that the development of pharmacological tools capable of modulating Pv-FS interneuron activity may represent a new therapeutic strategy to prevent the generalization of focal epilepsies.

References

Aradi I & Maccaferri G (2004). Cell type-specific synaptic dynamics of synchronized bursting in the juvenile CA3 rat hippocampus. *J Neurosci* 24, 9681–9692.

Ascoli GA, Alonso-Nanclares L, Anderson SA, Barrionuevo G, Benavides-Piccione R, Burkhalter A *et al.* (2008). Petilla terminology: nomenclature of features of GABAergic interneurons of the cerebral cortex. *Nat Rev Neurosci* 9, 557–568.

Avoli M, D'Antuono M, Louvel J, Kohling R, Biagini G, Pumain R, D'Arcangelo G & Tancredi V (2002). Network and pharmacological mechanisms leading to epileptiform synchronization in the limbic system *in vitro*. *Prog Neurobiol* 68, 167–207.

Bacci A, Huguenard JR & Prince DA (2005). Modulation of neocortical interneurons: extrinsic influences and exercises in self-control. *Trends Neurosci* 28, 602–610.

Bear MF (2005). Therapeutic implications of the mGluR theory of fragile X mental retardation. *Genes Brain Behav* 4, 393–398.

Brody DL & Yue DT (2000). Release-independent short-term synaptic depression in cultured hippocampal neurons. *J Neurosci* 20, 2480–2494.

Buchheim K, Schuchmann S, Siegmund H, Weissinger F, Heinemann U & Meierkord H (2000). Comparison of intrinsic optical signals associated with low Mg^{2+}- and 4-aminopyridine-induced seizure-like events reveals characteristic features in adult rat limbic system. *Epilepsia* 41, 635–641.

Chattopadhyaya B, Di Cristo G, Higashiyama H, Knott GW, Kuhlman SJ, Welker E & Huang ZJ (2004). Experience and activity-dependent maturation of perisomatic GABAergic innervation in primary visual cortex during a postnatal critical period. *J Neurosci* 24, 9598–9611.

Cobb SR, Buhl EH, Halasy K, Paulsen O & Somogyi P (1995). Synchronization of neuronal activity in hippocampus by individual GABAergic interneurons. *Nature* 378, 75–78.

de Curtis M & Gnatkovsky V (2009). Reevaluating the mechanisms of focal ictogenesis: The role of low-voltage fast activity. *Epilepsia* 50, 2514–2525.

Derchansky M, Jahromi SS, Mamani M, Shin DS, Sik A & Carlen PL (2008). Transition to seizures in the isolated immature mouse hippocampus: a switch from dominant phasic inhibition to dominant phasic excitation. *J Physiol* 586, 477–494.

Dreier JP & Heinemann U (1991). Regional and time dependent variations of low Mg^{2+} induced epileptiform activity in rat temporal cortex slices. *Exp Brain Res* 87, 581–596.

Drummond GB (2009). Reporting ethical matters in *The Journal of Physiology*: standards and advice. *J Physiol* 587, 713–719.

Durand DM, Park EH & Jensen AL (2010). Potassium diffusive coupling in neural networks. *Philos Trans R Soc Lond B Biol Sci* 365, 2347–2362.

Engel J Jr, Bragin A, Staba R & Mody I (2009). High-frequency oscillations: what is normal and what is not? *Epilepsia* 50, 598–604.

Fellin T & Carmignoto G (2004). Neurone-to-astrocyte signalling in the brain represents a distinct multifunctional unit. *J Physiol* 559, 3–15.

Fisher RS, Webber WR, Lesser RP, Arroyo S & Uematsu S (1992). High-frequency EEG activity at the start of seizures. *J Clin Neurophysiol* 9, 441–448.

Foldy C, Lee SH, Morgan RJ & Soltesz I (2010). Regulation of fast-spiking basket cell synapses by the chloride channel ClC-2. *Nat Neurosci* 13, 1047–1049.

Freund TF (2003). Interneuron diversity series: rhythm and mood in perisomatic inhibition. *Trends Neurosci* 26, 489–495.

Freund TF & Buzsaki G (1996). Interneurons of the hippocampus. *Hippocampus* 6, 347–470.

Freund TF & Katona I (2007). Perisomatic inhibition. *Neuron* 56, 33–42.

Frohlich F, Sejnowski TJ & Bazhenov M (2010). Network bistability mediates spontaneous transitions between normal and pathological brain states. *J Neurosci* **30**, 10734–10743.

Fujiwara-Tsukamoto Y, Isomura Y, Kaneda K & Takada M (2004). Synaptic interactions between pyramidal cells and interneurone subtypes during seizure-like activity in the rat hippocampus. *J Physiol* **557**, 961–979.

Gnatkovsky V, Librizzi L, Trombin F & de Curtis M (2008). Fast activity at seizure onset is mediated by inhibitory circuits in the entorhinal cortex *in vitro*. *Ann Neurol* **64**, 674–686.

Gomez-Gonzalo M, Losi G, Chiavegato A, Zonta M, Cammarota M, Brondi M, Vetri F, Uva L, Pozzan T, de Curtis M, Ratto GM & Carmignoto G (2010). An excitatory loop with astrocytes contributes to drive neurons to seizure threshold. *PLoS Biol* **8**, e1000352.

Hefft S & Jonas P (2005). Asynchronous GABA release generates long-lasting inhibition at a hippocampal interneuron-principal neuron synapse. *Nat Neurosci* **8**, 1319–1328.

Jefferys JG (1990). Basic mechanisms of focal epilepsies. *Exp Physiol* **75**, 127–162.

Jones RS & Lambert JD (1990). Synchronous discharges in the rat entorhinal cortex *in vitro*: site of initiation and the role of excitatory amino acid receptors. *Neuroscience* **34**, 657–670.

Katz B & Miledi R (1970). Further study of the role of calcium in synaptic transmission. *J Physiol* **207**, 789–801.

Kawaguchi Y & Kondo S (2002). Parvalbumin, somatostatin and cholecystokinin as chemical markers for specific GABAergic interneuron types in the rat frontal cortex. *J Neurocytol* **31**, 277–287.

Kovacs R, Kardos J, Heinemann U & Kann O (2005). Mitochondrial calcium ion and membrane potential transients follow the pattern of epileptiform discharges in hippocampal slice cultures. *J Neurosci* **25**, 4260–4269.

Lau D, Vega-Saenz de Miera EC, Contreras D, Ozaita A, Harvey M, Chow A, Noebels JL, Paylor R, Morgan JI, Leonard CS & Rudy B (2000). Impaired fast-spiking, suppressed cortical inhibition, and increased susceptibility to seizures in mice lacking Kv3.2 K$^+$ channel proteins. *J Neurosci* **20**, 9071–9085.

Li KX, Lu YM, Xu ZH, Zhang J, Zhu JM, Zhang JM, Cao SX, Chen XJ, Chen Z, Luo JH, Duan S & Li XM (2011). Neuregulin 1 regulates excitability of fast-spiking neurons through Kv1.1 and acts in epilepsy. *Nat Neurosci* **15**, 267–273.

Liang SL, Carlson GC & Coulter DA (2006). Dynamic regulation of synaptic GABA release by the glutamate-glutamine cycle in hippocampal area CA1. *J Neurosci* **26**, 8537–8548.

Losi G, Cammarota M, Chiavegato A, Gomez-Gonzalo M & Carmignoto G (2010). A new experimental model of focal seizures in the entorhinal cortex. *Epilepsia* **51**, 1493–1502.

Lovett-Barron M, Turi GF, Kaifosh P, Lee PH, Bolze F, Sun XH, Nicoud JF, Zemelman BV, Sternson SM & Losonczy A (2012). Regulation of neuronal input transformations by tunable dendritic inhibition. *Nat Neurosci* **15**, 423–430, S421–S423.

Lux HD, Heinemann U & Dietzel I (1986). Ionic changes and alterations in the size of the extracellular space during epileptic activity. *Adv Neurol* **44**, 619–639.

McGarry LM, Packer AM, Fino E, Nikolenko V, Sippy T & Yuste R (2010). Quantitative classification of somatostatin-positive neocortical interneurons identifies three interneuron subtypes. *Front Neural Circuits* **4**, 12.

McNamara JO (1999). Emerging insights into the genesis of epilepsy. *Nature* **399**, A15–22.

McNamara JO, Huang YZ & Leonard AS (2006). Molecular signaling mechanisms underlying epileptogenesis. *Sci STKE* **2006**, re12.

Markram H, Toledo-Rodriguez M, Wang Y, Gupta A, Silberberg G & Wu C (2004). Interneurons of the neocortical inhibitory system. *Nat Rev Neurosci* **5**, 793–807.

Miles R, Toth K, Gulyas AI, Hajos N & Freund TF (1996). Differences between somatic and dendritic inhibition in the hippocampus. *Neuron* **16**, 815–823.

Naylor DE, Liu H & Wasterlain CG (2005). Trafficking of GABA$_A$ receptors, loss of inhibition, and a mechanism for pharmacoresistance in status epilepticus. *J Neurosci* **25**, 7724–7733.

Neher E & Sakaba T (2008). Multiple roles of calcium ions in the regulation of neurotransmitter release. *Neuron* **59**, 861–872.

Ogiwara I, Miyamoto H, Morita N, Atapour N, Mazaki E, Inoue I, Takeuchi T, Itohara S, Yanagawa Y, Obata K, Furuichi T, Hensch TK & Yamakawa K (2007). Nav1.1 localizes to axons of parvalbumin-positive inhibitory interneurons: a circuit basis for epileptic seizures in mice carrying an *Scn1a* gene mutation. *J Neurosci* **27**, 5903–5914.

Oliva AA Jr, Jiang M, Lam T, Smith KL & Swann JW (2000). Novel hippocampal interneuronal subtypes identified using transgenic mice that express green fluorescent protein in GABAergic interneurons. *J Neurosci* **20**, 3354–3368.

Ortinski PI, Dong J, Mungenast A, Yue C, Takano H, Watson DJ, Haydon PG & Coulter DA (2010). Selective induction of astrocytic gliosis generates deficits in neuronal inhibition. *Nat Neurosci* **13**, 584–591.

Pare D, deCurtis M & Llinas R (1992). Role of the hippocampal-entorhinal loop in temporal lobe epilepsy: extra- and intracellular study in the isolated guinea pig brain *in vitro*. *J Neurosci* **12**, 1867–1881.

Perreault P & Avoli M (1989). Effects of low concentrations of 4-aminopyridine on CA1 pyramidal cells of the hippocampus. *J Neurophysiol* **61**, 953–970.

Perreault P & Avoli M (1991). Physiology and pharmacology of epileptiform activity induced by 4-aminopyridine in rat hippocampal slices. *J Neurophysiol* **65**, 771–785.

Perreault P & Avoli M (1992). 4-Aminopyridine-induced epileptiform activity and a GABA-mediated long-lasting depolarization in the rat hippocampus. *J Neurosci* **12**, 104–115.

Prince DA & Wilder BJ (1967). Control mechanisms in cortical epileptogenic foci. "Surround" inhibition. *Arch Neurol* **16**, 194–202.

Rivera C, Voipio J, Thomas-Crusells J, Li H, Emri Z, Sipila S, Payne JA, Minichiello L, Saarma M & Kaila K (2004). Mechanism of activity-dependent downregulation of the neuron-specific K-Cl cotransporter KCC2. *J Neurosci* **24**, 4683–4691.

Rutecki PA, Lebeda FJ & Johnston D (1987). 4-Aminopyridine produces epileptiform activity in hippocampus and enhances synaptic excitation and inhibition. *J Neurophysiol* **57**, 1911–1924.

Schevon CA, Weiss SA, McKhann G Jr, Goodman RR, Yuste R, Emerson RG & Trevelyan AJ (2012). Evidence of an inhibitory restraint of seizure activity in humans. *Nat Commun* **3**, 1060.

Schwartz TH & Bonhoeffer T (2001). *In vivo* optical mapping of epileptic foci and surround inhibition in ferret cerebral cortex. *Nat Med* **7**, 1063–1067.

Shin DS, Yu W, Fawcett A & Carlen PL (2010). Characterizing the persistent CA3 interneuronal spiking activity in elevated extracellular potassium in the young rat hippocampus. *Brain Res* **1331**, 39–50.

Staley KJ, Soldo BL & Proctor WR (1995). Ionic mechanisms of neuronal excitation by inhibitory GABA$_A$ receptors. *Science* **269**, 977–981.

Stanton PK, Jones RS, Mody I & Heinemann U (1987). Epileptiform activity induced by lowering extracellular [Mg^{2+}] in combined hippocampal-entorhinal cortex slices: modulation by receptors for norepinephrine and N-methyl-D-aspartate. *Epilepsy Res* **1**, 53–62.

Streit AK, Derst C, Wegner S, Heinemann U, Zahn RK & Decher N (2011). RNA editing of Kv1.1 channels may account for reduced ictogenic potential of 4-aminopyridine in chronic epileptic rats. *Epilepsia* **52**, 645–648.

Streit J, Luscher C & Luscher HR (1992). Depression of postsynaptic potentials by high-frequency stimulation in embryonic motoneurons grown in spinal cord slice cultures. *J Neurophysiol* **68**, 1793–1803.

Tan GH, Liu YY, Hu XL, Yin DM, Mei L & Xiong ZQ (2011). Neuregulin 1 represses limbic epileptogenesis through ErbB4 in parvalbumin-expressing interneurons. *Nat Neurosci* **15**, 258–266.

Thompson SM & Gahwiler BH (1989). Activity-dependent disinhibition. III. Desensitization and GABA$_B$ receptor-mediated presynaptic inhibition in the hippocampus *in vitro*. *J Neurophysiol* **61**, 524–533.

Timofeev I, Grenier F & Steriade M (2002). The role of chloride-dependent inhibition and the activity of fast-spiking neurons during cortical spike-wave electrographic seizures. *Neuroscience* **114**, 1115–1132.

Traub RD, Jefferys JG & Miles R (1993). Analysis of the propagation of disinhibition-induced after-discharges along the guinea-pig hippocampal slice *in vitro*. *J Physiol* **472**, 267–287.

Trevelyan AJ (2009). The direct relationship between inhibitory currents and local field potentials. *J Neurosci* **29**, 15299–15307.

Trevelyan AJ, Sussillo D, Watson BO & Yuste R (2006). Modular propagation of epileptiform activity: evidence for an inhibitory veto in neocortex. *J Neurosci* **26**, 12447–12455.

Trevelyan AJ, Sussillo D & Yuste R (2007). Feedforward inhibition contributes to the control of epileptiform propagation speed. *J Neurosci* **27**, 3383–3387.

Ullah G & Schiff SJ (2010). Assimilating seizure dynamics. *PLoS Comput Biol* **6**, e1000776.

Weissinger F, Buchheim K, Siegmund H & Meierkord H (2005). Seizure spread through the life cycle: optical imaging in combined brain slices from immature, adult, and senile rats *in vitro*. *Neurobiol Dis* **19**, 84–95.

Whittington MA, Traub RD & Jefferys JG (1995). Erosion of inhibition contributes to the progression of low magnesium bursts in rat hippocampal slices. *J Physiol* **486**, 723–734.

Zahn RK, Liotta A, Kim S, Sandow N & Heinemann U (2012). Reduced ictogenic potential of 4-aminopyridine in the hippocampal region in the pilocarpine model of epilepsy. *Neurosci Lett* **513**, 124–128.

Zhang ZJ, Koifman J, Damian SS, Ye H, Florez CM, Zhang L, Valiante TA & Carlen PL (2012). Transition to seizure: ictal discharge is preceded by exhausted presynaptic GABA release in the hippocampal CA3 region. *J Neurosci* **32**, 2499–2512.

Ziburkus J, Cressman JR, Barreto E & Schiff SJ (2006). Interneuron and pyramidal cell interplay during *in vitro* seizure-like events. *J Neurophysiol* **95**, 3948–3954.

Author contributions

The experiments were performed in the CNR Institute of Neuroscience, Padova section, Padova Italy. M.C., G.L. and G.C. conceived and designed the experiments, collected, analysed and interpreted the data, drafted the article or revised it critically for important intellectual content; A.C. and M.Z. collected and analysed the data. All authors approved the final version of the manuscript.

Q11

Acknowledgements

APPENDIX:

SELECTIVE STIMULATION OF INDIVIDUAL FAST SPIKING INTERNEURONS PREVENTS SEIZURE PROPAGATION IN A BRAIN SLICE MODEL OF FOCAL EPILEPSY

Mario Cammarota, Gabriele Losi and Giorgio Carmignoto

ADDITIONAL METHODS:

Analysis of afterdischarges. To evaluate in voltage-clamp recordings the delay between excitatory bursts from two neurons located at different distance from the epileptogenic focus, we calculated the cross-correlation between the time derivative of both signals, in time bins of 1000 ms separated by 30 ms and we represented the cross-correlation values in a pseudo-colors plot . We measured the lag corresponding to the maximal value of the cross-correlation before and after the change in direction of the afterdischarge.

Preventing depolarization block in Pv-FS-INs, but not in Som-INs, arrests ID propagation

If the depolarization block in Pv-FS-INs is a necessary condition to the local recruitment of PyNs into propagating IDs, one expects that ID propagation would be either delayed or blocked if the functional impairment in Pv-FS-INs is prevented. To test this possibility, an intense firing discharge was evoked in individual Pv-FS-INs by a sequence of depolarizing current pulses (500 ms duration at 0.5 or 1 Hz) applied through a patch pipette. Under these conditions, the double NMDA pulse failed to induce a depolarization block in the Pv-FS-IN and no ID was observed in 11 of a total of 12 NMDA stimulations (Figure 1 A,B). In the same neurons, when no current pulses were applied, the NMDA stimulation evoked both a depolarization block and a full ID

74

(left and right traces) in 13 out of 13 trials (n = 5 experiments). Similar intracellular current pulses applied to Som-INs always failed to prevent the depolarization block and the ID in these cells (n = 7 IDs from 3 experiments; Figure 1 A,B). The results reported above were further validated in Ca^{2+} imaging experiments. In all the performed experiments (n = 3), the sustained firing discharge evoked in individual Pv-FS-INs drastically reduced the recruitment of nearby neurons into propagating IDs. The experiment illustrated in Figure 1C shows the activity of a patched Pv-FS-IN distant from the focus and the Ca^{2+} change in neurons from the same recording field (Figure 1C) in response to double NMDA pulses applied in the absence or presence of a Pv-FS-IN stimulation. When the Pv-FS-IN was not stimulated (Figure 1C, left and right traces), an ID was successfully evoked and two neuronal clusters were subsequently recruited (red and blue traces). When current pulses were delivered to evoke an intense firing in the Pv-FS-IN (for details, see Methods), the ID propagated to neurons of the first cluster (red), but not to neurons of the second cluster (blue) surrounding the patched Pv-FS-IN (Figure 1C, middle traces). Noteworthy is that under these conditions neurons from the first cluster that were still recruited into the propagating epileptic discharge, but the ID duration in these neurons was reduced (-57 ± 5 %; n=24 neurons). Such an ID reduction might be linked to the existence of multiple foci of the afterdischarges that sustain the late ID phase. Indeed, during spontaneous IDs recorded in neocortical slices, afterdischarges have been described to travel also in the opposite direction with respect to that of ID propagation (Trevelyan et al., 2007). If neurons become sources of the afterdischarges as they are recruited into the ID wavefront, then the block of the recruitment process would reduce the afterdischarges in already recruited regions and shorten the overall ID duration, as we observed. To address this hypothesis we analyzed the timing of the afterdischarge in paired voltage-clamp recordings from two PyNs located at different distances from the

75

focus. We found that the ID wavefront propagated firstly to the neuron closer to the focus (Figure 1D, upper trace) and then to the more distant neuron (lower trace). During the clonic phase, however, the afterdischarges that initially propagated in the same direction as the ID wavefront, changed direction (Figure 1E). As revealed by the cross correlation diagram, after the switch in direction all the afterdischarges propagated from a distant region to the original site of ID generation (Figure 1D,E, lower panels). Similar results were obtained in 4 IDs from 3 PyN pairs. On the average, the direction switch occurred 7.97 ± 15 s after the t_{IE} in the more distant neuron. Before the direction switch, the afterdischarge in the neuron closer to the focus preceded by 30.5 ± 12.18 ms that in the more distant neuron, while after the switch it followed with a mean delay of 18.11 ± 6.4 ms (see Additional Methods).
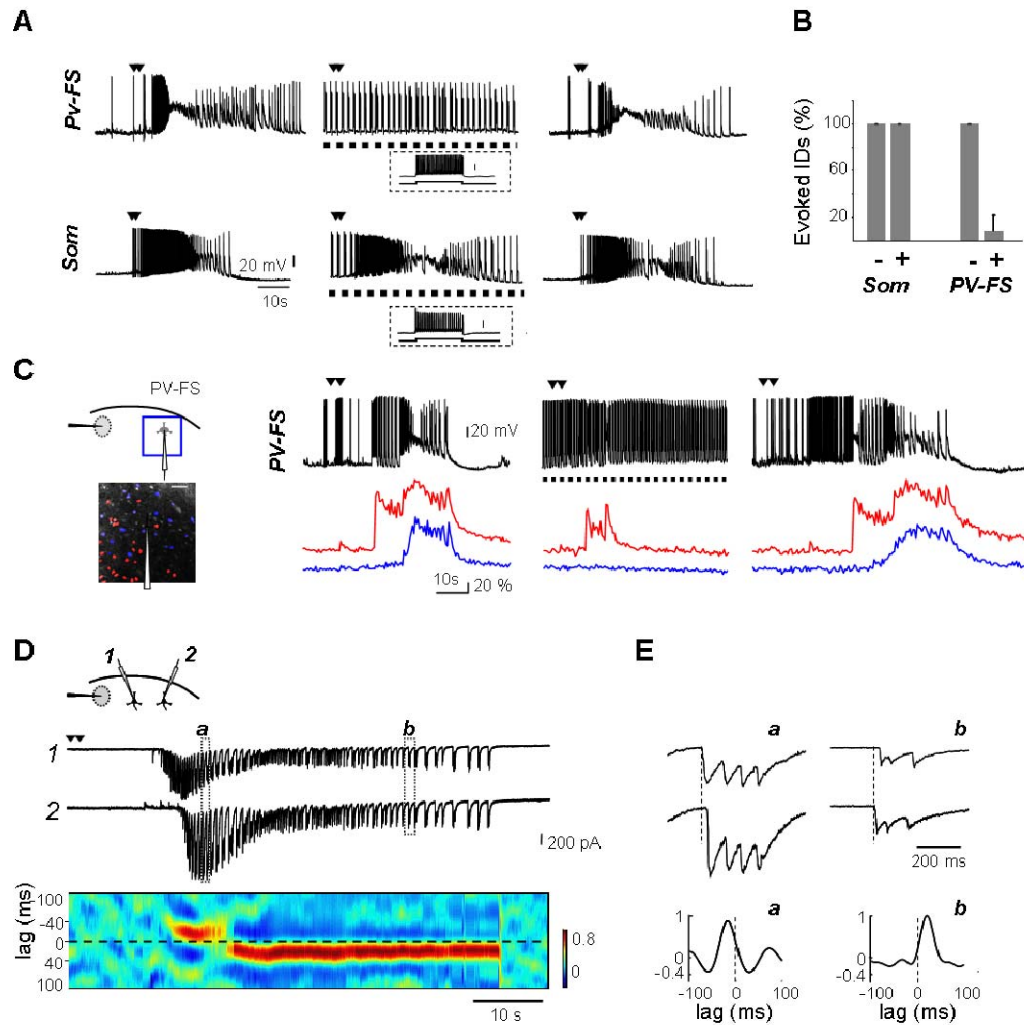
Figure 1: *Preventing depolarization block in Pv-FS-INs arrests ID propagation in layer V-VI of TeCx.* **A,** *Single current-clamp recordings from a Pv-FS-INs and a Som-IN. Steps of current were repeatedly injected to evoke firing activity (insets; see methods) that in the Pv-FS-IN, but not in Som-IN, prevented the depolarization block and the occurrence of a full ID.* **B,** *Summary of the average percentage of NMDA evoked IDs without (-) or during (+) stimulated firing of Som and PV-FS INs.* **C,** *Current-clamp recording from a Pv-FS-IN and simultaneous mean Ca2+ signal from two neuronal clusters (red and blue traces, their soma position is reported in right panel) according to their different recruitment time.* **D,** *Dual voltage-clamp recordings from two PyNs and pseudocolor plot of the cross-correlation (see methods) during a focal ID showing the switch of afterdischarge direction.* **E,** *Two afterdischarges at enlarged time scale with cross-correlation diagrams of the relative bin.*

77

WORK IN PROGRESS:

A GABA MEDIATED Ca^{2+} SIGNALLING IN CORTICAL ASTROCYTES

Gabriele Losi, Mario Cammarota, Letizia Mariotti and Giorgio Carmignoto

INTRODUCTION

Astrocytes can respond to the neuronal release of excitatory neurotransmitters such as glutamate with G-coupled protein receptor-mediated intracellular Ca^{2+} elevations (Porter and McCarthy, 1996, Pasti et al., 1997). The Ca^{2+} change triggers the release of diverse gliotransmitters, including glutamate, that affect neuronal excitability and modulate synaptic transmission. This discovery revolutionized the study of the brain and changed the basic concept that the function of the brain relies exclusively on neurons and neuron-to.neuron synaptic communication. While the vast majority of the studies on gliotransmission describe the interactions of astrocytes with excitatory neuronal network (for a review see Haydon and Carmignoto, 2006), little is known about the hypothesis that astrocytes can be also activted by synaptically released GABA and signal back to interneurons and/or principal neurons to modulate inhibitory and excitatory synaptic transmission.

It is noteworthy that feed-forward inhibition is highly active during ictal discharge propagation in the cortical network. A large amount of GABA is,, indeed, released by early activated interneurons to oppose ictal discharge propagation. This raised the question of whether such an intense activity of GABAergic interneurons can result in a strong activation of astrocytes.

METHODS:

Cortical slices from Enthorinal (EC), Temporal (TC) or Somatosensory (SCC) cortex of P15 wild type mice were obtained as described in the methods sections of the previous chapters. Slices were incubted with Sulforodamine 101 (SR101) to selectively labeled astrocytes (Nihemermaier et al., non mi ricordo come si scrive e data). We developed a new protocol in order to load slices with Fluo4-AM: slices were incubated with the Ca^{2+} indicator for 15 minutes only instead of 1h as commonly done. Under these conditions only a few neurons (5% of the total labeled cells) were loaded. Ca^{2+}-evoked fluorescence changes were measured by a confocal or two-photon microscope during either local pressure-pulses applied to a GABA (or Baclofen) - containing glass pipette or perfusion with the same agents alone or in conjunction with

a selective GABA$_B$ receptor antagonist (CGP or SCH). In the experiments performed on Tomato-floxed mice crossed with PV-CRE mice, the total number within the recording field of potentially responsive astrocytes was evaluated as the number of astrocytes responsive to the application of the mGluR agonist DHPG (50 μM). Only astrocytes that showed a Ca^{2+} increase greater then 3 standard deviation of their basal trace were considered responsive.

RESULTS

We first clarify whether GABA can evoke Ca^{2+} elevations in astrocytes. In Enthorinal Cortex (EC) slices loaded with both SR101 to selectively mark astrocytes (Nimmerjahn, 2004) and the Ca^{2+} sensitive dye Fluo4-AM (Figure 1A), we found that bath application of GABA (25 μm) activated a Ca^{2+} rise in a group of astrocytes (18 ± 6 astrocytes per recording field; Figure 1B). The GABA$_B$ antagonist CGP55485 (25 μm) almost completely abolished GABA effect on astrocytic Ca^{2+} (Figure 1B; n=3 slices). The GABA$_B$ agonist baclofen (25 μm) evoked a Ca^{2+} response similar to that evoked by GABA (19 ± 3 astrocytes, 11 experiments), and also in this case CGP55485 drastically reduced the number of activated astrocytes. (Figure 1B; see Methods). In temporal Cortex (TeCx) slices we also found that local baclofen applications (500 μm) evoked Ca^{2+} elevations in a large group of astrocytes. On the average, Baclofen local applications activated 10.1 ± 1.5 astrocytes (n = 8 experiments) that were located within a radius of approximately 150 μm from the Baclofen-containing pipette tip, inducing a mean fluorescence increase (ΔF/F$_0$) of 171 ± 16% (n = 60 astrocytes from 6 experiments; Figure 1C). This response was prevented by the GABA$_B$ antagonist SCH90911 (500 μm) locally applied 2 s before Baclofen applications (Figure 1C). These results clearly indicate that astrocyte respond to GABA through GABAB-mediated Ca2+ changes. We next tested whether GABA synaptically released by GABAergic interneurons activates astrocytic Ca^{2+} changes. Since we recently observed that parvalbumin positive fast spiking (Pv-FS) interneurons are a major source of the feed-forward inhibition that restrains focal ictal discharge propagation (Cammarota, 2013), we focussed on this interneuron subtype. We used a mouse line in which Pv-FS interneurons express a red fluorescent protein (Tomato-floxed mice crossed with PV-CRE mice) which allowed us to identify these cells in slices loaded with the green fluorescence dye Fluo-4. In order to preferentially

79

load astrocytes with the Ca^{2+} sensor we reduced the loading protocol duration (see Methods). We then performed patch-clamp recordings of a single Pv-FS interneuron and simultaneous Ca^{2+} imaging of nearby astrocytes before and during induction of high frequency action potential firing in the patched interneuron (trains of 80 Hz action potentials for 1000 ms, train frequency 0.5 Hz, induced by current injection through the patch pipette). Out of 74 astrocytes monitored, 24 displayed spontaneous activity. Twenty of these showed a significant increase in the frequency of Ca^{2+} oscillations after Pv-FS interneuron stimulation (p<0,02; Figure 2) (whereas amplitude did not increase significantly, the remaining 4 did not show any Ca^{2+} oscillations). In the remaining 50 astrocytes studied - which were not spontaneously active - we found that 19 cells displayed intense Ca^{2+} oscillations after Pv-FS interneuron stimulation. Notably in the presence of bath applied $GABA_B$ receptor antagonist SCH90911 (25 μM) almost all the responses of astrocytes were prevented. Altogether, these data show that firing activity in a single Pv-FS interneuron can evoke a $GABA_B$-mediated Ca^{2+} elevation in a group of neighbouring astrocytes.
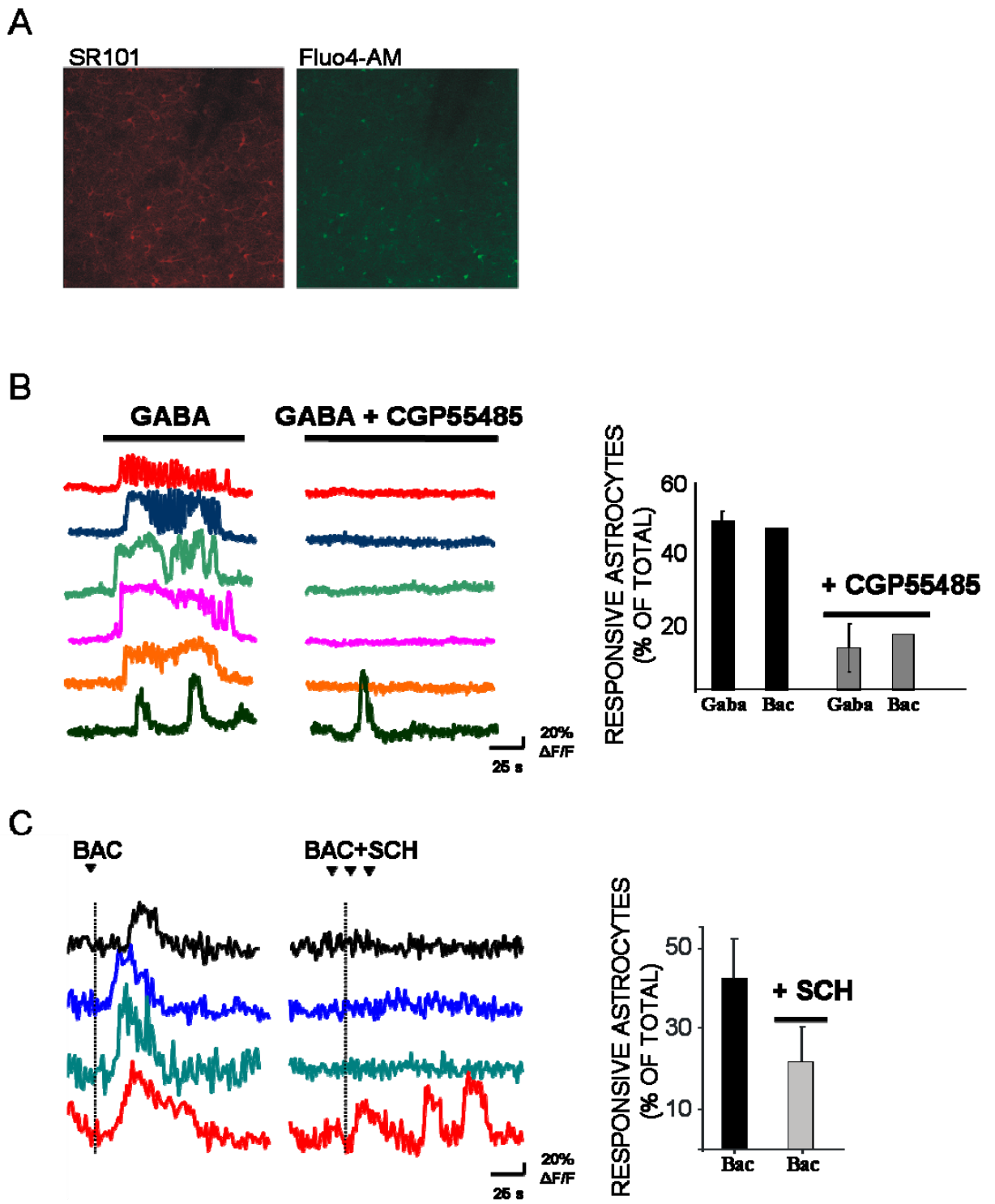
Figure 1: Astrocytes display a GABA$_B$-mediated Ca^{2+} signalling. A: 2-photon image of an EntCx slice loaded with SR101 and Fluo4-AM. B-C: Left: Ca^{2+} changes of astrocytes in response to GABA bath application (B) and to Baclofen local application (C), in control condition and during the application of GABA$_B$ antagonist CGP55485 (B) or SCH (C). Right: histograms summarizing the results.
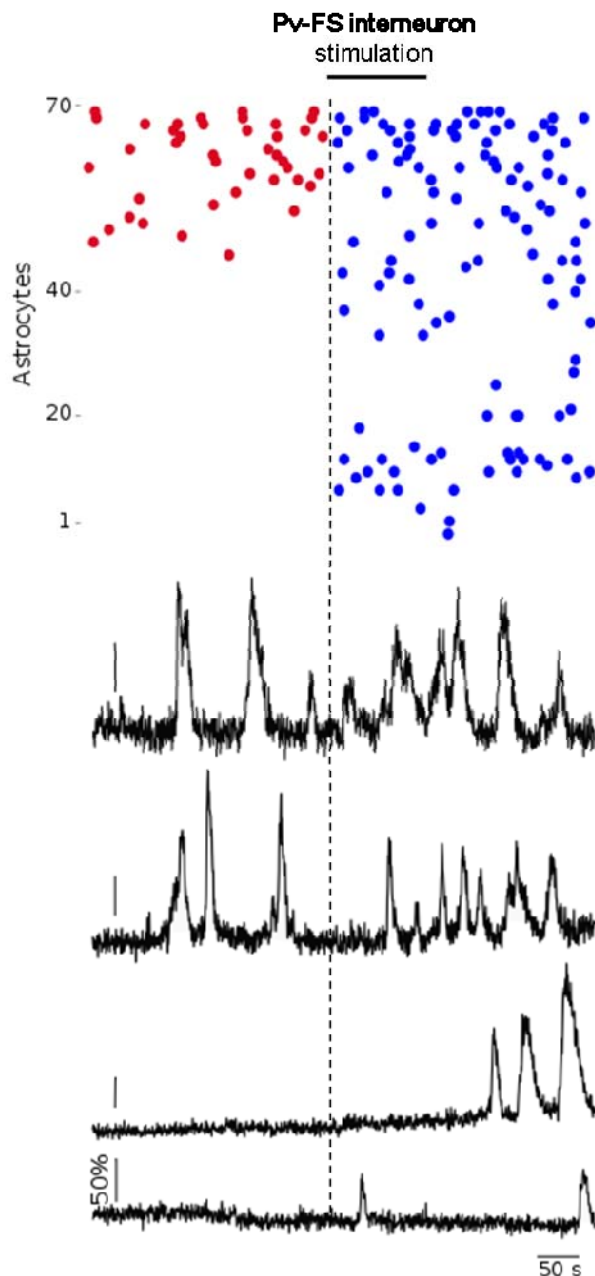
Figure 2: *Astrocytes Ca²⁻ signalling increases after the stimulation of a single Pv-FS interneuron. Top: raster plot of the Ca²⁺ activity of all the astrocytes monitored. Red and blu dots represent the peak of a Ca²⁺ oscillation respectevely before and after the start of the injection of current in the interneuron. Bottom: exemplificative traces.*

What are the consequences of $GABA_B$-mediated Ca^{2+} increases in astrocytes? In presence of TTX to block all neuronal activity, in TeCx slices we found that Baclofen (BAC) local applications evoked slow inward currents (SICs) in 5 out of 9 Pv-FS interneurons tested. Similar experiments were performed in somatosensory cortex slices from Pv-Cre/Tomato-floxed mice where numerous Pv interneurons express the tomato fluorescent protein. In this area, in 4 out of 5 Pv interneurons and in 5 out of 5 pyramidal neurons Baclofen induced a significant increase in SIC amplitude and frequency (Figure 3A-B). Interestingly, as a mean SICs in Pyramidal neurons were significantly larger than in FS interneurons, both in control and after $GABA_B$ activation

(Figure 3B). This result raises the possibility that $GABA_B$-mediated Ca^{2+} elevations in astrocytes result in a different effect in Pyr vs FS-interneurons.
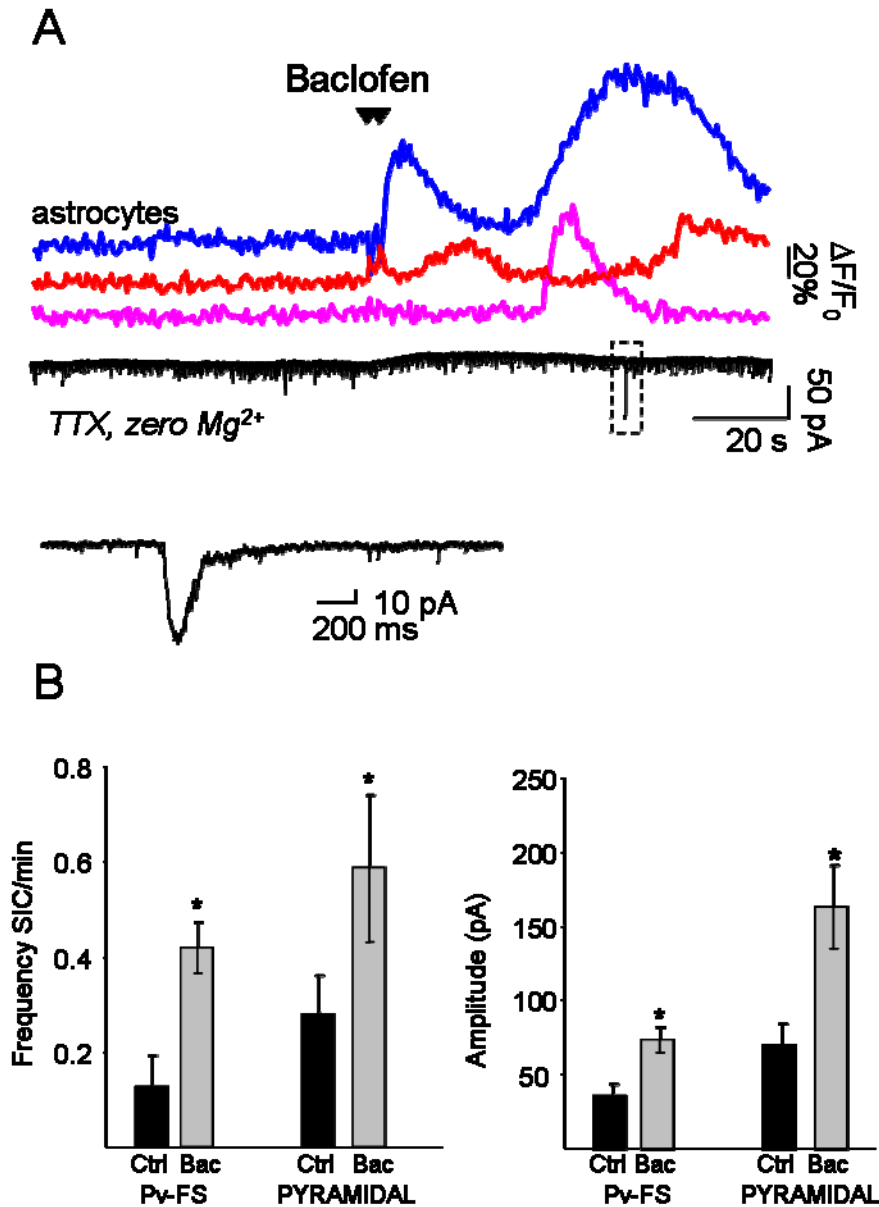

Figure 3: Ca2+ oscillations in astrocytes stimulated with GABAB receptor agonist induce SICs in Pv-FS interneurons and in pyramidal neurons. A: uppre traces: Ca2+ oscillations in astrocytes before and after the application of baclofen (black triangles). Central black trace: voltage-clamp recording from a Pv-FS interneuron. In the lower trace the boxed SIC is reported with higher magnification

CONCLUSIONS AND FUTURE PERSPECTIVES

Full understanding of the cellular mechanisms at the basis of generation, propagation and cessation of epileptic seizures represents one of the most complex and challenging problem in the pathophysiology of the brain. A seizure is comparable to a big electric tilt in the brain where thousands of neurons fire synchronous action potentials and release multiple inhibitory and excitatory transmitters. The problem became even more intricate when we consider the emerging concept that the function of the brain, and perhaps also the dysfunction of the brain, is based on a network of intensively interacting neurons and astrocytes rather than a network of only neurons. Exciting results have been published on the hidden capabilities of these cells to communicate with neurons in fundamental phenomena in brain function.

In my thesis I used a multidisciplinary experimental approach that was based on patch-clamp recordings coupled with confocal and 2-photon Ca^{2+} imaging in a newly developed model of focal ictal discharge in rodents brain slices. All our results indicate that a neuron-astrocyte reciprocal signaling can be deeply involved in the different phases of epileptiform activity. We showed that a release of glutamate from astrocytes – that were activated after an intense firing dischage was induced in a group on neurons by a local NMDA application - is a crucial event that generates a local hyperactivity of neurons and ultimately an epileptogenic focus that predisposes the neuronal network to seizure initiation. Seizure generation is, therefore, triggered by a concerted action of neurons and astrocytes, connected each other in an excitatory loop. The role of astrocytes in determining the threshold of ictal discharge generation was further corroborated by data obtained in a computational model of a neuron-astrocyte network. As regards the propagation of epileptic activity, we firstly investigated the role of GABAergic transmission in governing the spatial-temporal features of the recruitment of new neuronal territories into the propagating seizure. We found that one of the most abundant GABAergic interneurons in the grain, i.e., the parvalbumin expressing fast-spiking interneurons, play a crucial role in governing the timing of the recruitment of pyramidal neurons to the propagating ictal discharge. Preliminary results described in the last chapter of this thesis, raised the possibility that in areas distant from the focus astrocytes may establish with parvalbumin fast-spiking interneurons a series of reciprocal interactions that contribute to control

seizure propagation. This hypothesis will be specifically address in future experiments.

REFERENCES

Angulo, M. C., A. S. Kozlov, S. Charpak and E. Audinat (2004). Glutamate released from glial cells synchronizes neuronal activity in the hippocampus. *The Journal of Neuroscience* **24**(31): 6920-6927.

Bezzi, P., V. Gundersen, J. L. Galbete, G. Seifert, C. Steinhäuser, E. Pilati and A. Volterra (2004). Astrocytes contain a vesicular compartment that is competent for regulated exocytosis of glutamate. *Nature Neuroscience* **7**(6): 613-620.

Boison, D. (2005). Adenosine and epilepsy: from therapeutic rationale to new therapeutic strategies. *The Neuroscientist* **11**(1): 25-36.

Bowser, D. N. and B. S. Khakh (2004). ATP excites interneurons and astrocytes to increase synaptic inhibition in neuronal networks. *The Journal of Neuroscience* **24**(39): 8606-8620.

Carmignoto, G., L. Pasti and T. Pozzan (1998). On the role of voltage-dependent calcium channels in calcium signaling of astrocytes in situ. *The Journal of Neuroscience* **18**(12): 4637-4645.

Coco, S., F. Calegari, E. Pravettoni, D. Pozzi, E. Taverna, P. Rosa, M. Matteoli and C. Verderio (2003). Storage and release of ATP from astrocytes in culture. *Journal of Biological Chemistry* **278**(2): 1354-1362.

Dani, J. W., A. Chernjavsky and S. J. Smith (1992). Neuronal activity triggers calcium waves in hippocampal astrocyte networks. *Neuron* **8**(3): 429-440.

Di Castro, M. A., J. Chuquet, N. Liaudet, K. Bhaukaurally, M. Santello, D. Bouvier, P. Tiret and A. Volterra (2011). Local Ca^{2+} detection and modulation of synaptic release by astrocytes. *Nature Neuroscience*.

Eid, T., M. J. Thomas, D. D. Spencer, E. Runden-Pran, J. C. Lai, G. V. Malthankar, J. H. Kim, N. C. Danbolt, O. P. Ottersen and N. C. de Lanerolle (2004). Loss of glutamine synthetase in the human epileptogenic hippocampus: possible mechanism for raised extracellular glutamate in mesial temporal lobe epilepsy. *Lancet* **363**(9402): 28-37.

Fellin, T. and G. Carmignoto (2004). Neurone-to-astrocyte signalling in the brain represents a distinct multifunctional unit. *The Journal of Physiology* **559**(Pt 1): 3-15.

Gomez-Gonzalo, M., G. Losi, A. Chiavegato, M. Zonta, M. Cammarota, M. Brondi, F. Vetri, L. Uva, T. Pozzan, M. de Curtis, G. M. Ratto and G. Carmignoto (2010). An excitatory loop with astrocytes contributes to drive neurons to seizure threshold. *PLoS Biology* **8**(4): e1000352.

Gouder, N., L. Scheurer, J. M. Fritschy and D. Boison (2004). Overexpression of adenosine kinase in epileptic hippocampus contributes to epileptogenesis. *The Journal of Neuroscience* **24**(3): 692-701.

Haydon, P. G. and G. Carmignoto (2006). Astrocyte control of synaptic transmission and neurovascular coupling. *Physiological Reviews* **86**(3): 1009-1031.

Henneberger, C., T. Papouin, S. H. Oliet and D. A. Rusakov (2010). Long-term potentiation depends on release of D-serine from astrocytes. *Nature* **463**(7278): 232-236.

Hubert, G. W., M. Paquet and Y. Smith (2001). Differential subcellular localization of mGluR1a and mGluR5 in the rat and monkey substantia nigra. *The Journal of Neuroscience* **21**(6): 1838-1847.

Inyushin, M., L. Y. Kucheryavykh, Y. V. Kucheryavykh, C. G. Nichols, R. J. Buono, T. N. Ferraro, S. N. Skatchkov and M. J. Eaton (2010). Potassium channel activity and glutamate uptake are impaired in astrocytes of seizure-susceptible DBA/2 mice. *Epilepsia* **51**(9): 1707-1713.

Jourdain, P., L. H. Bergersen, K. Bhaukaurally, P. Bezzi, M. Santello, M. Domercq, C. Matute, F. Tonello, V. Gundersen and A. Volterra (2007). Glutamate exocytosis from astrocytes controls synaptic strength. *Nature Neuroscience* **10**(3): 331-339.

Kreft, M., M. Stenovec, M. Rupnik, S. Grilc, M. Kržan, M. Potokar, T. Pangršic, P. G. Haydon and R. Zorec (2004). Properties of Ca^{2+}-dependent exocytosis in cultured astrocytes. *Glia* **46**(4): 437-445.

Kuffler, S. W., J. G. Nicholls and R. K. Orkand (1966). Physiological properties of glial cells in the central nervous system of amphibia. *Journal of Neurophysiology* **29**(4): 768-787.

Kumaria, A., C. M. Tolias and G. Burnstock (2008). ATP signalling in epilepsy. *Purinergic Signalling* **4**(4): 339-346.

Lenzen, K. P., A. Heils, S. Lorenz, A. Hempelmann, S. Hofels, F. W. Lohoff, B. Schmitz and T. Sander (2005). Supportive evidence for an allelic association of the human KCNJ10 potassium channel gene with idiopathic generalized epilepsy. *Epilepsy Research* **63**(2-3): 113-118.

Li, L., V. Head and L. C. Timpe (2001). Identification of an inward rectifier potassium channel gene expressed in mouse cortical astrocytes. *Glia* **33**(1): 57-71.

Li, T., J. Quan Lan, B. B. Fredholm, R. P. Simon and D. Boison (2007). Adenosine dysfunction in astrogliosis: cause for seizure generation? *Neuron Glia Biology* **3**(4): 353-366.

Li, T., G. Ren, T. Lusardi, A. Wilz, J. Q. Lan, T. Iwasato, S. Itohara, R. P. Simon and D. Boison (2008). Adenosine kinase is a target for the prediction and prevention of epileptogenesis in mice. *Journal of Clinical Investigation* **118**(2): 571-582.

Losi, G., M. Cammarota and G. Carmignoto (2012). The role of astroglia in the epileptic brain. *Frontiers in Pharmacology* **3**: 132.

Malarkey, E. B. and V. Parpura (2011). Temporal characteristics of vesicular fusion in astrocytes: examination of synaptobrevin 2-laden vesicles at single vesicle resolution. *The Journal of Physiology* **589**(Pt 17): 4271-4300.

Mathern, G. W., D. Mendoza, A. Lozada, J. K. Pretorius, Y. Dehnes, N. C. Danbolt, N. Nelson, J. P. Leite, L. Chimelli, D. E. Born, A. C. Sakamoto, J. A. Assirati, I. Fried, W. J. Peacock, G. A. Ojemann and P. D. Adelson (1999). Hippocampal GABA and glutamate transporter immunoreactivity in patients with temporal lobe epilepsy. *Neurology* **52**(3): 453-472.

Matyash, V., V. Filippov, K. Mohrhagen and H. Kettenmann (2001). Nitric oxide signals parallel fiber activity to Bergmann glial cells in the mouse cerebellar slice. *Molecular and Cellular Neurosciences* **18**(6): 664-670.

McKhann, G. M., 2nd, J. Schoenfeld-McNeill, D. E. Born, M. M. Haglund and G. A. Ojemann (2000). Intraoperative hippocampal electrocorticography to predict the extent of hippocampal resection in temporal lobe epilepsy surgery. *Journal of Neurosurgery* **93**(1): 44-52.

Min, R. and T. Nevian (2012). Astrocyte signaling controls spike timing-dependent depression at neocortical synapses. *Nature Neuroscience*.

Navarrete, M. and A. Araque (2008). Endocannabinoids mediate neuron-astrocyte communication. *Neuron* **57**(6): 883-893.

Navarrete, M. and A. Araque (2010). Endocannabinoids potentiate synaptic transmission through stimulation of astrocytes. *Neuron* **68**(1): 113-126.

Navarrete, M., G. Perea, D. F. de Sevilla, M. Gomez-Gonzalo, A. Nunez, E. D. Martin and A. Araque (2012). Astrocytes mediate in vivo cholinergic-induced synaptic plasticity. *PLoS Biology* **10**(2): e1001259.

Nimmerjahn, A., E. A. Mukamel and M. J. Schnitzer (2009). Motor behavior activates Bergmann glial networks. *Neuron* **62**(3): 400-412.

Olsen, M. L. and H. Sontheimer (2008). Functional implications for Kir4.1 channels in glial biology: from K^+ buffering to cell differentiation. *Journal of Neurochemistry* **107**(3): 589-601.

Panatier, A., J. Vallee, M. Haber, K. K. Murai, J. C. Lacaille and R. Robitaille (2011). Astrocytes are endogenous regulators of Basal transmission at central synapses. *Cell* **146**(5): 785-798.

Pascual, O., K. B. Casper, C. Kubera, J. Zhang, R. Revilla-Sanchez, J. Y. Sul, H. Takano, S. J. Moss, K. McCarthy and P. G. Haydon (2005). Astrocytic purinergic signaling coordinates synaptic networks. *Science* **310**(5745): 113-116.

Pasti, L., A. Volterra, T. Pozzan and G. Carmignoto (1997). Intracellular calcium oscillations in astrocytes: a highly plastic, bidirectional form of communication between neurons and astrocytes in situ. *The Journal of Neuroscience* **17**(20): 7817-7830.

Perea, G. and A. Araque (2007). Astrocytes potentiate transmitter release at single hippocampal synapses. *Science* **317**(5841): 1083-1086.

Perea, G., M. Navarrete and A. Araque (2009). Tripartite synapses: astrocytes process and control synaptic information. *Trends in Neurosciences* **32**(8): 421-431.

Peters, A., S. L. Palay and H. d. F. Webster (1991). *The fine structure of the central nervous system: Neurons and their supportive cells.* O. U. Press. New York, Oxford University Press**:** 276-295.

Pinto, D. J., S. L. Patrick, W. C. Huang and B. W. Connors (2005). Initiation, propagation, and termination of epileptiform activity in rodent neocortex in vitro involve distinct mechanisms. *The Journal of Neuroscience* **25**(36): 8131-8140.

Porter, J. T. and K. D. McCarthy (1996). Hippocampal astrocytes in situ respond to glutamate released from synaptic terminals. *The Journal of Neuroscience* **16**(16): 5073-5081.

Proper, E. A., G. Hoogland, S. M. Kappen, G. H. Jansen, M. G. Rensen, L. H. Schrama, C. W. van Veelen, P. C. van Rijen, O. van Nieuwenhuizen, W. H. Gispen and P. N. de Graan (2002). Distribution of glutamate transporters in the hippocampus of patients with pharmaco-resistant temporal lobe epilepsy. *Brain* **125**(Pt 1): 32-43.

Sarac, S., S. Afzal, H. Broholm, F. F. Madsen, T. Ploug and H. Laursen (2009). Excitatory amino acid transporters EAAT-1 and EAAT-2 in temporal lobe and hippocampus in intractable temporal lobe epilepsy. *APMIS* **117**(4): 291-301.

Seifert, G., K. Schilling and C. Steinhauser (2006). Astrocyte dysfunction in neurological disorders: a molecular perspective. *Nature Reviews. Neuroscience* **7**(3): 194-206.

Serrano, A., N. Haddjeri, J. C. Lacaille and R. Robitaille (2006). GABAergic network activation of glial cells underlies hippocampal heterosynaptic depression. *The Journal of Neuroscience* **26**(20): 5370-5382.

Shigetomi, E., X. Tong, K. Y. Kwan, D. P. Corey and B. S. Khakh (2011). TRPA1 channels regulate astrocyte resting calcium and inhibitory synapse efficacy through GAT-3. *Nature Neuroscience*.

Takata, N., T. Mishima, C. Hisatsune, T. Nagai, E. Ebisui, K. Mikoshiba and H. Hirase (2011). Astrocyte calcium signaling transforms cholinergic modulation to cortical plasticity *in vivo*. *The Journal of Neuroscience* **31**(49): 18155-18165.

Takumi, T., T. Ishii, Y. Horio, K. Morishige, N. Takahashi, M. Yamada, T. Yamashita, H. Kiyama, K. Sohmiya, S. Nakanishi and et al. (1995). A novel ATP-dependent inward rectifier potassium channel expressed predominantly in glial cells. *The Journal of Biological Chemistry* **270**(27): 16339-16346.

Tanaka, K., K. Watase, T. Manabe, K. Yamada, M. Watanabe, K. Takahashi, H. Iwama, T. Nishikawa, N. Ichihara, T. Kikuchi, S. Okuyama, N. Kawashima, S. Hori, M. Takimoto and K. Wada (1997). Epilepsy and exacerbation of brain injury in mice lacking the glutamate transporter GLT-1. *Science* **276**(5319): 1699-1702.

Teichberg, V. I. (1991). Glial glutamate receptors: likely actors in brain signaling. *The FASEB Journal* **5**(15): 3086-3091.

Tessler, S., N. C. Danbolt, R. L. Faull, J. Storm-Mathisen and P. C. Emson (1999). Expression of the glutamate transporters in human temporal lobe epilepsy. *Neuroscience* **88**(4): 1083-1091.

Tian, G.-F., H. Azmi, T. Takano, Q. Xu, W. Peng, J. Lin, N. Oberheim, N. Lou, X. Wang, H. R. Zielke, J. Kang and M. Nedergaard (2005). An astrocytic basis of epilepsy. *Nature Medicine* **11**(9): 973-981.

Trevelyan, A. J., T. Baldeweg, W. van Drongelen, R. Yuste and M. Whittington (2007). The source of afterdischarge activity in neocortical tonic-clonic epilepsy. *The Journal of Neuroscience* **27**(49): 13513-13519.

Ventura, R. and K. M. Harris (1999). Three-dimensional relationships between hippocampal synapses and astrocytes. *The Journal of Neuroscience* **19**(16): 6897-6906.

Volterra, A. and J. Meldolesi (2005). Astrocytes, from brain glue to communication elements: the revolution continues. *Nature Reviews. Neuroscience* **6**(8): 626-640.

Wetherington, J., G. Serrano and R. Dingledine (2008). Astrocytes in the epileptic brain. *Neuron* **58**(2): 168-178.

Zhang, Q., T. Pangršic, M. Kreft, M. Kržan, N. Li, J.-Y. Sul, M. Halassa, E. Van Bockstaele, R. Zorec and P. G. Haydon (2004). Fusion-related release of glutamate from astrocytes. *Journal of Biological Chemistry* **279**(13): 12724-12733.